ADVANCED HYDROGELS FOR POLYMERIZED CRYSTALLINE

COLLOIDAL ARRAY MATERIALS

by

Kyle W. Kimble

B.S. Centre College, 1999

M.S. Indiana University, 2001

Submitted to the Graduate Faculty of

Department of Chemistry in partial fulfillment

of the requirements for the degree of

Doctor of Philosophy

University of Pittsburgh

2007

UNIVERSITY OF PITTSBURGH

_____

FACULTY OF ARTS AND SCIENCES

This dissertation was presented

By

<u>Kyle W. Kimble</u>

It was defended on

Oct. 5, 2007

and approved by

_____Adrian C. Michael

_____Alexander Star

_____David N. Finegold

_____

_____

_____Sanford A. Asher
            Committee Chairperson

ADVANCED HYDROGEL SYSTEMS FOR POLYMERIZED CRYSTALLINE COLLOIDAL ARRAY MATERIALS

Kyle W. Kimble, Ph.D.

University of Pittsburgh, 2007

We developed a novel photo-polymerized hydrogel material and a novel technique for embedding a crystalline colloidal array (CCA) within a thermo-reversible gelation polymer. The CCA lattice is locked into place within a polymeric hydrogel, forming a polymerized crystalline colloidal array (PCCA). The face-centered cubic (fcc) lattice into which the CCA self-assembles, Bragg diffracts light in the visible, near IR and UV regions of the spectrum.

We utilized the novel hydrogel composition to detect ammonia in both buffer solutions and human serum. Phenols attached to the hydrogel backbone cross-link upon the addition of hypochlorite in a sample containing ammonia. The cross-linking causes an increase in the elastic constant of the hydrogel which forces the gel to shrink, blue-shifting the wavelength of Bragg diffracted light proportional to the concentration of ammonia present in solution. The sensor functions within the clinically relevant ammonia interval with a 50 µM detection limit in 1:1 serum/buffer solutions.

A slight modification of this hydrogel material enabled its use within a bi-modular sensing approach for an organophosphorus (OP) nerve agent. The bi-modular sensing utilized the enzyme organophosphorus hydrolase (OPH) and the pH-sensitive group 3-aminophenol as recognition agents. OPH hydrolyzes OPs at basic pH and produces

protons. These protons lower the pH inside the hydrogel changing the phenolates to phenols, lowering the free-energy of mixing and blue-shifting the Bragg diffracted light wavelength proportional to the OP concentration. The sensor is reversible, functions in high-ionic strength media, and has a 0.2 μM OP detection limit in aqueous media.

We also developed a new technique for the synthesis of PCCA materials by embedding CCA within a thermo-reversible gelation polymer. Poly(vinyl alcohol) (PVA) in a solution of water and DMSO exhibits cononsolvency resulting in the formation of nanocrystallites, which act as physical cross-links. The hydrogel formed is thermo-reversible. It melts at 70°C and is optically clear when formed at temperatures below -10 ^{o}C. This gelation technique enables the facile synthesis of arbitrarily large PCCA materials.

ACKNOWLEDGEMENTS

TABLE OF CONTENTS

LIST OF TABLES

LIST OF FIGURES

Figure 10: Glutamate dehydrogenase converts 2-oxoglutarate and ammonium to glutamate and water. The quantity of NH_4^+ is monitored by UV absorbance of NAD^+ at 340 nm.

Figure 11: The proposed reaction mechanism for the Berthelot reaction consists of three steps: (a) ammonia reacts with hypochlorite to form monochloramine at basic pH, (b) monochloramine reacts with a phenol to form benzoquinone chlorimine, (c) benzoquinone chlorimine reacts with a second phenol to form an indophenol. (d) Sodium nitroferricyanide (III) dihydrate is a coupling reagent which increases the kinetics of steps (b).

Figure 12: The formation of indophenol cross-links results in an increase in the elastic restoring force of the hydrogel, which actuates an osmotic pressure, forcing water out of the hydrogel and thereby decreasing the volume of the gel. As a result, the spacing between diffracting planes in the PCCA decreases, and the wavelength of diffracted light blue-shifts proportional to NH_3 concentration.

Figure 13: Preparation of the PCCA and functionalization with 3-aminophenol. The poly(acrylamide) is first hydrolyzed to yield a carboxylic acid functionalized hydrogel. The 3-AMP is coupled via a standard carbodiimide coupling procedure.

Figure 14: The quantity of 3-aminophenol coupled to the hydrogel was determined by measuring the difference in absorbance of the blank and coupled hydrogel at 295 nm.

Figure 15: The absorbance spectra for standard solutions of 3-aminophenol in BBS. Inset is the Beer's law plot showing the determination of the molar absorbtivity.

Figure 16: The concentration of 3-AMP coupled to a blank gel increased linearly in relation to the hydrolysis time. The greater extent to which the amides on the hydrogel were converted to carboxylic acids resulted in the coupling of a higher concentration of 3-AMP through EDC coupling. In each case, the EDC coupling conditions, including the concentration of 3-AMP in the coupling solution, was kept constant and in excess.

Figure 17: Diffraction spectra of PCCA in presence of 600 μM OCl^-. The PCCA does not exhibit a consistent blue-shift, but the original peak diminishes as the secondary peak grows in intensity. The negative baseline results because of over-subtraction of the background.

Figure 18: The Hoffmann degradation, sometimes referred to as the Hoffman rearrangement, is a process where a primary amide is transformed into an isocyanate intermediate by the hypochlorite anion. The isocyanate is hydrolyzed forming a primary amine and carbon dioxide.

Figure 19: The synthesis of a PCCA. The monomers are added to a solution of the CCA. The initiator is added and the CCA is placed on the apparatus shown in Figure 8 for 3 hours. The hydrogel product will contain epoxide functionality.

Figure 20: Images showing turbidity caused by microsynerisis for blank hydrogels. Hydrogels made with high polymer content (40% and 30%) are transparent and hydrogels with low polymer content (20% and 10%) are opaque.

Figure 21: Response of the 30% polymer hydrogel for hyperphysiological concentrations of ammonia. The lack of spectral shift prompted the investigation into lower polymer hydrogels.

Figure 22: The relationship between the GA incorporated into the polymer (percent GA to total polymer content (w/w)) and the resulting spectral window for the response to 300 μM NH$_3$.

Figure 23: The sensing response to 300 μM NH$_3$ in BBS was dependent on the concentration of nitroprusside (NP) incorporated into the reaction solution. The maximum response occurs at ~0.0125 M NP.

Figure 24: The proposed reaction mechanism for the Berthelot reaction consists of three steps: (i) ammonia reacts with hypochlorite to form monochloramine at basic pH, (ii) monochloramine reacts with a phenol to form benzoquinone chlorimine, (iii) benzoquinone chlorimine reacts with a second phenol to form an indophenol. (iv) Sodium nitroferricyanide (III) dihydrate is a coupling reagent which increases the kinetics of step (ii).

Figure 25: The formation of indophenol cross-links results in an increase in the elastic restoring force of the hydrogel, which actuates an osmotic pressure, forcing water out of the hydrogel and thereby decreasing the volume of the gel. As a result, the spacing between diffracting planes in the PCCA decreases, and the wavelength of diffracted light blue-shifts proportional to NH$_3$ concentration.

Figure 26: Preparation and functionalization of PCCA via epoxide ring opening with 3-aminophenol.

Figure 27: Diffraction spectra of PCCA in presence of 300 μM NH$_3$. The PCCA blue-shifts continuously over the course of 120 min as NH$_3$ reacts with OCl$^-$ and 3-AMP to form an indophenol species which cross-links the hydrogel.

Figure 28: Diffraction blue-shift versus time for ammonia-sensing PCCA in BBS at pH 9.2 containing 600 μM OCl$^-$. The sensor displays distinctly different rates of diffraction shift for differing NH$_3$ concentrations; the control, containing no NH$_3$, actually red-shifts. The error bars are the average over the different time measurements of the standard deviation between replicate trials ($\lambda_{\text{diffraction}}$ = $\pm$ 1.46 nm, N = 3). The relative standard deviation remained fairly constant over time.

Figure 29: Calibration curve based on the response of our sensor to NH$_3$ in BBS (pH=9.2) containing 600 μM OCl$^-$ at 60 and 120 min. This sensor shows a linear response between 30 and 150 μM NH$_3$ at 60 min.

Figure 30: We measured the PCCA response of four spiked serum samples and an un-spiked sample. All samples contained 600 μM OCl⁻ and had a pH of 9. We found the serum contains NH_3 on the order of the physiological concentration for healthy adults. The error bars are the average of the standard deviation between replicate trials ($\lambda_{\text{diffraction}} = \pm 0.57$ nm, N = 3).

Figure 31: Calibration curve for the response of our sensor to NH_3 in a 1:1 solution of serum and BBS at 60 min. Concentrations of NH_3 were determined using the Vitros Autoanalyzer. Error bars are equal to the standard deviation ($\lambda_{\text{diffraction}} = \pm 0.57$ nm, N = 3).

Figure 32: A 3 cm x 3 cm TGCCA was fabricated between glass plates by using a 100 μm thick polyester spacer to separate the TGCCA from the adhesive used to seal the edges of the glass plates. The cell was divided into sixteen 9 mm square regions (A1 – D4) that were analyzed via UV-Vis transmission spectroscopy with a 5 mm diameter aperture.

Figure 33: a) A conical funnel, glass plates and a round bottom flask containing the fabricated TGCCA. The planar 16 cm x 16 cm sample shown has a thickness of 500 μm. Included for reference is a 15 cm ruler and a 25 mm scale-bar. The TGCCA in the round bottom flask and funnel have volumes of 50 ml. b) Reflectance spectra from each TGCCA.

Figure 34: TGCCA made with 5% 78 KD PVA and 110 nm diameter particles diffract different wavelengths of light depending on the colloid concentration. TGCCA materials can be made which diffract anywhere in the visible spectrum by controlling the colloid concentration.

Figure 35: All samples were maintained at −20°C for 3 hours and photographed after warming to room temperature. Sample (a) was cycled six times between −20°C and room temperature. a) 5% PVA in pure water. b) 5% PVA in a 50% DMSO/water. c) 5% PVA and 7.5% colloidal particles in pure water. d) 5% PVA and 7.5% colloidal particles in a 50% DMSO/water. e) 7.5% colloidal particles in pure water. f) 7.5% colloidal particles in 50% DMSO/water.

Figure 36: TEM image of a 180 nm PS colloidal particle incubated in a PVA solution. An ~10 nm layer of PVA appears to be adsorbed to the particle surface.

Figure 37: Photographs of CCA (left) thermally cycled to form TGCCA (right). The conditions for the thermal cycling are shown on photographs 1 and 2. On the right, average transmission spectra through four locations in both the CCA (black trace) and the TGCCA (red trace) are shown. The colloidal particles disorder, starting at the edges, with increasing thermal cycling.

Figure 38: a) Sixteen transmission spectra were taken of a single photo-polymerized PCCA and of a single TGCCA. Each spectrum comes from a different 9 x 9 mm

area of the PCCA and TGCCA. b) The average and best spectra from the sixteen spectra.

Figure 39: a) Room temperature diffraction spectra of TGCCA cross-linked by 1.5% glutaraldehyde solution after melting PVA physical cross-links. The diffraction peak wavelength is a function of the cross-linking time in b) 1.5% and c) 0.15% glutaraldehyde.

Figure 40: a) The diffraction spectra for a TGCCA functionalized with carboxylic acid groups exhibits a blue-shift in its diffraction wavelength as the carboxylate is protonated. b) The titration curves for a carboxyl and 3-amniophenol functionalized TGCCA.

Figure 41: OPH hydrolyzes methyl-paraoxon, an organophosphorus pesticide, into p-nitrophenolate and dimethylphosphate at basic pH, producing two protons in the process.

Figure 42: a) CCAs form due to electrostatic repulsion between particles. The particle spacing is such that the array Bragg diffracts visible light. The lattice is locked into place by a poly(2-hydroxyethyl acrylate) hydrogel network. The backbone is functionalized with both organophosphorus hydrolase (OPH) and 3-aminophenolate. As OPH reacts with methyl-paraoxon, p-nitrophenolate and dimethylphosphate, as well as two protons are produced. This produces a steady-state pH gradient between the interior and exterior regions of the hydrogel. The lower pH inside the hydrogel protonates the phenolates. As a result, the solubility of the hydrogel network decreases, which shrinks the hydrogel and blue-shifts the IPCCA diffraction. b) The diffraction peak of the IPCCA blue-shifts in response to the analyte concentration.

Figure 43: Preparation of the IPCCA and functionalization with 3-aminophenol and OPH. The 3-AMP is first coupled via epoxide ring opening. The pendant amides are subsequently hydrolyzed to form carboxylates, which are carbodiimide-coupled to amines on the OPH enzyme.

Figure 44: UV-VIS absorbance spectra of CCA-free hydrogels. a) displays the spectra at various stages of 3-AMP coupling. The blue line is the spectrum of a blank pHEA hydrogel prior to conjugation, the green spectrum is the blank after coupling with 3-AMP, and the red spectrum is after hydrolysis and rinsing. b) shows the spectra of a pHEA hydrogel with 4-amino-2-nitrophenol attached before (green) and after (red) OPH coupling. The blue difference spectrum represents the absorbance difference after coupling OPH. The peak at ~ 280 nm in the difference spectrum indicates OPH attachment. 4-amino-2-nitrophenol, which absorbs at ~ 430 nm instead of ~280 nm, was coupled instead of 3-AMP in order to avoid dominating overlap between the absorbance peaks of 3-AMP and OPH.

Figure 45: a) The solution pH versus the number of millimoles NaOH added. The pK_a of the borate buffer (pH ~ 9.2) and the 3-AMP (pH ~ 9.6) are apparent. b)

Diffraction red-shift of the PCCA as a function of the pH. We see that while the titration of the buffer occurs, there is very little response from the PCCA. But, as the phenol groups are titrated, we see the PCCA diffraction red-shifts. The inflection point in (b) occurs at the phenolate pK_a, indicating that the diffraction response is due to the phenol titration.

Figure 46: a)The PCCA diffraction wavelength as a function of methyl-paraoxon concentration in BTS. Inset is the range (0-24 µM methyl-paraoxon) used to calculate the limit of detection. b) shows the representative diffraction spectra of the PCCA at several methyl-paraoxon concentrations. The standard error in the measurement was $\sigma = 1.1$ nm for 2 replicates.

Figure 47: Time dependence of the diffraction blue shift at two different methyl-paraoxon concentrations. Steady-state is established within ~ 60 min. The diffraction red-shifts at longer times due to depletion of the analyte.

Figure 48: PCCA OP sensor diffraction wavelength as a function of methyl-paraoxon pesticide concentration in both BTS and filtered stream water. The sensor displays a 16% smaller response in stream water compared to its response in BTS. The inset shows the concentrations ≤ 24 µM methyl-paraoxon.

CHAPTER 1: Introduction

Polymerized Crystalline Colloidal Arrays (PCCA) hold great potential for advancements in analytical chemistry, optics, and sensor development. Currently, there is a great desire to prepare PCCA with alternative polymeric backbones enabling the development of PCCA materials for a greater range of applications. The hydrogel is responsible for how the PCCA responds to it environment and also dictates the optical properties, durability, biocompatibility, toxicity and handling characteristics. The number of different hydrogel compositions currently being used for PCCA materials is small, which has limited the development of new applications.

Current research in the area of PCCA materials has focused on the development of sensors that utilize the volume-responsive nature of the hydrogels actuated by specific chemical recognition events. This has led to a number of novel sensors for several important analytical targets. The most recently developed sensors target clinical analytes,[1] pesticides,[2] and heavy metals.[3] These sensors all utilized some variation of a poly(acrylamide) (pAMD) hydrogel, which was the first hydrogel reported for the synthesis of PCCA materials.[4] We will present research here on the development of new hydrogel systems which effectively embed the crystalline colloidal array. We will also present how these new PCCA materials can be used to develop sensors.

The primary focus of this dissertation is the development of two hydrogel materials, poly(hydroxyethyl acrylate) (pHEA) and poly(vinyl alcohol) (PVA). The

impetus for the development of both hydrogels was to create a point-of-care sensor for the determination of ammonia in bodily fluids. A diagnostic tool for monitoring hyperammonemia in bodily fluids could assist the treatment of patients afflicted with malfunctioning livers, urea cycle disorders, fatty acid oxidation defects, or organic acidaemias. The ammonia sensor could also be used as the integral component of an amino acid sensor. Utilizing a deaminase enzyme, a sensor for a specific amino acid could be developed which generates and then detects ammonia. Therefore, coupled to an enzymatic step, the ammonia sensor would be an amino acid sensor. Initially, our goal was to simply develop ammonia and amino acid sensors utilizing the pAMD hydrogel system, which had been successful for many other analytes. However, we found that the pAMD hydrogel was not compatible with our sensing mechanism. We will present here a pHEA hydrogel composition which enabled the development an ammonia sensor. We also used this pHEA hydrogel for the development of an organophosphorus sensor, demonstrating its general applicability.

While exploring alternative hydrogels to pAMD, we discovered a new class of CCA materials with a hydrogel comprised of physical cross-links formed through the thermo-reversible gelation. Our new mechanism for solidifying CCA has many advantages over photo-polymerization, the most significant of which are its reversibility and simplicity. These hydrogel materials were characterized in terms of their homogeneity and reversibility to ensure that the material had optical properties similar to the existing pAMD PCCA materials. We also incorporated covalent cross-links within these PVA PCCA, creating a thermally robust material. By attaching titratable groups to

the PVA backbone, we demonstrated that the physically cross-linked hydrogel would undergo volume phase transitions similar to those exhibited by photo-polymerized hydrogels, therefore establishing its potential for use as a sensor material.

References

1. Ben-Moshe M.; Alexeev V.L.; Asher S.A. Anal. Chem. 2006, 78 (14), 5149-5157.

2. Walker, J.P., Asher, S.A. Anal. Chem. 2005, 77, 1596-1600.

3. Asher, S.A.; Alexeev, V.L.; Goponenko, A.V.; Sharma, A.C.; Lednev, I.K.; Wilcox, C.S.; and Finegold, D.N. J. Am. Chem. Soc. 2003, 125, 3322-3329

4. Holtz, J. H., Asher, S. A., Nature 1997, 389, 829.

CHAPTER 2: Introduction to PCCA Sensing Materials

2.1 The Crystalline Colloidal Array (CCA)

Highly-charged, monodisperse colloidal particles will self-assemble into a periodic three-dimensional structure. Electrostatic repulsion between the highly-charged surface-groups is responsible for the self-assembly. Face-centered cubic (fcc) or body-centered cubic (bcc) lattices **(Figure 1)** form as the system finds a well-defined minimum energy state.[1,2] In the minimum energy state, identical electrostatic repulsions occur between all particles causing the distances between particles to become uniform **(Figure 2).**

fcc   bcc
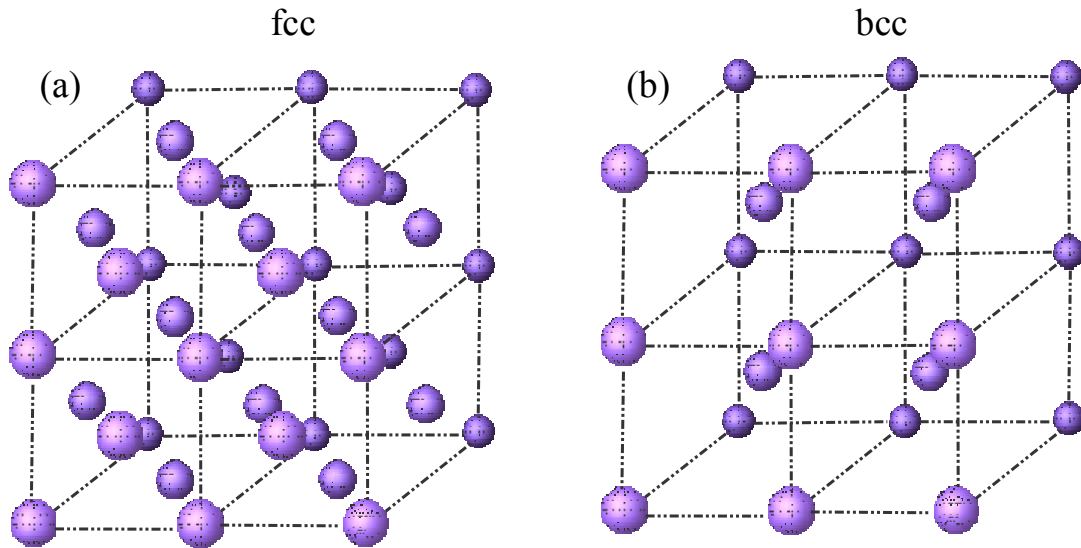
Figure 1: The (a) fcc and (b) bcc crystal lattice form when the particles self-assemble into an array. The concentration of ionic species and the particle density determines which structure will assemble.[1,2]

Colloidal particles organized into a crystalline structure are collectively called a crystalline colloidal array (CCA).[3] Electrostatic repulsive and van der Waals attractive forces combined result in a potential energy of interaction between particles. Dejaurin, Landau, Verwey, and Overbeek (DVLO) theory has been widely used to describe the repulsion between particles and is represented in the equations in **Figure 2**.[4]

(a)

Potential Energy of Interaction

charge

dielectric constant

sphere radius

$$U(r) = \frac{Z^2 e^2}{\varepsilon} \left[\frac{e^{\kappa a}}{1 + \kappa a} \right]^2 \frac{e^{-\kappa r}}{r}$$

(b)

Debye Layer Thickness

dissociated ions

Boltzmann's constant

ionic impurities

$$\kappa^2 = \frac{4\pi e^2}{\varepsilon k_B T} \left(n_p Z + n_i \right)$$

(c)
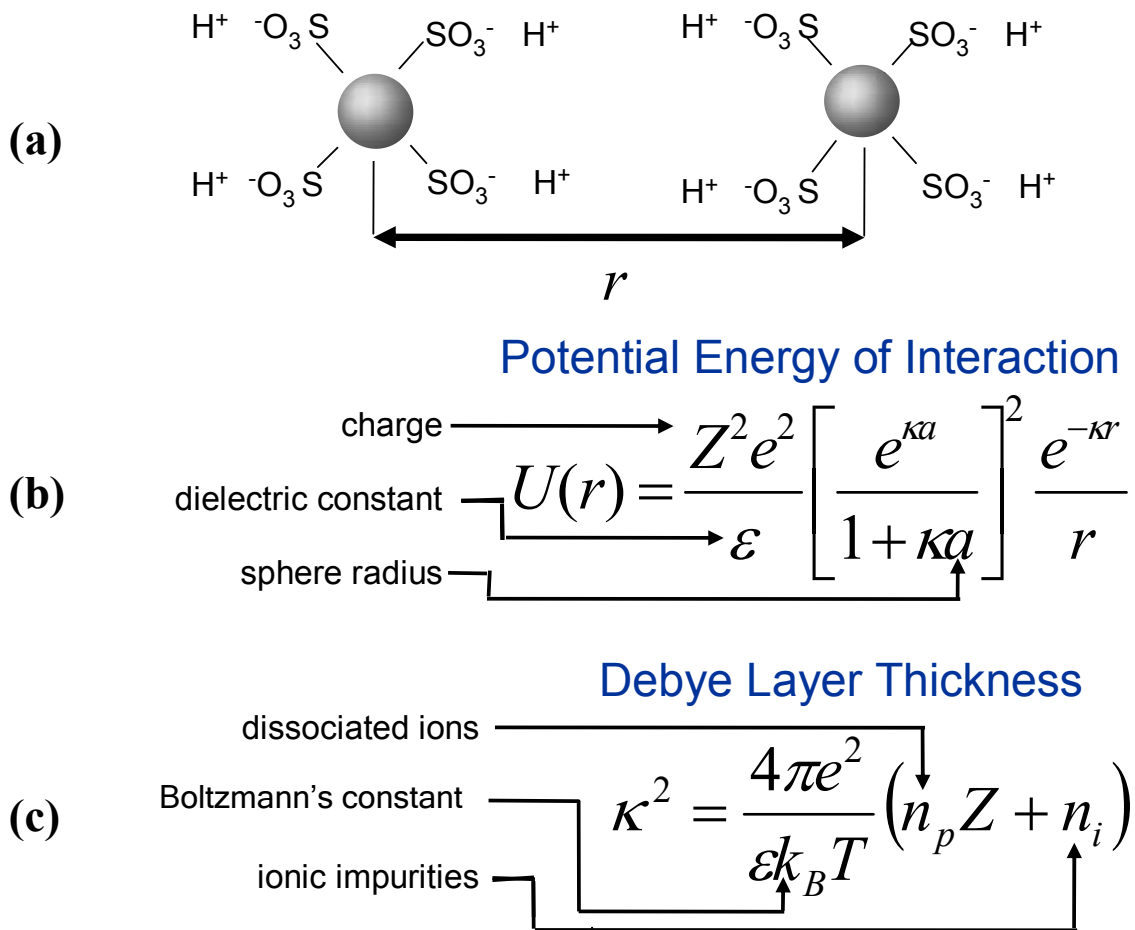
Figure 2: (a) Sulfonate groups provide surface charge to particles separated by a distance *r*. (b) The equation for potential energy of interaction is a function of the distance between particles. (c) The equation for Debye layer thickness relates ionic impurities to the potential energy of interaction.

As the distance between particles decreases, the electrostatic repulsion and the van der Waals attraction both become stronger, but the van der Waals attraction increases more dramatically and at small distances the particles will irreversibly aggregate. The addition of ionic species to a particle suspension decreases the Debye-layer thickness and weakens the electrostatic repulsion between particles. Colloidal particles exhibit aggregation at high ionic strengths but self-assemble into CCAs at low ionic strengths;[5,6,7] therefore, exhaustively de-ionizing a solution of monodisperse colloidal particles through dialysis and ion exchange resin causes them to form CCAs.[8,9,10,11]

CCAs are noted for their brilliant opalescence as they diffract ultra-violet, visible, or infra-red light depending on their crystal lattice spacing.[12] This diffraction is analogous to the more familiar diffraction exhibited by atomic crystals in the x-ray region of the electromagnetic spectrum.[13] The diffraction from the periodic structure follows Bragg's Law **(Equation 1)**, where m is the order of diffraction, λ is the diffracted wavelength, n is the refractive index, d is the lattice spacing and θ is the Bragg glancing angle**.**

$$m\lambda = 2nd \sin \theta \qquad \textbf{Equation 1}$$

CCAs have many potential applications due to their unique optical properties; however, the development and application of CCA materials is complicated by the particles' susceptibility to disorder which can be caused by any of the following: impact, freezing,

evaporation or ionic impurities. The instability of CCA solutions can be overcome by polymerizing a mesh-like network of polymers around the array, effectively "locking" the particles into position.[14,15,16,17]

2.2 Synthesis and Characterization of Nanoparticles

The use of emulsion polymerization to produce monodisperse particles was discovered by Alfrey et al.[18] at Dow Corning in the 1950's. Since its inception, the ability to produce a wide range of monodisperse particles with unique size, shape, and chemical properties has made emulsion polymerization a very important process in modern science and technology. Hiltner and Krieger were the first to notice that solutions of these monodisperse particles would Bragg diffract light when ionic impurities were removed.

Although any monodisperse particles having high surface charge will form an array in low ionic strength solutions, polystyrene colloidal particles are most frequently used. Cross-linked, highly charged, and highly monodisperse particles designed specifically for PCCAs were developed in the Asher laboratory and reported in 1999.[19,20] The particles' robust characteristics provide a CCA which can be used in the development of PCCA sensors based on various hydrogel systems. The optimal particle diameter for developing PCCA sensors is between 100 and 300 nm. Larger particles form PCCAs that diffract infrared light and smaller particles tend to scatter too weakly. Surface sulfonate groups are incorporated into the polymer through a vinyl-based sulfonate monomer. The sulfonate group is a strong acid with a pK_a of around 2. At

neutral pH, the electrostatic force between particles is strong due to the deprotonation of the sulfonate groups and the resulting surface charge.

To make 110 nm polystyrene spheres, a protocol developed by Reese is utilized with modifications primarily to the reactor apparatus.[19,20] A 500 ml split-head round-bottom reaction vessel (Ace Glass) is placed in an aluminum-cased heating mantle (Ace Glass) and connected to a temperature control unit (Ace Glass). 137 ml of nanopure H_2O and 0.172 g of $NaHCO_3$ buffer (Fisher) are mixed in the flask and purged with nitrogen for approximately 30 minutes. A mass of 18.5 g of MA-80 surfactant (Cytec) (10% solution with water w/w) is added. After 10 minutes, the nitrogen purge is removed, and the surface of the solution is blanketed with nitrogen. Styrene (GFS) and divinylbenzene (DVB, Aldrich) are mixed in a 125 ml Erlenmeyer flask and purged with nitrogen for 20 minutes. The reaction vessel is then heated to 50 ^{o}C and stirred at 125 RPM. Once the solution reaches 50 ^{o}C, the stirring is increased to 350 RPM, and the styrene/DVB mixture is introduced to the solution in a single shot. After waiting 5 minutes, 2.9 g of COPS-1 (Rhone-Poulenc) is added. Upon addition of COPS-1, the reaction is heated to 70 ^{o}C. Once the temperature becomes stable at 70 ^{o}C, 0.75 g of the initiator, ammonium persulfate ($N_2H_8S_2O_8$, Aldrich) is added using a 5 ml nanopure water wash. The polymerization is allowed to proceed for 3 hours after which the solution is cooled to room temperature and filtered through a nylon membrane (Small Parts, Inc.) with 35 μm mesh openings to remove clumps. The colloid is then dialyzed against nanopure water using 2,000,000 MWCO PVDF dialysis tubing (Spectrum Laboratories) for 6 days,

changing water twice daily. AG 501-X8 mixed-bed ion-exchange resin (Bio-Rad) is then

added and mixed for 1 hour by rolling end-over-end.

A typical reaction setup for the synthesis of polystyrene colloidal particles,

showing the arrangement of glassware and stirring unit, is shown in **Figure 3**.
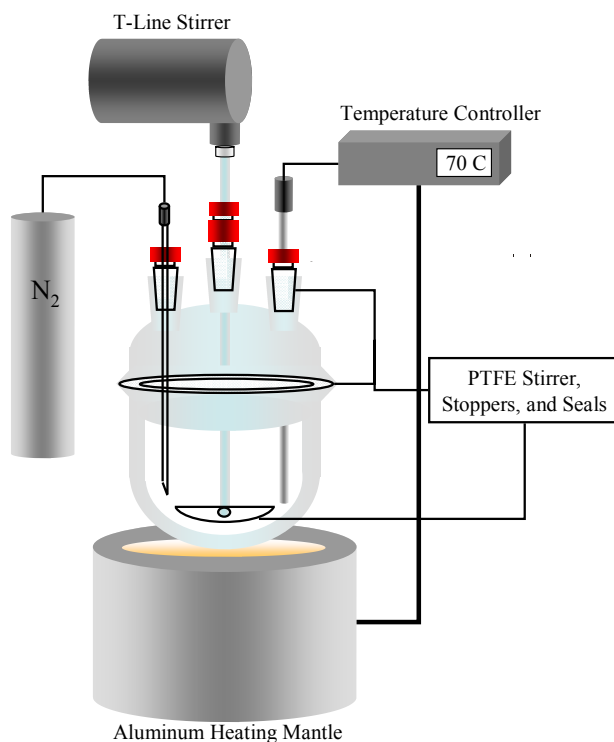
Figure 3: Apparatus for the synthesis of monodisperse colloidal particles through emulsion polymerization.

The cleaned colloidal particle suspension is a pale-blue liquid which diffracts

light in the UV region. Dilution of the suspension with water results in increased lattice

spacing of the particle suspension. This increase in lattice spacing results in a red-shift of

the diffraction. The suspension can be adjusted to any desired diffraction wavelength by

adding the appropriate quantity of water. **Figure 4** displays three colloidal solutions

which diffract different wavelengths of light because they have been diluted to different concentrations.
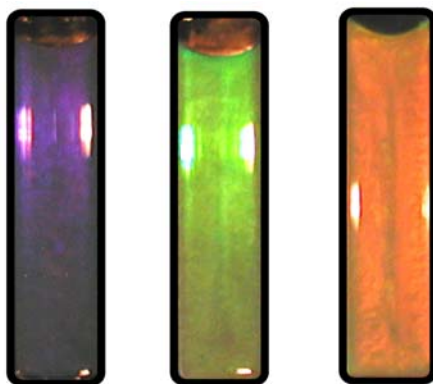
Figure 4: Colloidal suspensions diluted to three different concentrations resulting in different lattice spacing for the CCA. The difference in lattice spacing is apparent in the distinct colors. The violet CCA is the most concentrated and the orange is the least. *Image courtesy of Dr. Anjal Sharma.*

The primary analytical technique we use for particle characterization is dynamic light scattering (DLS) performed on a Zeta-Plus Particle Sizer (Brookhaven Instruments Corporation). While dynamic light scattering is quite accurate at establishing the particle size, the standard deviation of the particle diameter is best determined by transmission electron microscopy (TEM). Light scattering should not be used to determine the standard deviation of the particle size distribution because it is highly susceptible to agglomerates and "dust." Since the larger particles scatter more efficiently, even trace amounts can interfere with the autocorrelation function as it relates to the distribution of the particle population. The average particle is number weighted average and unaffected by a small number of highly scattering objects. The instrument manufacturer has integrated a software-based "dust filter" to reject data attributable to highly scattering objects. The TEM image **(Figure 5)** of the particles illustrates their high degree of

monodispersity. The particle size displayed here was determined to be 110 nm through DLS and 100 nm through TEM with a relative standard deviation of 5%. The deviation between the diameter reported through TEM and DLS is expected as the two techniques measure different properties of the colloidal particles. DLS determines the effective hydrodynamic radius of the particle which includes the shell of tightly associated water molecules and ions. The TEM measures the particle when dry. Although the particles are cross-linked, they tend to be slightly swollen in water due to the incorporation of the strong acid groups. Both of these would result in the particle size being measured by DLS to be slightly larger than the size measured by TEM.
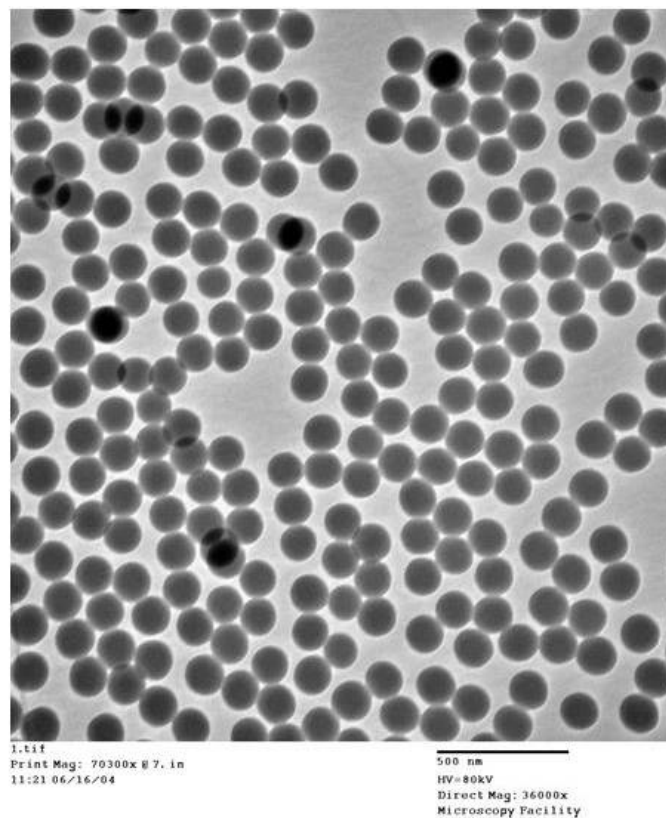
Figure 5: Representative TEM image of colloidal particles which self-assemble to form a CCA. Average size is 100 nm with a coefficient of variation of 5%.

2.3 The Polymerized Crystalline Colloidal Array (PCCA)

Formation of a cross-linked hydrogel in the solution surrounding the particles **(Figure 6)** results in the CCA being embedded within a hydrogel film.
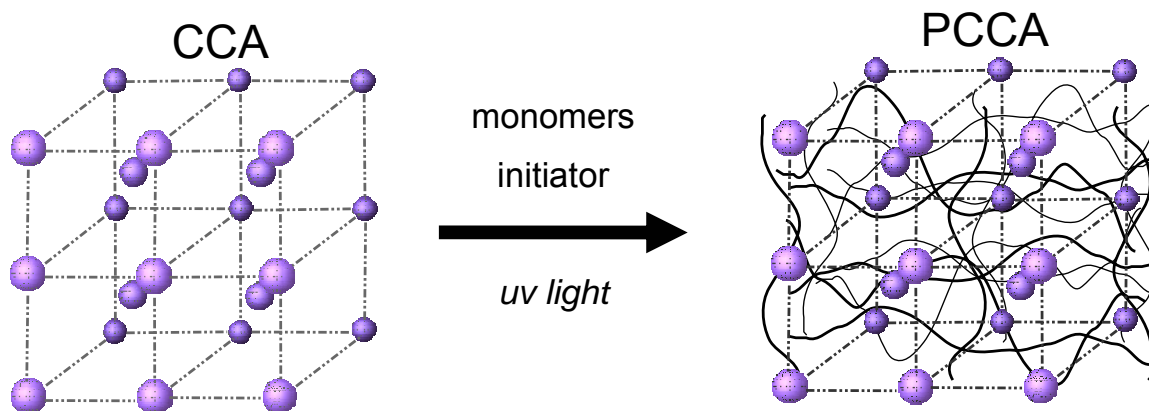
Figure 6: The addition of monomers and initiator to the CCA allow for the polymerization of a cross-linked hydrogel in the solution surrounding the particles, creating a PCCA.

Once the CCA is embedded within the polymer film it is called a polymerized CCA (PCCA). The CCA is stabilized through this process such that the robust hydrogel material can be utilized for more advanced applications.[21,22] In addition to the stability that the polymer hydrogel provides for the CCA, the polymer also provides a means of modifying the chemical functionality.[23,24]

Useful chemical functionality can be incorporated into the PCCA by selecting the appropriate monomers. Our lab routinely utilizes acrylamide and bis-acrylamide monomer compositions because of the many post-polymerization modifications which enable the modification of the chemical functionality. The acrylamide provides a site for chemical modification and the bis-acrylamide cross-links the hydrogel. A simple

chemical modification frequently used is the hydrolysis of the amides to form carboxylic acids. The carboxylic acids can then be coupled to molecules containing an amine through carbodiimide chemistries. The vast numbers of chemical modifications which the acrylamide enable are extensively described in the book by Hermanson.[25]

The PCCA can be transformed into a sensor by incorporating a molecular recognition agent onto the hydrogel backbone. The interaction between the molecular recognition agent and the analyte molecule induces an osmotic pressure change in the hydrogel. The osmotic pressure change results in a volume change and the concentration of analyte can be determined by monitoring the volume change. The change in volume results in the distance between the diffracting planes of colloidal particles embedded in the hydrogel to change. As the distance between the planes change, the wavelength of diffracted light shifts. Shifts in the diffracted wavelength are apparent because the observed color changes. The term intelligent PCCA or IPCCA has been used to describe this type of material because the concentration or presence of analyte can be determined through the shift in the diffraction wavelength.[23,24]

2.4 Monomers used for PCCA Synthesis

Colloidal particles in a CCA repel each other over macroscopic distances that are several times the diameter of the particles, up to 1 μm. Ionic impurities are capable of disordering the lattice,[26] which will result in a reduction of the intensity and eventual loss of Bragg diffraction. Polymerizing the CCA into a hydrogel network can prevent the disordering by "locking" the particles into an array.[7,11] The array ordering and the strong

diffraction is little affected by high ionic strengths and organic solvents that do not degrade the hydrogel. **Figure 7** shows the appearance of a CCA before polymerization and the same PCCA after polymerization.
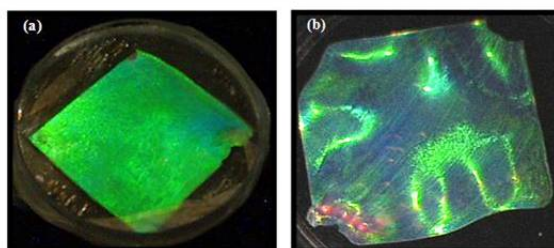
Figure 7: (a) A photograph of a CCA between two quartz plates contained by a parafilm spacer with a thickness of 125 μm. (b) After polymerization, the PCCA is structurally robust and still diffracts strongly despite having removed the quartz plates. Apparent inhomogenieties in the diffraction wavelength are the result of curves or waves in the PCCA resulting from the hydrogels flexibility. Homogeneity of the wavelength of maximum diffraction is generally within 10 nm over the entire hydrogel. *Image courtesy of Dr. Chad Reese.*

The following is the procedure for synthesizing a typical PCCA. Total volume is maintained at ~ 2 ml. Acrylamide (0.10 g, 1.4 mmol, Fluka), N,N'-methylenebisacrylamide (2.5 mg, 16.2 μmol, Fluka), colloid suspension (2.0 g, 5-10% w/w dispersion, polystyrene latex spheres, ~110 nm diameter, 26 in Nanopure water, AG501-X8 (D) ion exchange resin (~0.1 g, 20-50 mesh, mixed bed, Bio-Rad), and 10% DEAP (7.7 μL, 3.84 μmol; Diethoxyacetophenone; Aldrich) in DMSO (Fisher) are mixed in a 2-dram vial. Two quartz discs (Esco Products, Inc.) are clamped together with a 125 μm parafilm spacer (Pechiney Plastic) between them. The mixture is injected into the cavity between the quartz discs, and they are placed under a mercury arc lamp (Blak-Ray Model B-100A), which has a filter that allows only transmission of 366 nm UV light **(Figure 8)**. The mixture is left to polymerize under UV light for 2 hours. After two hours, the quartz cell is separated in nanopure water, and the PCCA is allowed to equilibrate.
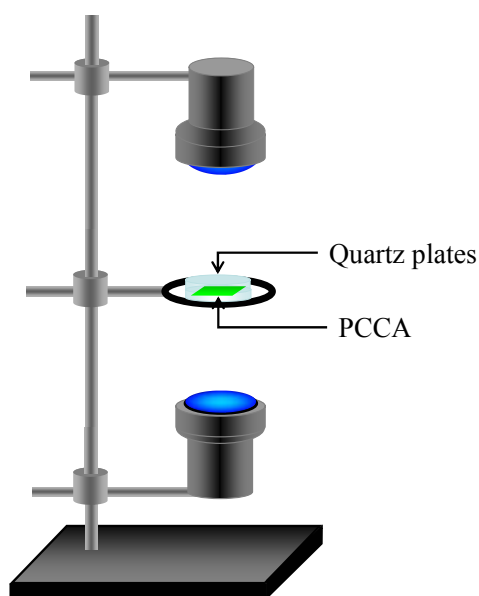
Figure 8: Apparatus for the synthesis of PCCA through UV polymerization. Two lights and careful calibration of radiative flux assure the reaction rate is equivalent on the top and bottom of the PCCA.

2.5 Thermodynamics of Hydrogels

Hydrogels have become an increasingly familiar material to most people through the widespread use of soft contact lenses and other hydrogel-based consumer products. Hydrogels are defined as materials in which cross-linked polymer networks are filled with an aqueous medium. Typical hydrogels have polymer chains which would ordinarily dissolve in an aqueous medium. However, linking together separate polymer chains into a single network results in a robust polymeric material which cannot dissolve but only swell in water. The volume of a hydrogel is dependent on three parameters which describe the total free energy of the system, as elucidated by Flory-Huggins theory[27] and Tanaka.[29] The free energy of the system (ΔG_T) is related to the osmotic

pressure and the volume of the hydrogel through the relationships seen in **Equation 2** and **Figure 9.**

$$\partial \Delta G_T / \partial V = \Pi_T = \partial / \partial V \, [\Delta G_I + \Delta G_E + \Delta G_M] = \Pi_I + \Pi_E + \Pi_M = 0 \qquad \textbf{Equation 2}$$

The volume-derivative of the total free energy (ΔG_T) is the total osmotic pressure (Π_T). The total osmotic pressure is the volume-derivative of the sum of the free-energies (where ΔG_I is the electrostatic free-energy, ΔG_E is the elastic free-energy, and ΔG_M is the free-energy of mixing). The osmotic pressures associated with those free-energies are Π_I, Π_E, and Π_M respectively. Equation 2 predicts how the hydrogel network volume will respond to the chemical environment as it approaches equilibrium. Free-energy changes result in osmotic pressure changes, and osmotic pressure changes result in volume changes (swelling or shrinking).

$$\Delta G_{tot} = \Delta G_{ion} + \Delta G_{elas} + \Delta G_{mix}$$

$$\Pi_{tot} = \frac{\partial \Delta G_{tot}}{\partial \Delta V} = \Pi_{mix} + \Pi_{ion} + \Pi_{elas}$$

$$\Pi_{mix} = \frac{-RT}{V_s} \left[\ln\left(1 - \frac{V_0}{V}\right) + \frac{V_0}{V} + \chi\left(\frac{V_0}{V}\right)^2 \right]$$

$$\Pi_{ion} = \frac{1}{N_{Av}\, k_B\, T} \left(\frac{i\, c_p}{z_-} - v_i\, (c_s^* - c_s) \right)$$

$$\Pi_{elas} = \frac{-RT \cdot n_{cr}}{V_0\, N_{Av}} \left[\left(\frac{V_0}{V}\right)^{1/3} - \frac{1}{2}\frac{V_0}{V} \right]$$

Figure 9: Sensors, to date, have responded to analyte through changes to χ, the Flory-Huggins interaction parameter, $i*c_p$, the charge density on the hydrogel, or n_{cr}, the number of cross-links. Other parameters: R is the gas constant, k_b is the Boltzmann constant, N_{Av} is Avogadro number, T is the absolute temperature, V_0 is the volume of the hydrogel in pure water, V is the volume of the hydrogel in the presence of analyte, V_s is the molar volume of the solvent, z_- is the valence of the counter-ion, c_s^* is the concentration of mobile ions in the external solution bath, and c_s is the mobile ion concentration in the hydrogel.

The mechanism of response utilized for a particular sensor will be dependent on the nature of the analyte for which the sensor will be designed. **Figure 9** relates the free energy of mixing to the sum of the osmotic pressures and shows the parameters which can be influenced in order to actuate a hydrogel volume change.

2.5.1 Sensors Utilizing ΔG_M

The free energy of mixing of the hydrogel contains an entropic term which relates to the hydrogel's tendency towards establishing equivalent concentrations of ions in the hydrogel and ions in solution (analogous to the entropy increase associated with homogeneous distribution of a solute in a solvent) and an enthalpic component stemming from the interaction of the polymer chains with the solvent (analogous to the extent of solubility of a solute in a solvent). Instead of describing the solubility in terms of a k_{sp}, as would be done for a salt, the interaction of a polymer with a solvent is defined by the Flory-Huggins interaction parameter χ.   This empirical term is specific to the composition of the polymer and changes according to the solvent. Changes to the polymer through the attachment of an analyte or changes in conformation of bound groups can cause changes in the solubility of the hydrogel. Small χ values are associated with strong solvation of the polymer by the solvent. A hydrogel in a solvent with a small χ value will be more swollen than the same hydrogel in a solvent for which it has a larger χ parameter.

An example of a responsive PCCA based on ΔG_M is the temperature sensing intelligent PCCA. This sensor was made by incorporating a CCA into a poly(N-isopropyl acrylamide) (NIPAM) hydrogel. This sensor utilizes the free-energy of mixing of the hydrogel with pure water. NIPAM has a volume phase transition that is driven by the temperature dependent free energy entropic term. At low temperatures, the hydrophobic hydrogel forces the surrounding water into a highly ordered structure. As the temperature increases the entropic penalty for this order becomes too great and the hydrogel minimizes its surface area to minimize the total free energy. The hydrogel shrinks as the temperature increases. The sensor was made such that it diffracted at 700 nm (appeared red) when at 11 ^{o}C and diffracted at 450 nm (appeared blue) when at 35 ^{o}C. Another sensor which relies upon the free energy of mixing to cause a hydrogel volume transition is the optical switch developed by Kamenjicki et al.[28] An azobenzene derivative was attached to the hydrogel backbone in a position in which it was a cross-linker. When the azobenzene isomerizes from the *trans*-form to the *cis*-form, it causes a change in the solubility of the hydrogel. The *cis*-form is more soluble, so the volume of the hydrogel increases during the isomerization from *trans*- to *cis*-. This results in a red-shift in the diffraction. The transition from *trans*- to *cis*- occurs when the azobenzene is subjected to UV light, while subjecting the azobenzene to visible light results in the *trans*-isomer. The sensor appears blue when in visible light, but becomes red with exposure to UV light.

2.5.2 Sensors Utilizing ΔG_I

The electrostatic free energy also affects the volume of the hydrogel and can be used to make a sensor. When charged groups are bound to the hydrogel, for example due dissociation of strong acid groups covalently bound to the hydrogel, the local concentration of ionic charges inside the hydrogel can be greater than the concentration outside the gel. Not only do the bound charges repel each other due to the electrostatic interaction potential, but the associated counter-ions also affect the volume of the hydrogel. The counter-ions associated with the covalently bound charge groups change the chemical potential of water inside the hydrogel. The resulting electrochemical gradient is called a Donnan potential. In low ionic strength solutions, the Donnan potential causes water to flow either in or out of the hydrogel. The extent of volume change is proportional to the number of bound charges.[29]

There have been several sensors developed which rely on the change in ionic free energy (ΔG_I) to actuate a visible color change. One such photonic crystal chemical sensor responds to pH and ionic strength.[30] This sensor was synthesized by hydrolyzing the poly(acrylamide) hydrogel resulting in acrylamide groups being converted into carboxylate groups. These carboxylate groups were found to have a pK_a of 5.2. With a pK_a of 5.2, the carboxylic acid groups are protonated and uncharged at low pH values and the carboxylate groups are deprotonated and charged at high pH values. At pH = 9.0, the carboxylate groups are completely ionized and further increases in pH no longer resulted in the hydrogel swelling. In fact, addition of base to the solution increases the ionic strength and causes the gel to shrink. As the ionic strength is increased, the Donnan

potential is reduced and the hydrogel shrinks. From neutral pH, the hydrogel shrinks (resulting in a blue-shift of the diffraction) as the pH is reduced. The shrinking is due to the acid groups being protonated. As the groups are protonated, the Donnan potential associated with the counter-ions decreases.

Another example of a PCCA sensor which utilizes the charge-based sensing motif is a low-ionic strength carbohydrate sensor developed by Asher et al.[31] Amino-phenylboronic acid is attached to PCCA and serves as the molecular recognition agent towards vicinal *cis*- diols like those found in carbohydrates. The phenylboronic acids bind carbohydrate molecules which lower the pK_a of the boronate groups. Because of the drop in the pK_a, the boronic acid groups become boronate anions. The ionic groups attached to the hydrogel actuate an osmotic pressure change and the diffraction shifts in response to the concentration of glucose present in solution. As with the pH and ionic strength sensor, the Donnan potential is attenuated as the ionic strength of the solution increases. Therefore the sensor becomes much less sensitive at concentrations of salt greater than 10 mM. The ionic response of hydrogels is only useful for sensing in solutions with low ionic strength, and this precludes its use in biological samples.

For biological analytes, the inability to operate at physiological ionic strengths severely limits the application of a sensor based on ionic free energy. However, when not working in high ionic strength media, it is possible to take advantage of the extraordinary sensitivity of this sensing mechanism to detect molecules at very low concentrations. One such sensor, developed by Walker and Asher,[32] is capable of

detecting concentrations as low as 4.26 fM of parathion, an organophosphorus pesticide. In this sensor the enzyme acetylcholinesterase binds the organophosphorus compound irreversibly and creates a volume change by generating an anionic phonsphonyl species. The charged species generates a Donnan potential which results in the hydrogel swelling (observed as a diffraction red-shift) in response to the organophosphorus molecule.

2.5.3 Sensors Utilizing ΔG_{elas}

The volume of the hydrogel is impacted by the number of cross-links holding the hydrogel together. The cross-links provide a restoring force and constrain the hydrogel volume.

Sensors utilizing the formation of cross-links to cause a volume phase transition and the corresponding diffraction wavelength shift are particularly interesting due to their robust response irregardless of the ionic strength of the testing solution. Several sensors have been designed containing molecular recognition agents which bind analytes to form additional cross-links within the hydrogel. The elastic restoring force of the hydrogel is increased with the new cross-link and it contracts, blue-shifting the wavelength of diffracted light.

An example of a simple PCCA sensor which relies upon the free energy of elasticity is the aqueous metal cation sensor developed by Asher et.al.[33] 8-hydroxyquinoline group are attached to the hydrogel via EDC-coupling. When the stoichiometric ratio of the cation to the ligand is 1:2 or less, the cations form a

21

bisliganded complex with two 8-hydroxyquinoline groups. This bisliganded complex is effectively a covalent cross-link since the binding constant for the complex is large (Cu^{2+}, 10^{22} M^{-2}). As the cross-links form, the diffraction blue shifts. At cation to ligand ratios greater than 1:2, the cations break the bisliganded complex in favor of the monoliganded complexes. As the cross-links are broken, the PCCA diffraction red-shifts, and the gel swells. The sensor can be made such that the concentration of analyte can be determined visually or by using a spectrophotometer.

The importance of glucose as a clinical analyte prompted Alexeev et al.[34] to improve the aforementioned photonic crystal carbohydrate sensor such that it could function in high ionic strength solutions typical of biological matrices. The improved glucose sensor uses the same poly(acrylamide) hydrogel with pendant phenylboronic acid groups, but also incorporates pendant poly(ethylene glycol) or 15-crown-5 groups into the hydrogel matrix. These functional groups are prepositioned such that glucose self-assembles them into a supramolecular complex which effectively increases the number of cross-links in the hyrdrogel. The concentration of glucose is then sensed by the hydrogel volume decrease that causes the diffraction wavelength to blue-shift.

References

1. Monovoukas, Y., Gast, A. P., *J. Colloid Interface Sci.* **1989, 128**, 533.

2. Hachisu, S.; Kobayashi, Y.; Kose, A. *J. Colloid Interface Sci.* **1973**, 42(2), 342-348.

3. Rundquist, P. A., Photinos, P., Jagannathan, S., Asher, S. A., *J. Chem. Phys.*, **1989, 91**, 4932.

4. Behrens, S.H.; Christl, D.I.; Emmerrzael, R.; Schurtenberger, P. Borkovec, M. *Langmuir* **2000**, 16, 2566-2575.

5. Hiltner, P. A., Papir, Y. S., Krieger, I. M., *J. Phys. Chem.* **1971, *75***, 1881.

6. Carlson, R. J., Asher, S. A., *Appl. Spec.* **1984, *38***, 297.

7. Asher, S. A., Holtz, J. H., Liu, L., Wu, Z., *J. Am. Chem. Soc.* **1994, *116***, 4997.

8. Liu, L., Li, P., Asher, S. A., *J. Am. Chem. Soc.* **1997, *119***, 2729.

9. Okubo, T., *Acc. Chem. Res.* **1988, *21***, 281.

10. Asher, S. A., Flaugh, P. L., Washinger, G., *Spectroscopy* **1986, *1***, 26.

11. Asher, S.A., U.S. Patents 4,627,689 (**1986**)., 4,632,517 (**1986**), 5,281,370 (**1994**), 5,452,123 (**1995**).

12. Hiltner, P. A., Krieger, I. M., *J. Phys. Chem.* **1969, *73***, 2386.

13. Krieger, I. M., O'Neill, F. M., *J. Am. Chem. Soc.* **1968, *90***, 3114.

14. Weissman, J. M., Sunkara, H. B., Tse, A. S., Asher, S.A., *Science* **1996, *274***, 959.

15. Pan, G., Sood, A. K., Asher, S.A., *J. Appl. Phys.* **1998, *84***, 83.

16. Pan, G., Tse, A. S., Kesavamoorthy, R., Asher, S. A., *J. Am. Chem. Soc.* **1998, *120***, 6518.

17. Ito, K., Nakamura, H., Ise, N., *J. Chem. Phys.* **1986, *85***, 6136.

18. Alfrey, T.Jr.; Bradford, E.B.; Vanderhoff, J.W.; *J. Opt. Soc. Am.* **1954** 44,603-609.

19. Reese, C.E. *Ph.D. Thesis*, **2003,** The University of Pittsburgh.

20. Reese, C.E., Guerrero, C.D., Weissman, J.M., Lee, K., Asher, S.A., *J. Coll. Int. Sci.* **2000**, *232*, 76.

21. Pan, G., Kesavamoorthy, R., Asher, S. A., *J. Am. Chem. Soc.* **1998,** *120,* 6525.

22. Pan, G., Kesavamoorthy, R., Asher, S. A., *Phys. Rev. Letters.* **1997,** 78, 3860.

23. Holtz, J. H., Asher, S. A., *Nature* **1997,** *389*, 829.

24. Holtz, J. H., Holtz, J. S. W., Munro, C., Asher, S. A., *Anal. Chem.* **1998,** *70*, 780.

25. Hermanson, G.T. *Bioconjugate Techniques.* **1996**, Academic Press, New York.

26. Hachisu, S., Kobayashi, Y., Kose, A., *J. Col. Int. Sci.* **1973, 42**, 342.

27. Flory, P.J. *Principles of Polymer Chemistry* : Cornell University Press; New York, **1953.**

28. Kamenjicki, M.; Lednev, I.K.; Mikhonin, A.; Kesavamoorthy, R.; Asher, S.A. *Adv. Funci. Mater.* **2003**, 13 (10) 774.

29. Tanaka, T.; Niccolini, C., Ed.in *Structure and Dynamics of Biopolymers*, Series E: Dordrecht, **1986**, pp. 237-257.

30. Lee, K.; Asher, S.A. *J. Am. Chem. Soc.* **2000**, *122*, 9534-9537.

31. Asher, S.A.; Alexeev, V. L.; Goponenko, A.V., Sharma, A.C.; Lednev, I.K.; Wilcox, C.S., Finegold, D.N. *J. Am. Chem. Soc.* **2003**, *125*, 3322-3329.

32. Walker, J.P.; Asher, S.A. *Anal. Chem.* **2005**, 77, 1596-1600.

33. Asher, S.A., Sharma, A.C., Goponenko, A.V., Ward, M.M. *Anal. Chem.* **2003,** *75*, 1676-1683.

34. Alexeev, V.L.; Sharma, A.C.; Gopenenko, A.V. Das, S.; Lednev, I.K.; Wilcox, C.S.; Finegold, D.N.; Asher, S.A. *Anal. Chem.* **2003**, 75 (10) 2316-2323.

CHAPTER 3: *Sensing Ammonia*

3.1 The Importance of Ammonia as a Clinical Analyte

Blood ammonia results from the metabolic breakdown of dietary protein, generated primarily in the liver, muscles, and kidneys.[1] It is derived specifically from the deamination of α-amino nitrogens of amino acids and is toxic when persistent at elevated levels. Hyperammonaemia, levels greater than 100 μM in neonates, or greater than 40 μM for all others, results primarily from one of four groups of clinical diagnoses: urea cycle disorders (UCDs), organic acidaemias (OAs), fatty acid oxidation defects (FAOs) or malfunctioning of the liver.[2,3] Hyperammonaemia results in damage to the central nervous system, including altering the transit of amino acids, water, and electrolytes across the neuronal membrane. Ammonia can also inhibit the generation of both excitatory and inhibitory postsynaptic potentials.[4,5] The symptoms of this condition in infants are irritability, lethargy, and vomiting within the first 24 hours after birth. Seizures, hypotonia (poor muscle tone), respiratory distress, coma and death can occur if undiagnosed. Children with moderate or mild enzyme deficiencies may not be symptomatic as infants, but their symptoms can develop to include hyperactive behavior, sometimes accompanied by screaming and self-injurious behavior, and refusal to eat meat or other high-protein foods. Symptoms may also include frequent vomiting in response to high-protein meals, lethargy, and delirium. As in infants, undiagnosed or untreated cases can result in coma and death. Adult symptoms of hyperammonemia include inappropriate behavior, clumsiness, drowsiness, memory loss, slurred speech, confusion, episodes of delirium, lethargy, and stroke-like symptoms. The onset of these adult symptoms is often

diagnosed by mental health professionals as the symptoms are more commonly associated with mental illnesses. Persistence of a hyperammonemic state causes irreversible damage to the brain resulting in mental retardation. The rarity of these diseases coupled with the diversity of symptoms often leads to misdiagnosis.

Treatment of urea cycle disorders consists of tightly restricting dietary protein intake and physically removing ammonia from blood through blood exchange transfusion and peritoneal dialysis. There are also new therapies available which supplement the missing urea cycle products (arginine or citrulline) and optimize ammonia levels through protein restriction with added essential amino acids. Excess ammonia concentrations can also be lowered by diverting ammonia to alternate pathways by prescribing benzoate to the patients. Frequent blood tests and hospitalizations are required to monitor and to control the disorder. Although hyperammonemia is generally caused by rare genetic diseases, the requisite frequency of testing places a high demand on both the clinical laboratories and the affected patients and their families.[6] Furthermore, the routine screening of blood ammonia levels will lower the frequency of misdiagnosis and potentially treat borderline patients before hyperammonemia causes retardation or other neurological damage.

Ammonia in the body is distributed between ammonia gas and ammonium ions according to the equilibrium:

$$NH_{3\,(gas)} + H^+ \leftrightarrow NH_4^+ \qquad \textbf{Equation 3}$$

Since the pK_a of ammonium is 8.9 at 37 ^{o}C, at physiological pH of 7.4, 97% is in the form of the ammonium ion and 3% is in the form of ammonia gas. Following convention, the term ammonia will be used to refer to the sum of the ammonia and the ammonium. The contribution of various organs and the local concentrations of ammonia throughout the body have been extensively reviewed by Huizenga et al. They report that while there are different concentrations of ammonia in venous and arterial blood the two are correlated such that capillary blood can be used to determine blood ammonia levels. Further complicating the determination of ammonia, drawn blood begins to generate ammonia through deamination in the red blood cells immediately after the draw. Blood from a healthy person can be stored at 4° C for an hour, but patients with compromised urea cycles must have their blood analyzed or treated within 15 minutes of the draw in order to obtain accurate results. This strict time frame and need for immediate testing presents significant obstacles for the accurate determination of ammonia.[7]

3.2 Current Technologies for the Determination of Ammonia

Currently, blood ammonia levels are typically determined utilizing an enzyme-based assay in the clinical laboratory. The enzyme glutamate dehydrogenase converts 2-oxoglutarate and ammonium to glutamate and water.[2,8,9,10] The UV absorbance at 340 nm is monitored as the NADH cofactor is converted to NAD^+ as seen in **Figure 10**.
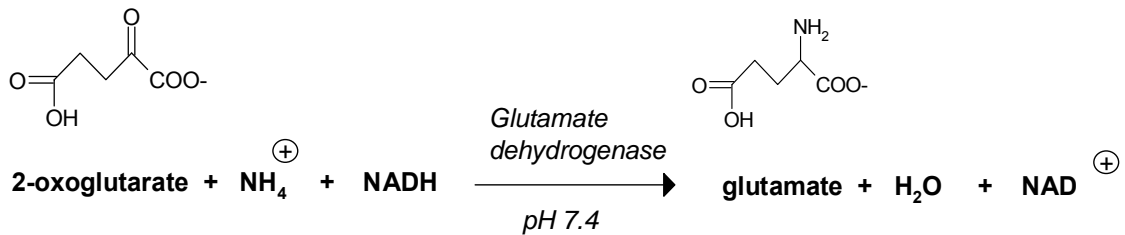
Figure 10: Glutamate dehydrogenase converts 2-oxoglutarate and ammonium to glutamate and water. The quantity of NH_4^+ is monitored by UV absorbance of NAD^+ at 340 nm.

There are numerous other technologies which have been developed to detect ammonia in biological fluids. Unlike the direct enzymatic method mentioned above, most of these processes involve two steps. The first step is separation of ammonia gas from the biological matrix and the second step is sequestration of the ammonia in a media such that the quantity can be determined. The means of separating ammonia from the blood include distillation, aeration, ion-exchange, microdiffusion, protein precipitation, dialysis, or Kjeldahl extraction.[11,12,13,14] There have been several methods based on the alkaline liberation of gaseous ammonia and transport through a gas-permeable membrane. The subsequent determination of the liberated ammonia is then accomplished through colorimetry, titration, ion-selective electrochemistry, fluorometry, coulometry, mass spectrometry, second-derivative spectrometry, optical waveguide spectroscopy, HPLC, and capillary isotachophoresis. [1,15]

There are also several technologies which have been developed which combine separation and determination into a single process. Two such devices have been developed which are designed to be point-of-care analyzers. An instrument developed by Careside, Inc. separates ammonia from the whole blood or plasma matrix by utilizing gas

permeable thin films and alkaline liberation of ammonia. After passage through the gas permeable membrane, the ammonia is dissolved in an acidic solution where the ammonium interacts with bromophenol blue changing the color from yellow to blue green.[16] Arkray, Inc., another manufacturer of commercially available point-of-care blood ammonia diagnostic kits uses microdiffusion of ammonia around a spacer and subsequent determination based on bromocresol green changing color.[17] This technology has been referred to in the literature as the Blood Ammonia Checker II (BAC II).[18,19] This instrument is currently being used abroad but is not available in the United States.

3.3 The Berthelot or Indophenol Reaction

A colorimetric approach to sensing ammonia which has been extensively utilized is the Berthelot, or indophenol, reaction. The reaction is named for the French chemist Marcellin Berthelot because he discovered and described the colorimetric reaction in 1859.[20] In this reaction, ammonia (NH_3) and hypochlorite (OCl^-) form monochloramine. The monochloramine then reacts with two phenols to form indophenol as seen in **Figure 11.** The concentration of ammonia is determined by monitoring the absorbance of the dye molecule at ~ 640 nm. This reaction has been studied extensively in solution for various absorbing phenolic species, hypohalite sources, catalysts, and applications. An exhaustive review of the reaction was presented by Searle in 1984.[21] Searle presented three different possible mechanisms; however, the mechanism described here and in **Figure 11** is the most commonly accepted.[22]
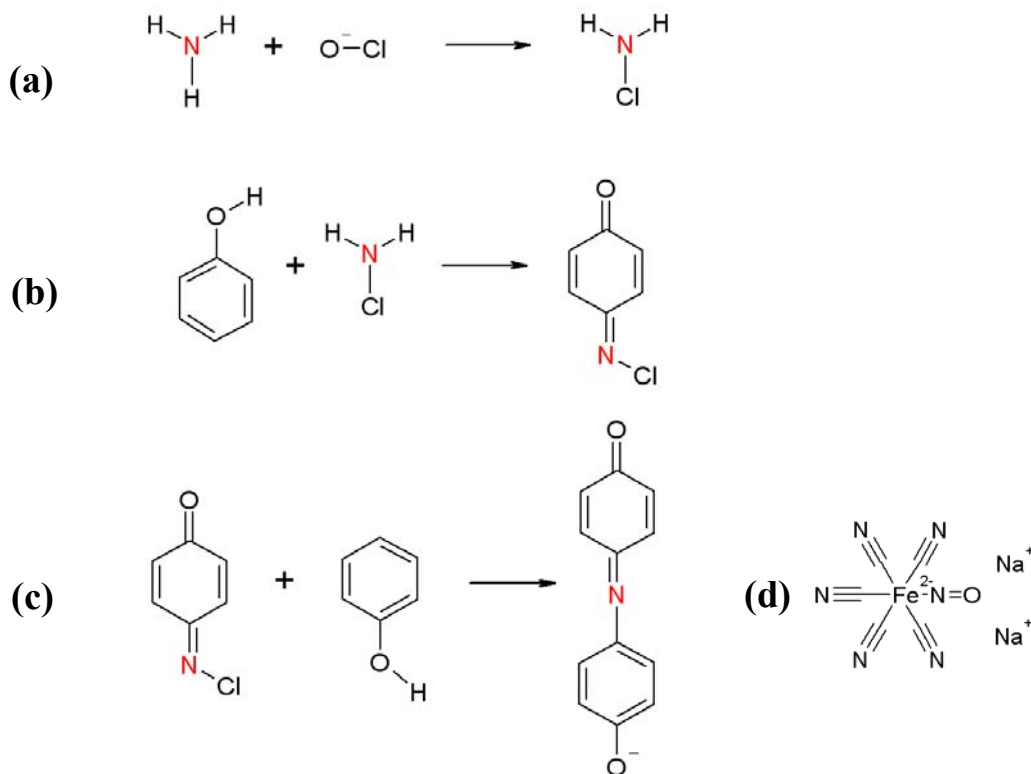
Figure 11: The proposed reaction mechanism for the Berthelot reaction consists of three steps: (a) ammonia reacts with hypochlorite to form monochloramine at basic pH, (b) monochloramine reacts with a phenol to form benzoquinone chlorimine, (c) benzoquinone chlorimine reacts with a second phenol to form an indophenol. (d) Sodium nitroferricyanide (III) dihydrate is a coupling reagent which increases the kinetics of steps (b).

The first step in the Berthelot reaction is the very fast ($k = 3.2 \times 10^6$ [M*sec]$^{-1}$) reaction between hypochlorite and ammonia. The ammonia has a reaction order of 1 in this reaction and the catalyst NP does not affect the rate of this step. The second step is the reaction between monochloramine and phenol to yield a benzoquinone chlorimine. This step of the reaction is rate limiting. The rate of this step is also strongly influenced by the presence of NP. The final step of the reaction is between the chlorimine and phenol. This step has a rate constant of $k = 3.2 \times 10^6$ [M*sec]$^{-1}$. It is significantly faster than the hydrolysis of the chlorimine which is a competing reaction. However, the product of the

chlorimine hydrolysis also reacts to form the indophenol. The reaction has been optimized to work in a number of different applications which has lead to numerous versions of the "ideal" reaction conditions.

3.3.1 Reagents and Concentrations

There has been extensive use of different phenols and hypohalite sources for the determination of ammonia through the Berthelot reaction. Among the most frequently used are phenols with substitutions which lead to the activation of the position *para*- to the hydroxyl. Thymol, salicylic acid, cresol, and *o*-phenylphenol have all been shown to be successful using appropriate conditions. Salts of salicylic acid have found widespread use as non-carcinogenic alternatives to phenol.[23] The concentrations which have led to the best analytical determinations of ammonia have varied greatly. Ideally the concentration of ammonia to be determined would dictate the concentration of the phenolic compound to be used. Literature sources indicate that there is a steady increase in rate as the concentration of phenol increases up to a plateau at which additional phenol does not contribute and can actually diminish response. Molar excesses up to 3 orders of magnitude have been described in the literature as the optimal concentration in respect to the ammonia. The optimal concentration of various substituted phenols may differ significantly from that of phenol.

The hypohalite sources which are used most frequently are sodium hypochlorite and hypobromite. Other molecules which hydrolyze to form hypochlorite have also been used effectively. One such compound, sodium dichloroisocyanurate, has been used

extensively in specific applications where interferences are not present.[24] It was found by Seely et al.[25] that the sodium dichloroisocyanurate reacts with proteins and amines resulting in a negative interference leading to the ammonia concentration being reported erroneously low. The ideal concentration of hypochlorite is also dependent on the concentration of ammonia to be detected. A two to thirty-fold molar excess in respect to the ammonia has been shown to be optimal in different applications.[21]

Although NP has most prevalently been used as the catalyst for this reaction, several other alternatives have also been utilized. Originally manganese (II), iron, and chromium ions were used to catalyze the reaction and are still used in some applications.[26] Small amounts of acetone were also found to increase the rate of the reaction. These catalysts were all inferior to NP, however, and it is used almost exclusively today. The actual mechanism by which NP catalyzes the reaction is through the stabilization of the monochlorimine facilitating the reaction with the phenol to form benzoquinone chlorimine. However, there is some debate about the nature of the actual chemical species that is stabilizing the monochlorimine. While NP has five cyano-groups and one nitrito- group, it has been suggested that the active molecule is aquapentacyanoferrate. Since NP is actually consumed during the reaction, it has been suggested that it is more appropriately called a coupling reagent as opposed to a catalyst.

3.3.2 The Effect of pH

The pH of the solution is critical to the Berthelot reaction. Both the ammonia and the hypochlorite are in acid-base equilibrium before they react, as seen in **Equation 4 and 5**.

$$HOCl + H_2O \leftrightarrow OCl^- + H_3O^+ \qquad \textbf{Equation 4}$$

$$NH_3 + H_2O \leftrightarrow NH_4^+ + OH^- \qquad \textbf{Equation 5}$$

In a solution buffered to pH = 9, the equilibrium lie such that ammonia (NH_3) and hypochlorite(OCl^-) are the favored species. Furthermore, the formation of the monochlorimine is also dependent upon the pH of the solution. It is reported that the formation of monochloramine is favored when the pH of the solution is between of 8.5 - 11.0.[27] The catalyst, sodium nitroferricyanide (III) dihydrate (Nitroprusside or NP), becomes important when discussing the effect of pH on the stability of chloramines as it has been found that the NP stabilizes monochloramine. This stabilization occurs as the iron center loses a complexed water molecule in favor of a monochloramine complex. It has been reported that when using the catalyst, the rate of the reaction is far less dependent on the pH of the solution.[22]

3.3.3 Development Time and Temperature

The uncatalyzed Berthelot reaction is known to take up to an hour to reach full color development.[28] Catalyzed, the reaction has been shown to reach full color development in as little as 6 minutes when working at 37 °C. The disadvantage of working at higher temperatures is the rate at which the blue color, indophenol dye, fades. Using a solid-state approach, Lau et al., achieved full response from a sensor in less than 3 minutes.

3.3.4 Interferants

Gips et al. reported many species present in serum or blood samples could interfere with the Berthelot reaction when present at elevated concentrations. They actually used the interference to diagnose specific disease states. For example, it was found that hyper-physiological concentrations of amino acids could prevent the determination of the ammonia concentration. They concluded the Berthelot reaction was impeded because the hypochlorite reacted with the amino acids and was not available in sufficient quantity to react with ammonia. It was reported that this interference could be so strong for patients experiencing endogenous hepatic coma or pre-coma, that the hyperaminoacidemia would nullify the formation of the indophenol entirely. This contrasted strongly with exogenous hepatic coma, where the amino acid levels are not elevated and the ammonia levels result in the formation of high concentrations of the indophenol.[29] While this interference could be used to diagnose certain conditions, the interference of amino acids is problematic for the determination of ammonia in serum

and blood especially when the amino acid levels are not known. In a more comprehensive study, Ngo et al.[30] systematically examined possible interferences to the Berthelot reaction. The conclusion of their work was that compounds without amine functionality rarely interfere. However, aliphatic compounds with primary or secondary amines could interfere. Furthermore, even tertiary and aromatic amines could interfere if the concentrations were abnormally high. Other compounds such as dimethyl sulfoxide, sodium sulfide, ascorbic acid, thiols, and thioureas also interfere with the reaction. They concluded that the interference was due to the benzoquinone's reactivity towards amines. Their results also supported the previous conclusion that amines reduce the concentrations of hypochlorite resulting in sub-optimal concentrations for the conversion of ammonia into monochloramine.

3.4 Ammonia Responsive pAMD PCCA

3.4.1 Introduction

Our goal was to move the Berthelot reaction onto our PCCA platform to eliminate some of the drawbacks described above. The primary advantage of the PCCA platform is that the change in the absorbance from the Berthelot reaction cannot be monitored visually when done in solution because physiological concentrations of NH_3 result in very small indophenol absorbance changes. Not only does this require the use of a spectrophotometer to measure these subtle changes, but the indophenol molecule is also subject to photo-degradation.

We also sought to design a sensing material that can be incorporated into a sensing device for home or bed-side point-of-care NH_3 monitoring. To accomplish this, the sensor element must be inexpensive, reproducible, and robust. It must also be chemically sensitive, accurate, and capable of sensing ammonia from very small volumes of capillary blood (20 μL). Finally, it must display information in a format that is easily interpreted.

We sought to develop an NH_3 sensor based on our previously developed PCCA photonic crystal sensing technology (**Figure 1**).[31(a-n)] Our PCCA utilize an array of highly charged colloidal particles embedded in a hydrogel matrix. The array of particles Bragg diffracts light in the visible spectral region. Our molecular recognition agent, 3-aminophenol (3-AMP), is covalently attached to the hydrogel. The sensing approach mirrors the solution based Berthelot reaction except the phenol utilized is attached to the hydrogel backbone. The OCl^- and NH_3 react in the test solution to form monochloramine, which in turn reacts with two of the pendant 3-aminophenols to create a new cross-link in the hydrogel. The mechanism for response is the formation of cross-links in the hydrogel matrix that causes an increase in the elastic restoring force of the hydrogel network and actuates an osmotic pressure inside the gel which causes the hydrogel to shrink in proportion to the amount of NH_3 present in solution. This results in a decrease in the spacing between diffracting planes of the embedded colloidal array and a blue-shift in the wavelength of light diffracted by the sensor. Our NH_3 sensor relies upon changes in the elastic free-energy of the hydrogel caused by the formation of cross-

links. The diffraction blue-shift can be directly correlated with the amount of NH_3 present in the analyte solution.

Figure 12: The formation of indophenol cross-links results in an increase in the elastic restoring force of the hydrogel, which actuates an osmotic pressure, forcing water out of the hydrogel and thereby decreasing the volume of the gel. As a result, the spacing between diffracting planes in the PCCA decreases, and the wavelength of diffracted light blue-shifts proportional to NH_3 concentration.

The wavelength of light (λ_o) diffracted follows Bragg's law: $\lambda_o = 2\,nd\,\sin\,\theta$. In our sensor, the light is diffracted by the fcc 111 plane of the embedded particle array. λ_o depends on the plane spacing, d, the refractive index of the system, n, and the incident angle of the light, θ, which is the Bragg glancing angle. Since we are sampling back-diffraction (reflectance) from light normally incident to the 111 plane of the array, $\sin\,\theta$ is unity.

3.4.2 Experimental

PCCA Preparation

We synthesized an acrylamide hydrogel like those previously made within our group.[32(a-c)] **Figure 13** depicts the synthesis, hydrolysis and functionalization of the

PCCA. Acrylamide (0.10 g, 1.4 mmol, Fluka), N,N'-methylenebisacrylamide (2.5 mg, 16.2 μmol, Fluka), a colloid suspension (2.0 g, 5-10% w/w dispersion, polystyrene latex spheres, 120 nm diameter in Nanopure water (Barnstead), AG501-X8 (D) ion exchange resin (~0.1 g, 20-50 mesh, mixed bed, Bio-Rad) and 10% DEAP (7.7 μL, 3.84 μmol; Diethoxyacetophenone; Aldrich) in DMSO (Fisher) were mixed in a 2-dram vial. The mixture, which was centrifuged to remove the ion exchange resin, was injected between two quartz disks separated by a 125 μm-thick Parafilm spacer. The cell was exposed to 365 nm UV light from mercury lamps (Blak Ray) for 2 hours. A poly(acrylamide) (pAMD) hydrogel network forms around the CCA, resulting in a pAMD Polymerized CCA (PCCA) The cell enclosing the PCCA was then opened in Nanopure water and the PCCA film allowed to equilibrate.

Hydrolysis of the pAMD

We hydrolyzed the amide groups to yield carboxylic acid groups. The PCCA was then hydrolyzed in a 50 mL solution of NaOH (0.1 M, J.T. Baker) containing 10 % v/v N,N,N',N'-tetramethylethylenediamine (TEMED, Aldrich) for 150 min. The hydrolyzed PCCA was washed for 2 hrs with 150 mM NaCl (J.T. Baker). UV-VIS Spectra were recorded to confirm that phenols remained attached to the hydrogel after hydrolysis.
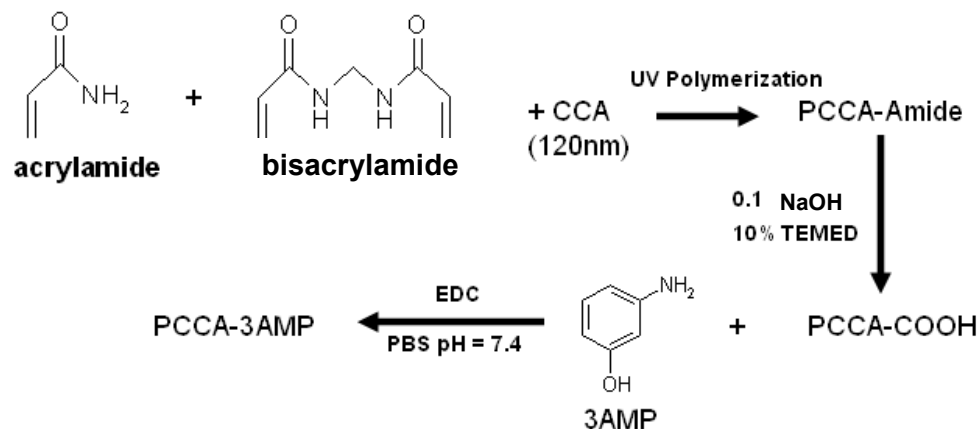
Figure 13: Preparation of the PCCA and functionalization with 3-aminophenol. The poly(acrylamide) is first hydrolyzed to yield a carboxylic acid functionalized hydrogel. The 3-AMP is coupled via a standard carbodiimide coupling procedure.

Attachment of 3-Aminophenol

0.5 g of 3-aminophenol (3-AMP, 4.6 mmol, Sigma) were dissolved in 10 ml DMSO (J.T. Baker) and then diluted to 50 ml with 50 mM phosphate buffer solution (PBS, Pierce Biotechnology). The PCCA was incubated for 4 hours in the 3-AMP solution to allow sufficient time for diffusion into the hydrogel. Next, 0.5 g of 1-ethyl-3-(3-dimethylaminopropyl) carbodiimide hydrochloride (EDC, 0.52 mmol, Pierce Bitoechnology) was dissolved into solution surrounding the PCCA. After the EDC solution was added, and the reaction was allowed to proceed for 2 hrs. The 3-AMP functionalized PCCA was rinsed repeatedly in 150 mM NaCl (J.T. Baker).

Diffraction Measurements

The diffraction of the PCCA was monitored using a fiber-optic diode spectrometer with a tungsten halogen light source (Ocean Optics) using a reflectance probe. A PCCA (1 cm x 1cm x 125 μm) was attached to a plastic Petri dish, and was

equilibrated with 5 ml of 50 mM BBS containing sodium nitroferricyanide (III) dihydrate (Nitroprusside, NP, 0.0188 g, 0.0125 M, Aldrich). A standard NH_3 solution was prepared by dissolving 0.03 g NH_4Cl (5.6 mmol, J.T. Baker) in BBS and diluting to a total volume of 30 ml. A NaOCl solution was prepared by diluting 2.4 ml NaOCl (5% in H_2O, 1.8 μmol, J.T. Baker) in BBS to a total volume of 30 ml. An initial diffraction spectrum of the PCCA was collected, and then an aliquot of the stock NH_3 solution was added to each piece of PCCA. After allowing the NH_3 to equilibrate for 5 min., a 28 μl aliquot of the OCl^- solution was added. In a control measurement, a PCCA with 3-AMP attached was exposed to 600 μM NaOCl solution with no NH_3 present, and diffraction spectra were collected according to the above protocol.

3.4.3 Results and Discussion

Selection and Optimization of the Molecular Recognition Group

The molecular recognition molecule utilized by our sensor is 3-aminophenol (3-AMP). Historically, the Berthelot reaction involves two phenol molecules reacting to form an indophenol. Later modifications to that procedure incorporated several different related molecules for reasons mostly associated with the toxicity of phenol. Salicylic acid was a common choice as the rate of the reaction was similar to that of phenol, but it avoided the detrimental toxicity. For our sensor, we sought a phenol which we could couple to our hydrogel efficiently and that also reacted well with chloramines to form the indophenol cross-link. Two logical choices were 2-aminophenol and 3-aminophenol. The amine groups provide an easy pathway for coupling to the hydrogel and in both cases the position *para-* to the hydroxyl group would still be available for the reaction with

chloramine. Other molecules which we hypothesized might work were phenol and aniline. Phenol could be coupled to the hydrogel through its hydroxyl (an epoxide ring opening reaction at higher pH) and would still have an available *para-* position and sterically would be the best fit. Aniline was also considered as it could also be easily coupled to the hydrogel and is electronically similar to phenol.

We synthesized and coupled the aforementioned molecular recognition molecules to a series of identical PCCAs. Blank hydrogels (void of colloidal particles) were simultaneously synthesized so we could analyze the effectiveness of our coupling procedure using UV-Vis. The sensors' response to 300 μM NH_3 was tested to determine which molecular recognition molecule generated the maximum spectral window and reaction rate. Our coupling procedures for attaching 3-aminophenol, 2-aminophenol, and aniline were sufficient as evident from the absorbance at 295 nm. However, the attempt to couple phenol did not result in an absorbance increase at 295 nm indicating that little or no coupling of phenol had occurred. **Figure 14** shows the hydrogel before and after the coupling of 3-aminophenol. The quantity of 3-aminophenol on the hydrogel was then calculated using the molar absorbtivity determined through a Beer's law plot. The spectra of the standard dilutions and the Beer's law plot can be seen in **Figure 15**.

When the PCCAs were tested for response to ammonia, only the hydrogel coupled with 3-aminophenol responded with a substantial blue-shift in the diffraction wavelength. The hydrogel coupled with 2-aminophenol responded with a very slight blue-shift while the aniline hydrogel red-shifted slightly. Further tests were not run on

the hydrogel coupled with phenol since we had concluded it did not couple to the hydrogel. It was concluded that 3-aminophenol was the best reagent tested for use in our sensor and we continued to optimize the reaction around this molecular recognition moiety.
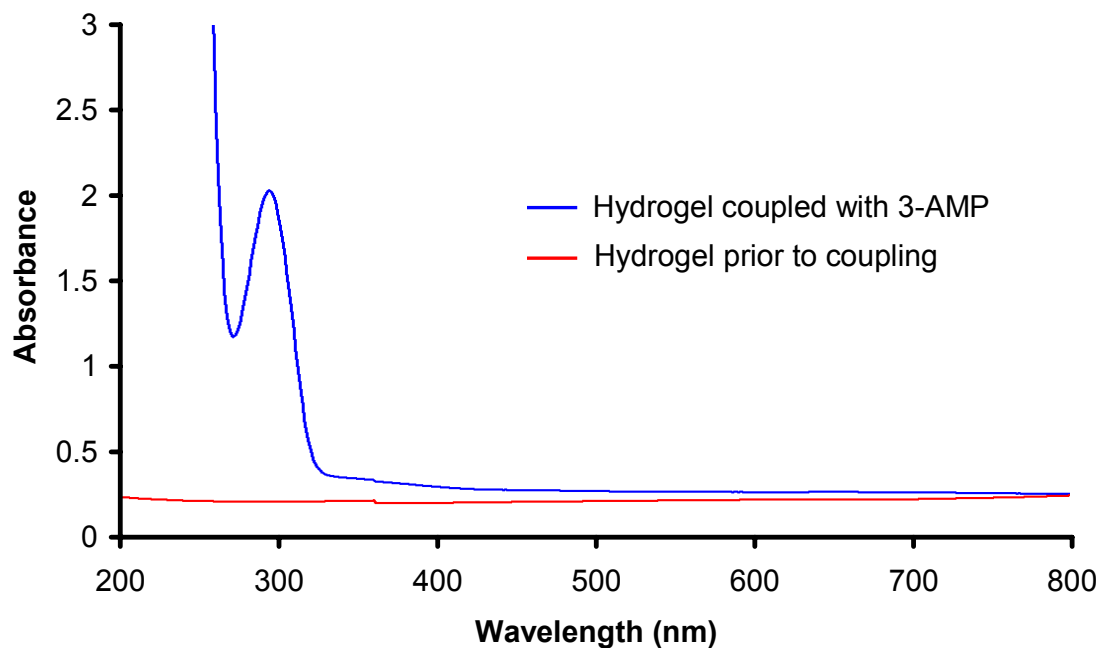
Figure 14: The quantity of 3-aminophenol coupled to the hydrogel was determined by measuring the difference in absorbance of the blank and coupled hydrogel at 295 nm.

Determination of 3-AMP Coupling Efficiency

A clear gel (hydrogel in which CCA solution is replaced with pure H_2O) was prepared and functionalized according to the above protocol. UV-VIS spectra of the blank gel were measured by a Varian Cary 5000 UV-VIS spectrophotometer to confirm attachment of 3-AMP by monitoring the absorbance at 290 nm. In order to determine the concentration of 3-AMP coupled to the hydrogel, we made standard dilution of 3-AMP and established the molar absorptivity from a Beer's Law plot **(See Figure 15)**.
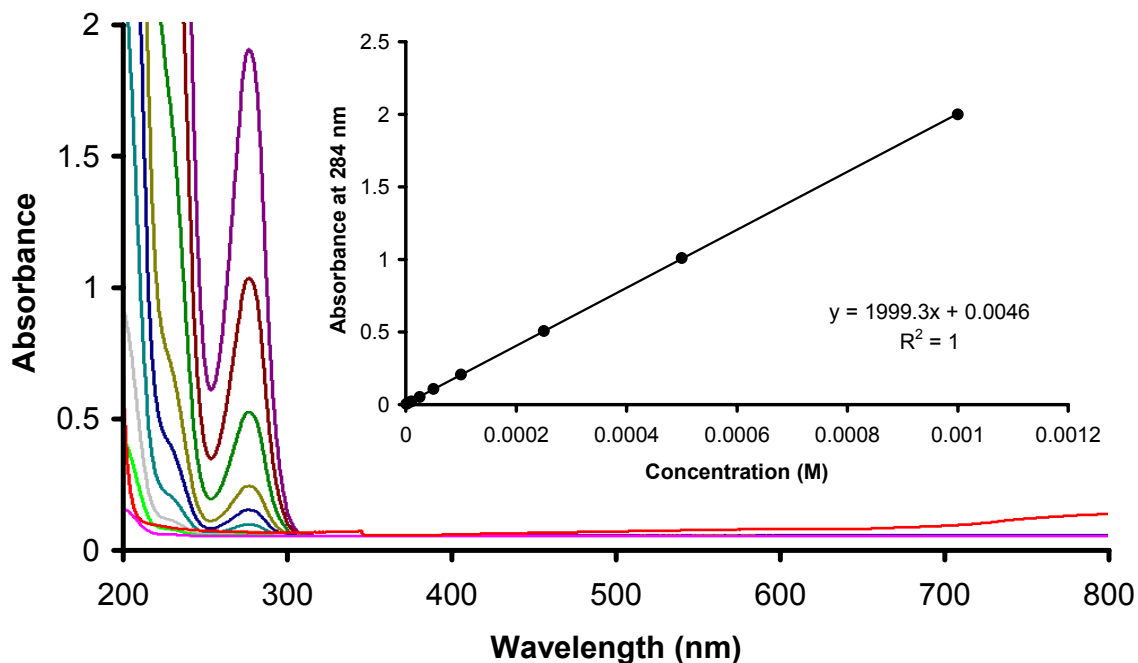
Figure 15: The absorbance spectra for standard solutions of 3-aminophenol in BBS. Inset is the Beer's law plot showing the determination of the molar absorbtivity.

We then optimized the 3-AMP coupling to a blank hydrogel by varying the hydrolysis time. It was our hypothesis that we could modify the 3-AMP concentration by varying the concentration of carboxylic acid groups on the hydrogel. The hydolysis of polyacrylamide results in pendant carboxylic acid groups. We determined the appropriate hydrolysis time by removing portions of the hydrogel from the hydrolysis solution at four different times. We then coupled 3-AMP to each of these materials and determined the concentration of coupled 3-AMP through its absorbance at 290 nm. Each absorbance measurement was done in a 50 mM BBS solution with a pH of 9.2 **(See Figure 16)**.
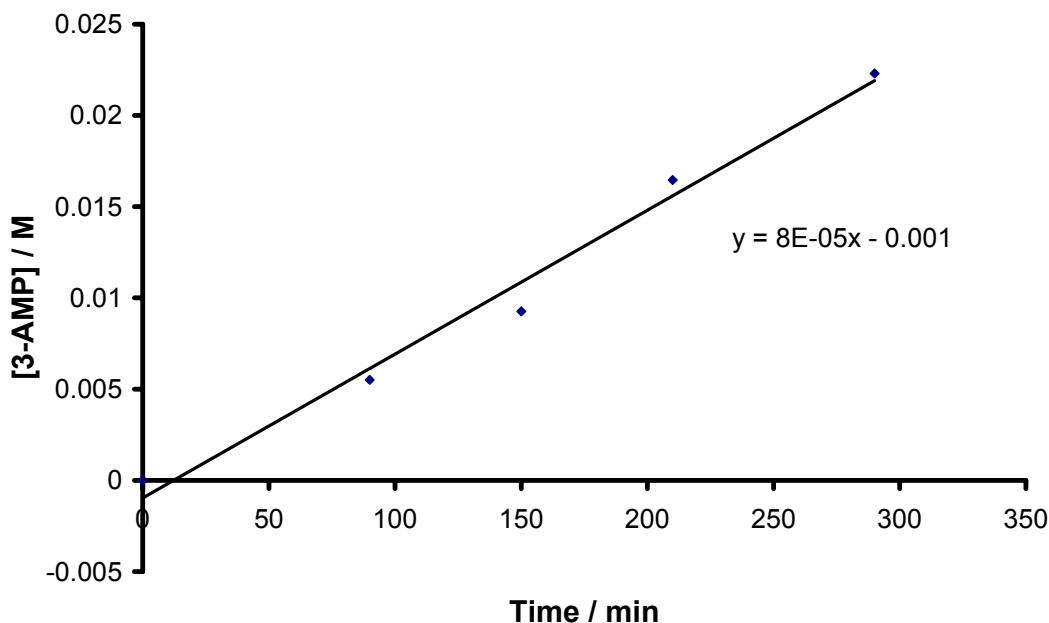
Figure 16: The concentration of 3-AMP coupled to a blank gel increased linearly in relation to the hydrolysis time. The greater extent to which the amides on the hydrogel were converted to carboxylic acids resulted in the coupling of a higher concentration of 3-AMP through EDC coupling. In each case, the EDC coupling conditions, including the concentration of 3-AMP in the coupling solution, was kept constant and in excess.

The relationship between the concentration of 3-AMP on the hydrogel and the hydrolysis time was roughly linear. We found that we were able to increase the concentration of 3-AMP by 80 μM for every minute the hydrogel was hydrolyzed. We chose to hydrolyze our ammonia sensing PCCA for 150 minutes, which we calculated had a 3-AMP concentration of ~ 10 mM. While longer times allowed the incorporation of greater concentrations of 3-AMP, it also caused the hydrogel to swell to the extent the diffraction shifted into the IR. Because we sought a PCCA that diffracted in the visible region of the spectra, we did not study the properties of PCCA which had been hydrolyzed for longer than 300 min.

Diffraction Shift Due to Hypochlorite

Prior to examining the response to solutions containing ammonia and hypochlorite, the sensor's response to hypochlorite and ammonia individually was first tested. The PCCA exhibited no change in diffraction wavelength upon the addition of ammonia without hypochlorite present. However, significant diffraction shifts were observed when hypochlorite was added to the testing solution. **Figure 17** shows the manner in which the diffraction spectrum (measured as reflectance) changes over time for 600 μM OCl⁻ in BBS.
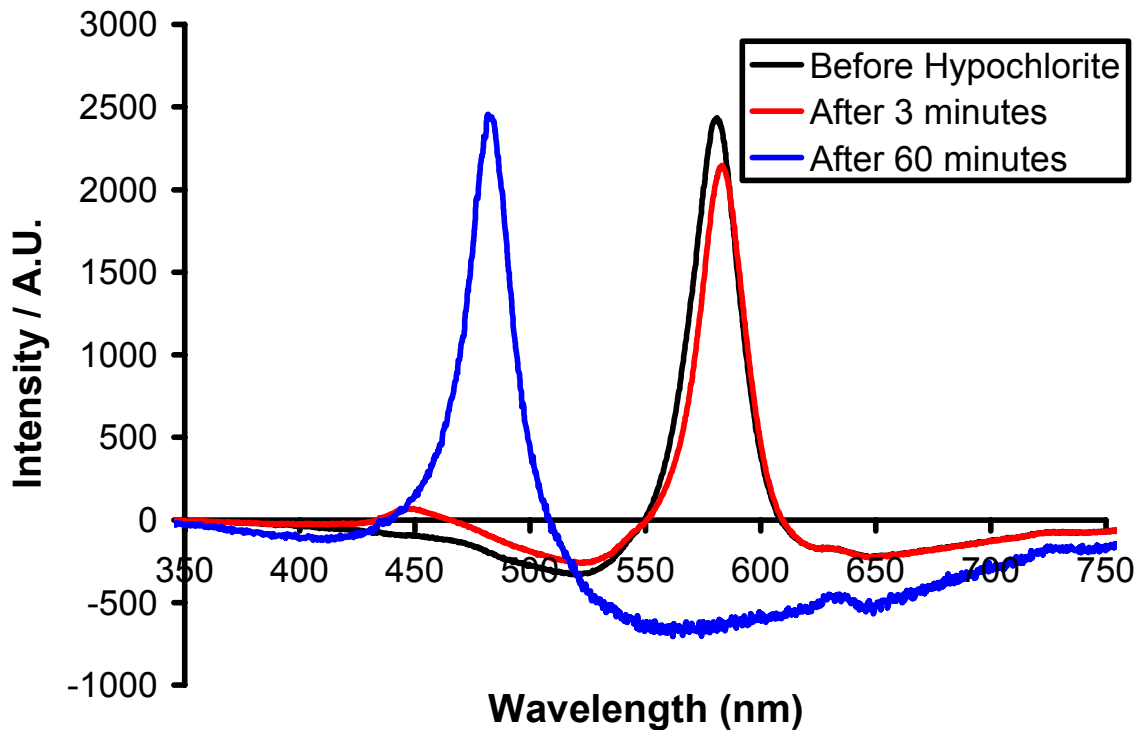
Figure 17: Diffraction spectra of PCCA in presence of 600 μM OCl⁻. The PCCA does not exhibit a consistent blue-shift, but the original peak diminishes as the secondary peak grows in intensity. The negative baseline results because of over-subtraction of the background.

Initially, the diffraction wavelength red-shifts slightly while diminishing in intensity. This is followed by a gradual degradation in diffraction intensity of the original diffraction peak contemporaneous with a gradual growth of another peak. The original diffraction wavelength here was ~ 580 nm and the new peak was observed at ~ 480 nm. Several other concentrations of hypochlorite (300 μm, 1200 μm, and 1800 μm OCl⁻) were tested and each behaved similarly. The main difference was that at higher concentrations the changes occurred faster.

We attempted to use this material as a sensor by first introducing ammonia to the solution, then adding hypochlorite. The response to solutions containing both ammonia and hypochlorite was a gradual decrease in the original diffraction peak as multiple peaks at other wavelengths appeared. This deviated significantly from our previous experiences with PCCA materials, which would exhibit a continuous shift between two diffraction wavelengths. The cause of the discontinuous spectral response and the failed hypochlorite control needed to be understood prior to attempting to develop an ammonia senor based on this PCCA.

Through the control experiment utilizing hypochlorite, we hypothesized that our hydrogel backbone was reacting with hypochlorite. The reaction between hypochlorite and the poly-acrylamide hydrogel was anticipated, but the extent to which it would prevent the development of a sensor was not understood until the experiments were attempted. The chemistry of this adverse reaction is known as the Hofmann degradation, the transformation of primary amides into primary amines in the presence of hypochlorite

(Figure 18). The magnitude of the interaction between the hydrogel and the hypochlorite necessitated the development of either a hypochlorite-free sensing mechanism or the development of a more robust hydrogel which would not react with hypochlorite.
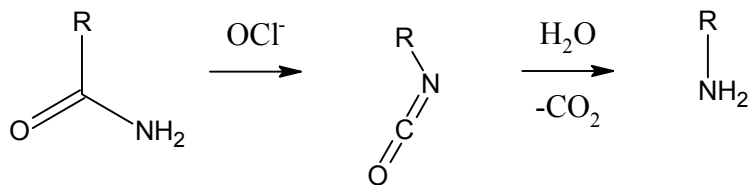
Figure 18: The Hoffmann degradation, sometimes referred to as the Hoffman rearrangement, is a process where a primary amide is transformed into an isocyanate intermediate by the hypochlorite anion. The isocyanate is hydrolyzed forming a primary amine and carbon dioxide.

Summary

The pAMD based PCCA is incompatible with the Berthelot reaction based sensing approach because the amide groups are susceptible to reaction with the hypochlorite.

References

1. Huizenga, J.R.; Gips, C.H.; Tangerman, A. *Ann. Clin. Biochem.* **1996**, 33, 23-30.

2. Tietz, N.W.; *Clinical Laboratory Guide to Laboratory Tests*. 3rd ed. Philadelphia, W.B. Saunders, **1995**.

3. Pesce, A.J. and Kaplan, L.A. *Methods in Clinical Chemistry* C.V. Mosby Company, St. Louis, MO, **1987**, 1089.

4. Hazell, A.S.; Butterworth, R.F. *Experimental Biology and Medicine* **1999,** 222 (2) 99.

5. Campion, M. Blood Ammonia: a critical measurement, *BIMDG Bulletin Spring 2003*, 13.

6. Bachmann, C. *Eur. J. of Pediatr.* **2003,** 162, S29 - S33.

7. Huizenga, J.R.; Tangerman, A.; Gips, C.H. *Ann. Clin. Biochem.* **1994**, 31, 529-543.

8. Mondzac, A.; Ehrlich, G.E.; Seegmiller, J.E. *J. Lab. Clin. Med.* **1965,** 66, 526-531.

9. Van Anken, H.C.; Schiphorst, M.E. A *Clin. Chim. Acta* **1974**, 56, 151-157.

10. Bostian, KA; Betts, GF. *Biochem. Journal* **1978**,173, 773-786.

11. Mann, L.T. *Anal. Chem.* **1963**, 35(13), 2179-2182.

12. Reay, P.F. *Anal. Chim. Acta* **1985**, 176, 275-278.

13. Lau, K.T.; Edwards, S.; Diamond, D. *Sens. Actuators B.* **2004**, 98, 12-17.

14. Daridon et al. *Sens. Actuators B.* **2001**, 76, 235-243.

15. Zellmer, S.; Katenborn, G.; Rothe, U.; Lehnich, H.; Lasch, J.; Pauer, H.D. *Anal. Biochem.* **1999**, 273, 163-167.

16. http://www.careside.com/pdfs/Ammonia.pdf

17. http://www.arkray.co.jp/english/products/ammonia.html

18. Huizenga, J.R. *Clin. Chim. Acta* **1992**, 153-155.

19. Huizenga, J.R.; Gooitzen, M.D.; Gips, C.H.; *Clin. Chim. Acta* **1996**, 73-82.

20. Berthelot, M.; *Repert. Chim. Appl. I* **1859**, 284.

21. Searle, P.L. *Analyst*. **1984,** 109: 549-568.

22. Harfmann, R.G.; Crouch, S.R. *Talanta* 36: **1989,** 261-269.

23. Krom, M.D. *Analyst* **1980**, 105, 1249.

24. Juttner, F. *Fresnius J. Anal. Chem.* **1999**, 363, 128-129.

25. Seeley, J.H.; Petitclerc, J.C.; Benoiton, L. *Clin. Chim. Acta*, **1967,** 18, 85.

26. Tsuboi, T.; Hirano, Y.; Shibata, Y.; Motomizu, S. *Analytical Sciences*. **2002**, 18, 1141-1144.

27. Qiang, Z.; Adams, C.D. *Environ. Sci. Technol.* **2004**, 38, 1435-1444.

28. Lau, K.T.; Edwards, S.; Diamond, D. *Sens. Actuators B*, **2004,** 98, 12-17.

29. Gips, C.H.; Reitsema, A. *Clin. Chem. Acta* **1971**, 33, 257-259.

30. Ngo, T.T.; Phan, A.P.H.; Yam, C.F.; Lenhoff, H.M. *Anal. Chem.* **1982**, 54, 46-49.

31. Historical perspective on PCCA development:

    a) Krieger, I.M.; and O'Neill, F.M. *J. Am. Chem. Soc.* **1968**, *90*, 3114.

    b) Hiltner, P.A.; and Krieger, I.M. *J. Phys. Chem.* **1969**, *73*, 2386.

    c) Hiltner, P.A.; Papir, Y.S.; and Krieger, I.M. *J. Phys. Chem.* **1971**, *75*, 1881.

    d) Carlson, R.J.; and Asher, S.A. *Appl. Spec.* **1984**, *38*, 297.

    e) Runquist, P.A.; Photinos, P.; Jagannathan, S.; and Asher, S.A. *J. Chem. Phys.* **1989**, *91*, 4932.

    f) Asher, S.A.; Holtz, J.H.; Liu, L.; and Wu, Z. *J. Am. Chem. Soc.* **1994**, *116*, 4997.

    g) Weissman, J.M.; Sunkara, H.B. Tse, A.S.; and Asher, S.A. *Science,* **1996**, *274*, 959.

h) Ito, K.; Nakamura, H.; and Ise, N. *J. Chem. Phys.* **1986**, *85*, 6136.

i) Monovoukas, Y.; and Gast, A.P. *J. Colloid Interface Sci.* **1989**, *128*, 533.

j) Okubo, T. *Acc. Chem. Res.* **1988**, *21*, 281.

k) Asher, S.A. U.S. Patents 4,627,689 (**1986**), 4,632,517 (**1986**), 5,281,370 (**1994**), 5,452,123 (**1995**).

l) Holtz, J.H.; and Asher, S.A. *Nature* **1997**, *389*, 829.

m) Holtz, J.H.; Holtz, J.S.; Munro, C.; and Asher, S.A. *Anal. Chem.* **1998**, *70*, 780.

n) Pan, G.; Kesavamoorthy, R.; and Asher, S.A. *J. Am. Chem. Soc.* **1998**, *120*, 6525

32. a) Asher, S.A.; Holtz, J.; Liu, L.; Wu, Z.; *J. Am. Chem. Soc.* **1994**, *116*, 4997-4998.

b) Holtz, J.H.; Asher, S.A. *Nature* **1997**, *389*, 829-832.

c) Holtz, J.H.; Holtz, J.S.; Munro, C.H; Asher, S.A. *Anal. Chem*. **1998**, *70*, 780-791.

CHAPTER 4: A Novel Poly(hydroxyethyl acrylate) Hydrogel Sensor Material

4.1 Selection and Optimization of the pHEA Hydrogel

4.1.1 Introduction

As we showed in the previous chapter, a pAMD hydrogel is not compatible with our ammonia sensing mechanism. After finding that pAMD was not an adequate material, we were faced with the choice of which hydrogel would be the best candidate for the development of an ammonia sensor. We researched the feasibility of using poly(hydroxyethyl methacrylate) (pHEMA) hydrogels because they have been extensively utilized for medical devices, specifically soft contact lenses.[1,2,3] We also expected that functionalizing pHEMA hydrogels would be easy because of the favorable reactivity ratios between the hydoxyethyl methacrylate monomer and the epoxy containing monomers, such as glycidal methacrylate and glycidal acrylate. One potential drawback we discovered is that researchers have reported that pHEMA cross-linked with dimethacrylates containing greater than 39% water, exhibited significant turbidity.[4] We synthesized several pHEMA hydrogels at various monomer contents and our observations confirmed the validity of those reports. Hydrogel formulations in which the HEMA content was less than 60% of the total reaction mixture resulted in turbid hydrogels. The turbidity was observed in hydrogel polymerized with and without the inclusion of CCA, therefore we concluded that the turbidity was intrinsic to the hydrogel composition.

This turbidity results from the well-known phenomenon in hydrogel systems called microsyneresis. Syneresis is a term used to describe phase separation. Macrosyneresis is the term describing systems which have separated into macro-scale distinct phases, like precipitation of a bulk from a solution. The term microsyneresis means that the phase separation within a system occurs over very small length scales. In terms of hydrogels, the term is used for systems in which small regions of the dense polymer phase is distributed in the solvent phase.[5] Hydrogels exhibiting microsyneresis are sometimes referred to as microgels.[6] The phase separations in the hydrogel result in a refractive index modulation over distances comparable to the wavelength of light. These modulations efficiently scatter light and make the hydrogel appear turbid. Our sensors utilize diffraction from the CCA embedded within the hydrogel; the randomly distributed refractive index modulations either obscure the Bragg diffraction due to dominating diffuse scattering or they disorder the CCA. Throughout the development of our ammonia sensor, we synthesized hydrogels without colloidal particles in parallel with the PCCAs. These "blank" hydrogels were then visually inspected for microsyneresis.

4.1.2 Experimental

Syntehesis of pHEA PCCA

Hydroxyethylacrylate (HEA, 0.94 g, 8.1 mmol, Sigma), Poly(ethylene glycol dimethacrylate-200) (PEGDMA-200, 0.09 g, 0.25 mmol, Polysciences), glycidyl acrylate (GA, 0.04 g, 0.37 mmol, Sigma) and ethylene glycol (1.95 g, 31 mmol, J.T. Baker) are mixed and exposed to Al_2O_3 (Sigma) in order to remove the inhibitor. The mixture is centrifuged to separate the monomer from the Al_2O_3, and 1.015 g of the de-inhibited

monomer is added to an aliquot of colloid suspension (1.0 g, 5-10% w/w dispersion, polystyrene latex spheres, 106 nm). Another 1.015 g of monomer mixture is added to 1.0 g H_2O to prepare a colloid-free clear hydrogel, which can be used for UV-VIS absorbance measurements. AG501-X8 (D) ion exchange resin (~ 0.1 g, 20-50 mesh, mixed bed, Bio-Rad) and 10 % diethoxyacetophenone (DEAP, 10 uL, 4 umol, Aldrich) in DMSO (J.T. Baker) are mixed with the suspension in a 2-dr vial. The colloidal particles self-assemble into a CCA in the reaction mixture and the mixture appear opalescent. The mixture is centrifuged to eliminate air bubbles generated by mixing and is injected between two quartz discs separated by a 125 μm thick Parafilm spacer. The ion exchange resin is excluded because the size of the resin particles are larger than the 125 μm spacer size. The film is exposed to 365 nm UV light from mercury lamps (Blak Ray) for 3 hrs **(Figure 8)**.
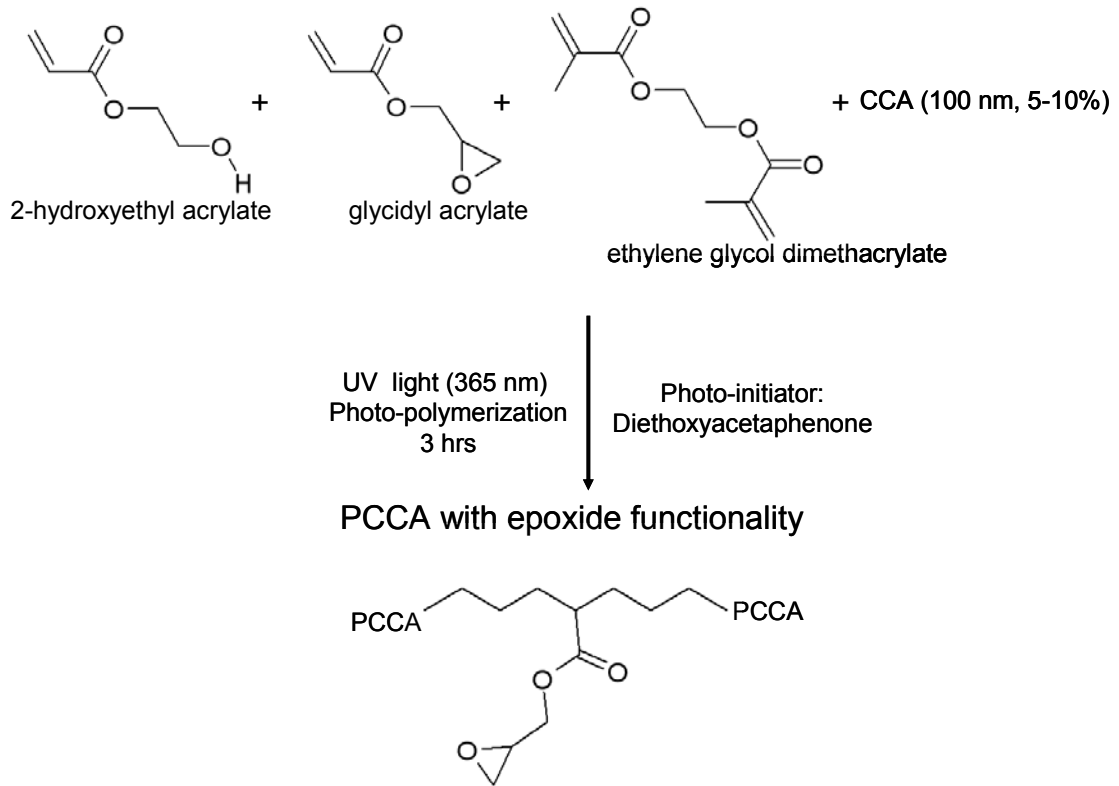
Figure 19: The synthesis of a PCCA. The monomers are added to a solution of the CCA. The initiator is added and the CCA is placed on the apparatus shown in Figure 8 for 3 hours. The hydrogel product will contain epoxide functionality.

A pHEA hydrogel network with PEGDMA cross-links forms around the CCA, resulting in a PCCA. The cell enclosing the hydrogel is opened in Nanopure water and the PCCA is allowed to equilibrate with water. The reaction scheme for the polymerization of the PCCA is seen in **Figure 19**.

4.1.3 Results and Discussion

Dense Gel Sensor

To avoid the microsynerisis associated with HEMA hydrogels, we developed a hydrogel based around 2-hydroxyethylacrylate (HEA). HEA is more soluble in aqueous solutions than HEMA because it lacks a methyl group on the acrylate. pHEA-based hydrogels also exhibited microsynerisis, but only at a much higher water content. We were able to synthesize clear hydrogels in pure water with polymer contents as low as 28%. **Figure 20** shows images of several hydrogels with polymer compositions ranging from 40% polymer to 10% polymer. The hydrogels made with 40% and 30% polymer are clear, while the hydrogels made with 20% and 10% polymer are turbid. The turbidity is caused by light scattering from the unordered polymeric micro-domains.
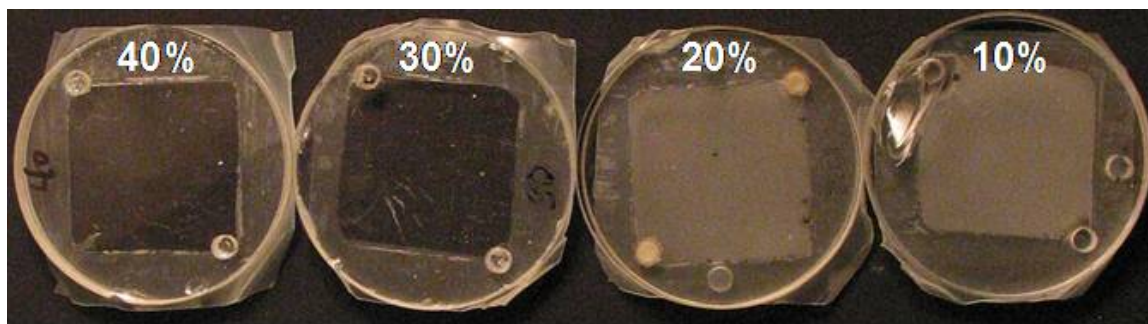
Figure 20: Images showing turbidity caused by microsynerisis for blank hydrogels. Hydrogels made with high polymer content (40% and 30%) are transparent and hydrogels with low polymer content (20% and 10%) are opaque.

It was initially determined that pHEA hydrogels with a polymer content of 30% were the lowest polymer content which could be made without significant microsyneresis. We developed a sensor utilizing this material that responded to ammonia

in buffer solutions. **Figure 21** shows the response of a 30% polymer hydrogel to various hyper-physiological concentrations of ammonia. While the spectral window of the sensor was small, it was our first demonstration that the new hydrogel we were developing was capable of sensing ammonia. The need for further optimization was apparent because the hydrogel lacked sensitivity over the clinical reference interval.
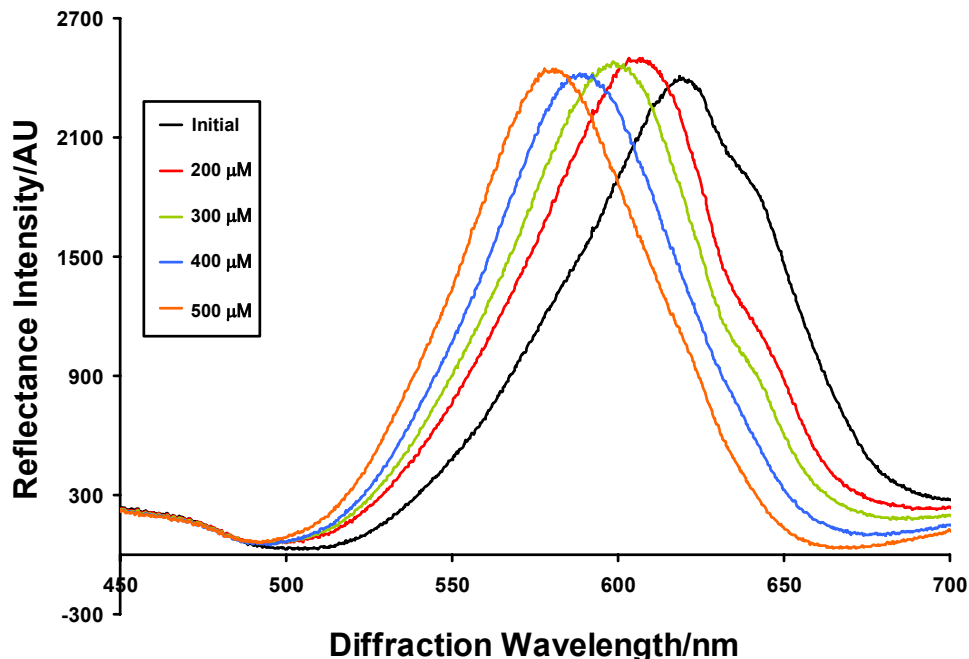
Figure 21: Response of the 30% polymer hydrogel for hyperphysiological concentrations of ammonia. The lack of spectral shift prompted the investigation into lower polymer hydrogels.

Our sensor was designed to change diffraction wavelengths in response to the formation of new crosslinks. Therefore, the number of crosslinks in the original hydrogel should impact the spectral response. For highly crosslinked hydrogels, the crosslinks formed in response to the presence of ammonia would result in a relatively small change in the overall number of crosslinks. This would result in a very small hydrogel volume

change and only a small change in the diffraction wavelength. In contrast, lightly cross-linked hydrogels should exhibit proportionally more shrinking.

However, we did not observe a significant improvement in the shrinking response with the lower crosslink density sensors. In fact, we determined that the response was essentially independent of the original crosslink density. We hypothesized that the hydrogel was behaving more like a plastic than a typical elastic hydrogel. At 30% polymer content, we hypothesize that the restoring forces which prevent the polymer from adopting other configurations derive not only from covalent crosslinks, but also from the physical crosslinks associated with the entanglement of the polymer chains. Entanglement of the hydrogel chains act as effective crosslinks which constrain the hydrogel from changing volume. This polymer entanglement has been utilized to synthesize hydrogels without any true covalent crosslinks.[7] Although our sensor was responsive to ammonia, it was clear that it was not behaving according to the relationship described in **Figure 9**, which relates osmotic pressure of elasticity to the number of crosslinks. In light of these findings we developed lower polymer content hydrogels so that the formation of crosslinks would result in PCCA diffraction shifts.

The Utilization of Solvents to Synthesize Low-Polymer Hydrogels

The use of co-solvents added to the aqueous solution can prevent microsynerisis during polymerization of the hydrogel. CCA require a predominantly aqueous environment, but a co-solvent can be added to increase the solubility of the forming polymer hydrogel. We tested several co-solvent systems in an attempt to lower the

polymer content of the hydrogel such as methanol, ethanol, DMSO, and EG. Another approach to preventing microsynerisis was addition of water soluble polymers including poly(vinyl alcohol) (PVA), poly(vinyl pyrollidone) (PVP), and poly(ethylene oxide) (PEO). While the co-solvent approach was based on increasing the solubility of the forming polymer gel, it was our hypothesis that the dissolved polymer could stabilize the hydrogel polymer during polymerization and prevent the phase separation which causes microsynerisis. In both cases, we expected that the co-solvent or stabilizing polymer could be removed after polymerization. Unfortunately, we found that the addition of PVA and PVP to the polymerization did not affect the microsynerisis. However, the incorporation of co-solvents into the polymerization mixture did allow us to minimize microsynerisis.

PCCA synthesized in a mixture of EG and water showed the best diffraction at the lowest percent polymer. Hydrogel compositions with as little as 15% polymer could be made without exhibiting microsynerisis. Furthermore, the diffraction did not degrade when the EG was washed from the gel after polymerization. While the typical PCCA made with 15% polymer exhibited no microsynerisis, the polymerization was not consistently reproducible and microsynerisis was observed occasionally despite incorporation of the co-solvent. We increased the polymer content to 18% because polymerizations at that composition were more reproducible. We suspect the lack of reproducibility at 15% polymer was due to a larger temperature dependence of microsyneresis at this lower polymer content. Slightly increasing the polymer content allowed us to reproducibly synthesize our PCCA sensor.

Optimization of Glycidyl Acrylate/3-AMP

The quantity of 3-AMP incorporated into the hydrogel depends on the concentration of GA incorporated into the hydrogel. We found that the reaction between 3-AMP and GA is 89% efficient by dividing the moles of incorporated GA by the number of moles of 3-AMP attached determined through UV-Vis absorption spectrometry. We varied the concentration of GA in the polymerization and utilized the concentration which exhibited the greatest sensing response. We found that spectral window was the greatest for a GA concentration of 1.25% (w/w) of the total polymer. **Figure 22** shows the relationship between the GA incorporated into the polymer and the resulting spectral window for the response to 300 μM NH_3.
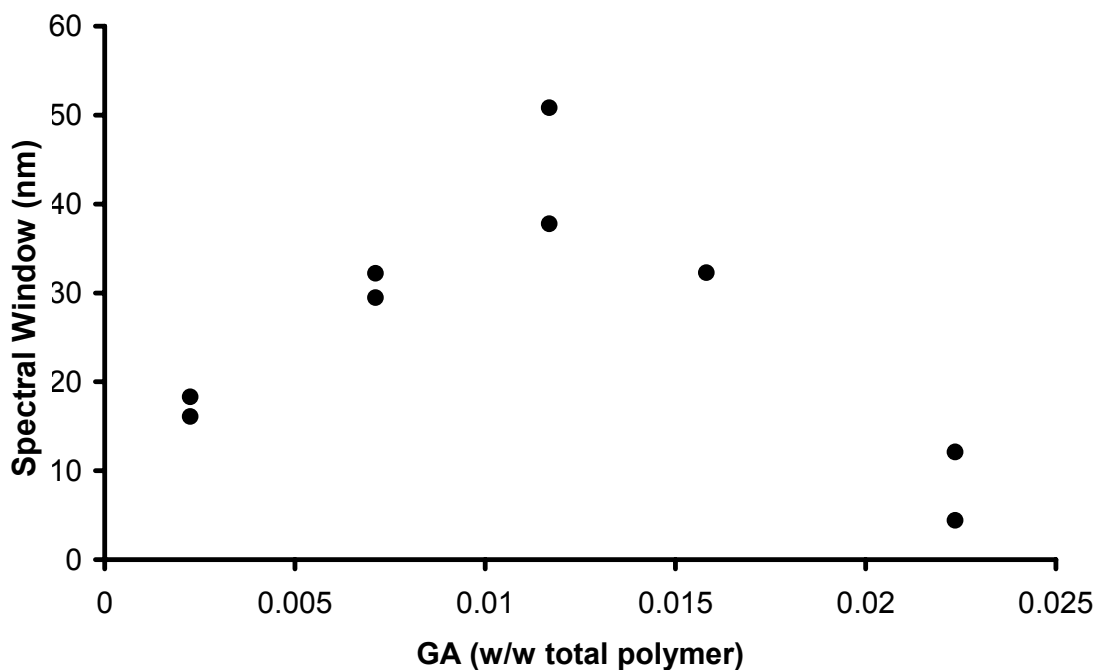
Figure 22: The relationship between the GA incorporated into the polymer (percent GA to total polymer content (w/w)) and the resulting spectral window for the response to 300 μM NH_3.

The trials were run in duplicate at slightly different total polymer content; this can be seen as the multiple data points for each concentration. The narrow range of concentrations studied stems from the inability to incorporate higher concentrations of GA into the hydrogel. GA is very hydrophobic and attempts to incorporate higher concentrations resulted in increased microsynerisis. As the concentration of GA is increased the hydrogel's diffraction intensity declines and the diffraction peak broadens. Concentrations of GA over 2.5% led to turbid hydrogels with visually evident microsynerisis. The optimal concentration of GA in the hydrogel limited the concentration of 3-AMP in our sensor. We determined through UV-Vis spectroscopy (as shown in **Figure 15** and **Figure 16**) that the concentration of 3-AMP in our sensor was 24 mM (80 times greater than the highest concentration of ammonia we were trying to sense, 300 μm). While in excess, we would have preferred coupling even larger concentrations of 3-AMP to the PCCA because literature suggests that even larger excesses are preferable (molar excess of one-hundred to one-thousand times).

Optimization of hypochlorite and NP

We sought to develop an ammonia sensor useful for the clinically relevant range (11- 300 μmol NH_3/L). The optimal concentration of hypochlorite and NP were determined for this range of ammonia concentrations. The literature reports that the ratio of hypochlorite to ammonia should be at least 2:1, because this is the minimum ratio for efficient generation of monochloramine from ammonia. Therefore, we utilized 600 μM hypochlorite.

We determined the optimal NP concentration by determining the sensing response at different NP concentrations. The concentration range tested was based on the literature values reported for the solution-based Berthelot reaction. **Figure 23** shows the affect of the NP concentration on the spectral window. A concentration of ~0.0125 M was determined to be optimal.
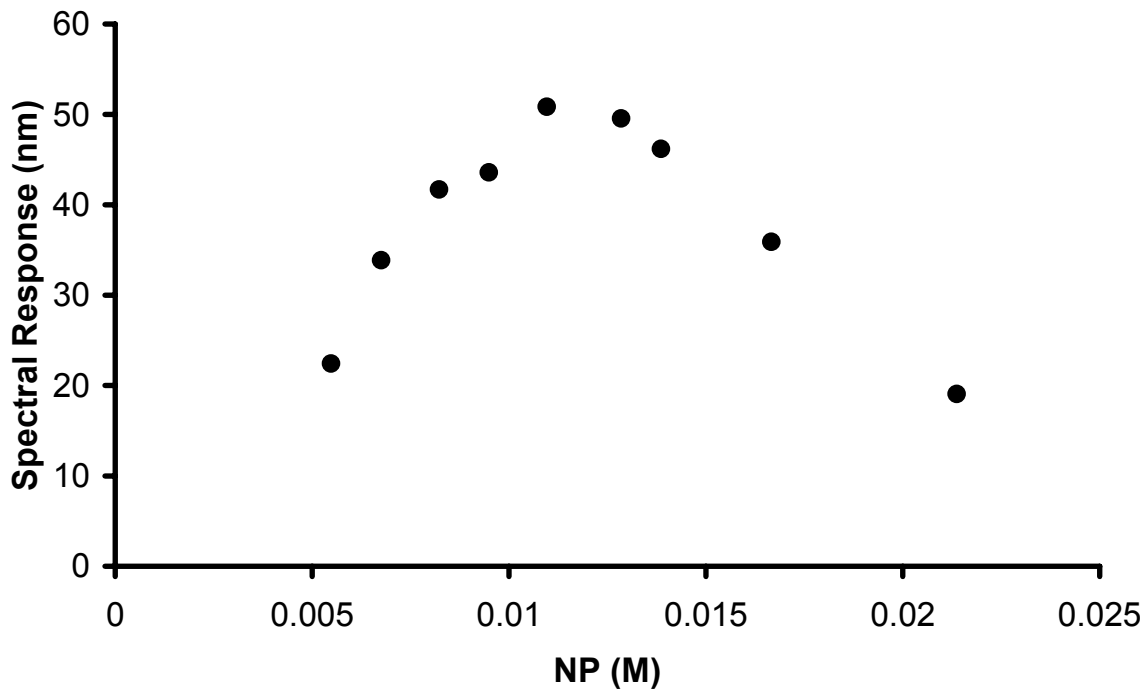
Figure 23: The sensing response to 300 μM NH$_3$ in BBS was dependent on the concentration of nitroprusside (NP) incorporated into the reaction solution. The maximum response occurs at ~0.0125 M NP.

References

1. Nicolson, P.C.; Vogt, J. *Biomaterials* **2001** 22, 3273-3283.

2. Hacioglu, B.; Berchtold, K.A.; Lovell, L.G.; Nie, J.; Bowman, C.N.; *Biomaterials* **2002**, 23, 4057-4064.

3. Elliott, J.E.; Anseth, J.W.; Bowman, C.N. *Chem. Eng. Sci.* **2001**, 56, 3173-3184.

4. Okay, O. *Prog. Polym. Sci.* **2000**, 25, 711-779.

5. Huglin, M.B.; Yip, D.C.F.; *Macromolecules* **1992**, 25, 1333-1337.

6. Graham, N.B.; Cameron, A. *Pure & Appl. Chem.* **1998**, 6, 1271-1275.

7. Trieu, H.; Qutubuddin, S. *Polymer* **1995**, 36, 13, 2531-2539.

4.2 Progress towards the Development of a Point-of-Care Photonic Crystal Ammonia Sensor

> - work in this portion of the chapter was a collaboration with J. P. Walker. My contribution to this project (~50%) was general oversight and direction, development of the ammonia sensitive PCCA hydrogel material, and optimization of conditions for the Berthelot reaction.

4.2.1 Introduction

Ammonia within bodily fluids results from the metabolic breakdown of dietary proteins, and is generated primarily in the liver, muscles, and kidneys.[1]   It is derived specifically from the deamination of the α-amino nitrogen of amino acids and is toxic when persistent at elevated levels. Hyperammonemia, venous blood levels of ammonia greater than 100 μM NH_3 in neonates, or greater than 40 μM NH_3 for all others, results primarily from one of four groups of diagnoses: urea cycle disorders (UCDs), organic acidemias (OAs), fatty acid oxidation defects (FAOs) and liver malfunctioning.[2,3]

Hyperammonemia results in damage to the central nervous system, including altering the transit of amino acids, water, and electrolytes across the neuronal membrane. Ammonia can also inhibit the generation of both excitatory and inhibitory postsynaptic potentials.[4,5]   The routine screening of ammonia levels should allow for treatment of at-risk patients before hyperammonemia causes retardation, neurological damage or death. The frequency of testing required to avoid the physical ramifications of hyperammonemia places a high demand on both the clinical laboratories and on the affected patients and families.[6]

Blood ammonia levels are currently determined utilizing an enzyme-based assay in which the enzyme glutamate dehydrogenase converts 2-oxoglutarate and ammonium to glutamate and water. In this reaction, the UV absorbance of the NADPH cofactor is monitored as it is converted to $NADP^+$.[2,7,8,9] This test requires sophisticated laboratory instrumentation and testing is typically done in clinical laboratories. Further complicating ammonia determinations, whole blood samples begin to generate ammonia immediately after the draw due to deamination of proteins in the red blood cells (RBCs). Blood from a healthy person can be stored at 4° C for an hour, but patients with urea cycle defects must have their blood analyzed or treated within 15-30 min of the blood draw in order to obtain accurate results. This need for immediate testing presents significant obstacles for the accurate determination of ammonia and demands that the patient be tested in close proximity to the clinical laboratory.[10]

There are numerous other technologies which have been developed to detect ammonia in bodily fluids. Unlike the direct enzymatic method mentioned above, most of these are two-step processes. The first step separates ammonia from the biological matrix, and the second step is a quantitative determination. The means of separating ammonia from the blood include distillation, aeration, ion-exchange, microdiffusion, protein precipitation, or Kjeldahl extraction.[11-14] Several methods have been developed which are based on the alkaline liberation of gaseous ammonia and transport through a gas-permeable membrane. The subsequent determination of the ammonia is performed by colorimetry, titration, ion-selective electrochemistry, fluorometry, conductometry, mass spectrometry, second-derivative spectrometry, optical waveguide spectroscopy, HPLC, or

capillary isotachophoresis.[15] Several technologies have also been developed which combine liberation and quantitation into one procedure. These techniques were discussed at length in the recent review by Huizenga et al.[10]

A colorimetric approach to sensing ammonia which has been successful in solution is the Berthelot, or indophenol, reaction.[16] In this reaction, ammonia (NH_3) reacts with a hypochlorite (OCl^-) to form a monochloramine, which in turn reacts with two phenols to form an indophenol dye **(Figure 24).** The concentration of NH_3 can be determined by monitoring the absorbance of the dye molecule at $\lambda = 640$ nm. This reaction has been extensively studied in solution for various absorbing phenolic species and hypohalite sources.[17] Various catalysts have also been explored as a means of increasing reaction kinetics. The most prevalently used catalyst is sodium nitroferricyanide (III) dihydrate (Nitroprusside, NP). Several researchers have effectively demonstrated the coupling of alkaline liberation of NH_3 with the Berthelot determination.[10]

The Berthelot reaction has some drawbacks. The change in the absorbance from the Berthelot reaction cannot be monitored visually because physiological concentrations of NH_3 result in small indophenol absorbance changes. Not only does this require the use of a spectrophotometer to measure these subtle changes, but the indophenol molecule is also subject to photodegradation. The Berthelot method is also known to suffer from interferences from other amine-containing molecules present in the analyte matrix.[18,19]
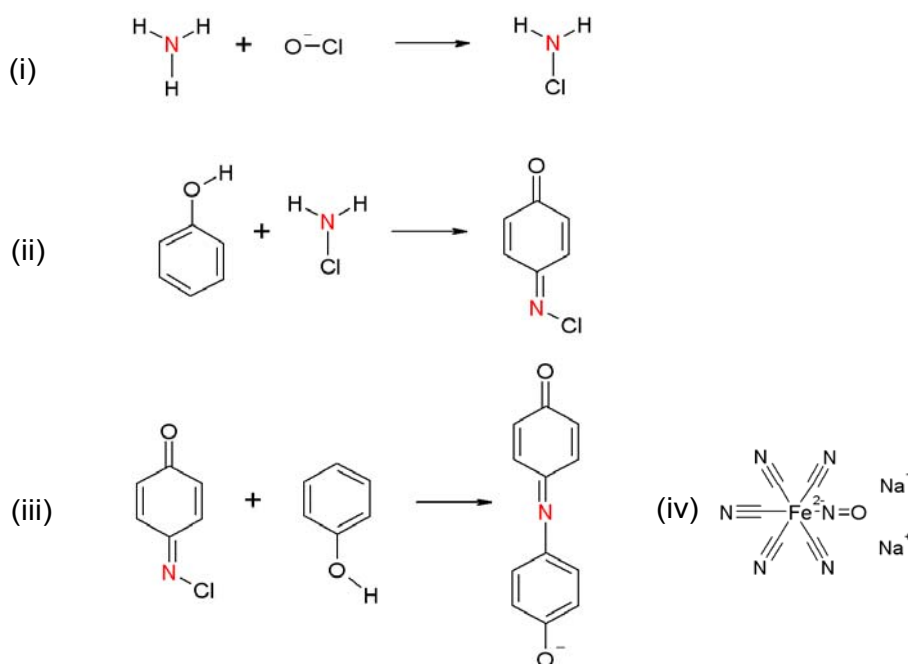
Figure 24: The proposed reaction mechanism for the Berthelot reaction consists of three steps: (i) ammonia reacts with hypochlorite to form monochloramine at basic pH, (ii) monochloramine reacts with a phenol to form benzoquinone chlorimine, (iii) benzoquinone chlorimine reacts with a second phenol to form an indophenol. (iv) Sodium nitroferricyanide (III) dihydrate is a coupling reagent which increases the kinetics of step (ii).

Building on the paradigm of home glucose monitoring, we seek to design a sensing material that can be incorporated into a new technology for home or bed-side point-of-care NH_3 monitoring. To accomplish this, the sensor must be inexpensive, reproducible, and robust. It must also be chemically sensitive, accurate, and capable of sensing very small volumes of capillary blood (20 μL). Finally, it must display information in a format that is easily interpreted.

Our NH_3 sensor is based on our previously developed PCCA photonic crystal sensing technology (**Figure 25**).[20-33] Our PCCAs utilize an array of highly charged

colloidal particles embedded in a hydrogel matrix. The array of particles Bragg diffracts light in the visible spectral region. Our molecular recognition agent, 3-aminophenol, is covalently attached to the hydrogel. The OCl^- and NH_3 react in the test solution to form monochloramine, which in turn reacts with two of the pendant 3-aminophenols to create a new cross-link in the hydrogel.

Figure 25: The formation of indophenol cross-links results in an increase in the elastic restoring force of the hydrogel, which actuates an osmotic pressure, forcing water out of the hydrogel and thereby decreasing the volume of the gel. As a result, the spacing between diffracting planes in the PCCA decreases, and the wavelength of diffracted light blue-shifts proportional to NH_3 concentration.

The formation of cross-links in the hydrogel matrix increases the elastic restoring force of the hydrogel network and actuates an osmotic pressure inside the gel which causes the hydrogel to shrink in proportion to the amount of NH_3 present in solution. This results in a decrease in the spacing between diffracting planes of the embedded colloidal array and a blue-shift in the wavelength of light diffracted by the sensor. Our NH_3 sensor relies upon changes in the elastic free-energy of the hydrogel caused by the formation of cross-links. The diffraction blue-shift can be directly correlated with the amount of NH_3 present in the analyte solution. We have also recently improved our modeling of these PCCA sensing volume phase transitions.[34]

The wavelength of light (λ_o) diffracted follows Bragg's law: $\lambda_o = 2\,nd\sin\theta$. In our sensor, the light is diffracted by the fcc 111 plane of the embedded particle array. λ_o depends on the plane spacing, d, the refractive index of the system, n, and the incident angle of the light, θ, which is the Bragg glancing angle. Since we are sampling back-diffraction (reflectance) from light normally incident to the 111 plane of the array, $\sin\theta$ is unity.

4.2.2 Experimental

PCCA Preparation

Figure 26 depicts the final product polymer backbone after synthesis and functionalization of the PCCA. 2-hydroxyethyl acrylate (2-HEA, 0.94 g, 8.1 mmol, Sigma), Poly(ethylene glycol-200) dimethacrylate (PEGDMA-200, 0.09 g, 0.25 mmol, Polysciences), glycidyl acrylate (GA, 0.04 g, 0.37 mmol, Sigma) and ethylene glycol (1.95 g, 31 mmol, J.T. Baker) were mixed and treated with Al_2O_3 in order to remove the inhibitor from the monomers. The mixture was centrifuged to separate the monomer from the Al_2O_3. 1.015 g of this solution was mixed with the colloid suspension (1.0 g, 5-10% w/w dispersion, polystyrene latex spheres, 110 nm). AG501-X8 (D) ion exchange resin ($\sim$ 0.1 g, 20-50 mesh, mixed bed, Bio-Rad) and 10 % diethoxyacetophenone (DEAP, 10 µL, 4 µmol, Aldrich) in DMSO (J.T. Baker) were mixed into the suspension in a 2-dr vial. After 15 min, the mixture was centrifuged to remove the ion-exchange resin and was injected between two quartz discs separated by a 125- µm thick Parafilm spacer. The colloidal particles self-assemble into a crystalline colloidal array (CCA), resulting in a

68

liquid film which diffracts light. The film was exposed to UV light (λ=365 nm) from mercury lamps (Blak Ray) for 3 hrs. A pHEA hydrogel network with PEGDMA cross-links forms around the CCA, resulting in a polymerized CCA (PCCA). The cell enclosing the hydrogel was opened in Nanopure water and the PCCA was allowed to equilibrate with water.
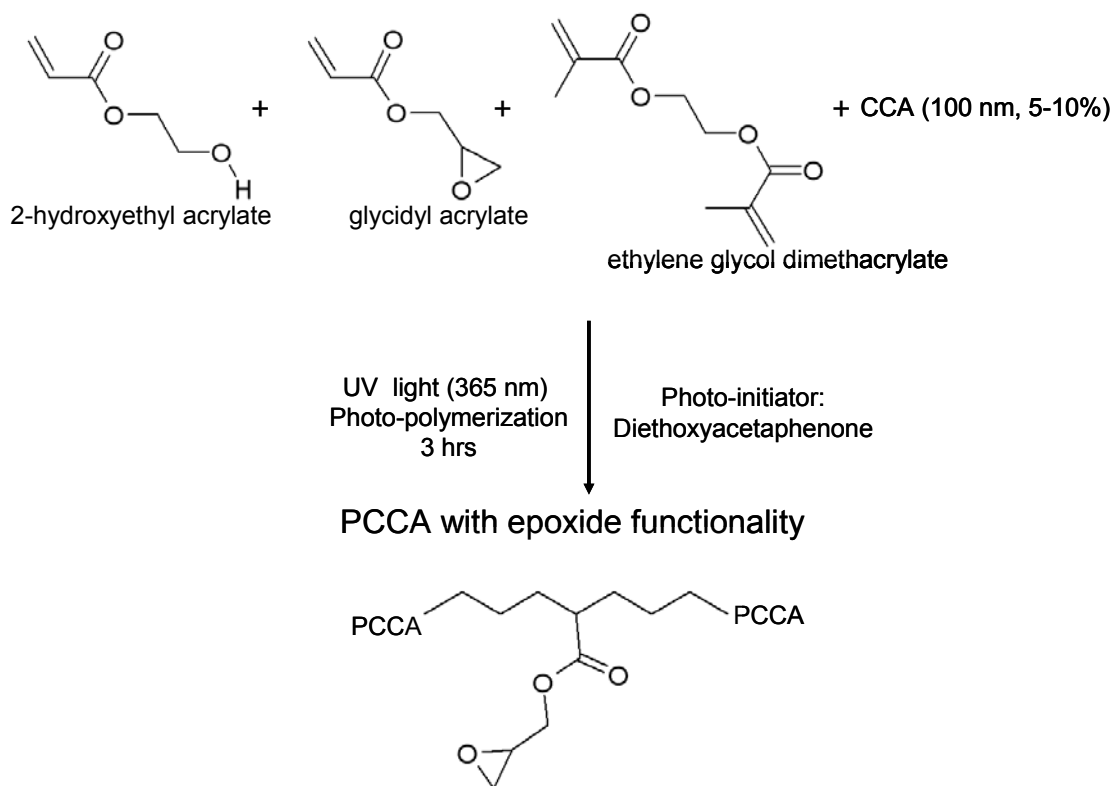
Figure 26: Preparation and functionalization of PCCA via epoxide ring opening with 3-aminophenol.

Attachment of 3-Aminophenol

The PCCA was placed into a 50 mM buffer solution (BBS, pH 9.2, J.T. Baker) to equilibrate before coupling. 0.5 g of 3-aminophenol (3-AMP, 4.6 mmol, Sigma) were dissolved in 10 ml DMSO (J.T. Baker) and then were diluted to 50 ml with 50 mM BBS.

The solution and PCCA were placed in a 125 ml plastic container (Nalgene) and were allowed to react for ~ 8 hours. After reacting, the PCCA was rinsed every hour for 6 hours with BBS. A blank gel (hydrogel without colloid) was prepared and functionalized according to the above protocol. UV-VIS spectra of the blank gel were measured by a Varian Cary 5000 UV-VIS spectrophotometer to confirm attachment of 3-AMP by monitoring the absorbance at $\lambda = 290$ nm.

Diffraction Measurements

The diffraction of the PCCA was monitored using a fiber-optic diode spectrometer with a tungsten halogen light source (Ocean Optics) using a reflectance probe. The light is completely diffracted by the first 10-20 μm thickness of the PCCA due to the high diffraction efficiency of the embedded CCA.[24]

A PCCA (1 cm x 1cm x 125 μm) was attached to a plastic Petri dish, and was equilibrated with 5 ml of 50 mM BBS containing sodium nitroferricyanide (III) dihydrate (Nitroprusside, NP, 0.0188 g, 0.0125 M, Aldrich). A standard NH_3 solution was prepared by dissolving 0.03 g NH_4Cl (5.6 mmol, J.T. Baker) in BBS and diluting to a total volume of 30 ml. A NaOCl solution was prepared by diluting 2.4 ml NaOCl (5% in H_2O, 1.8 μmol, J.T. Baker) in BBS to a total volume of 30 ml. An initial diffraction spectrum of the PCCA was collected, and then an aliquot of the stock NH_3 solution was added to each piece of PCCA. After allowing the NH_3 to equilibrate for 5 min., a 28 μl aliquot of the OCl⁻ solution was added. The diffraction spectra were recorded at pre-selected 5 min time intervals for a total of 120 min. The process was performed for NH_3 concentrations

of 30, 75, 150, and 300 μM NH_3, each solution contained 600 μM NaOCl. In a control measurement, a PCCA with 3-AMP attached was exposed to 600 μM NaOCl solution with no NH_3 present, and diffraction spectra were collected according to the above protocol.

The response of a PCCA, synthesized without GA or 3-AMP, was monitored to establish that the attached 3-AMP was responsible for the blue-shift observed. This PCCA was tested in 0 and 300 μM NH_3 solutions containing 600 μM NaOCl.

The response of the PCCA to NH_3 was also tested in a solution which was isotonic to physiological fluid (~ 150 mM NaCl) in order to determine whether salinity affects the response of the sensor. The response of the sensor to concentrations of 100, 200, and 300 μM NH_3 was determined according to the aforementioned protocol in solutions containing 50 mM BBS and 100 mM NaCl.

The sensor was tested in 5 ml of a 1:1 solution of BBS and male human serum from whole blood (Sigma). BBS (pH = 9.2) mixed with the serum resulted in a pH of 9.0. Four separate samples were spiked with concentrations of 30, 75, 150, and 300 μM NH_3. A fifth solution was not spiked, and was used in order to determine the spectral response generated from the NH_3 originally present in the sample. OCl^- was added to the solutions after equilibration (15 min), and diffraction spectra were recorded for 120 min. These five samples were also analyzed using a Vitros Chemistry Autoanalyzer System which uses the direct enzymatic determination.[9]

The sensor was tested in 5 ml solutions of BBS and Bovine Serum Albumin (BSA, 35 mg/ml in BBS, Sigma). The response of the sensor to the addition of OCl^- without NH_3 was determined.

4.2.3 Results and Discussion

The normal physiological range of NH_3 in capillary blood is 19-54 µg NH_3/ dL (11-32 µM NH_3) according to Tietz[2] or 31-122 µg NH_3/ dL (18-72 µM NH_3) according to Pesce.[3] The neurological manifestations of elevated blood NH_3 are expected above 250 µg NH_3/ dL (147 µM NH_3.[3] A sensor capable of determining the concentration of NH_3 from 10-300 µM NH_3 in blood would be a valuable asset to the medical community.

Figure 27 shows the manner in which the diffraction spectrum (measured as reflectance) changes over time for 300 µM NH_3 in BBS.
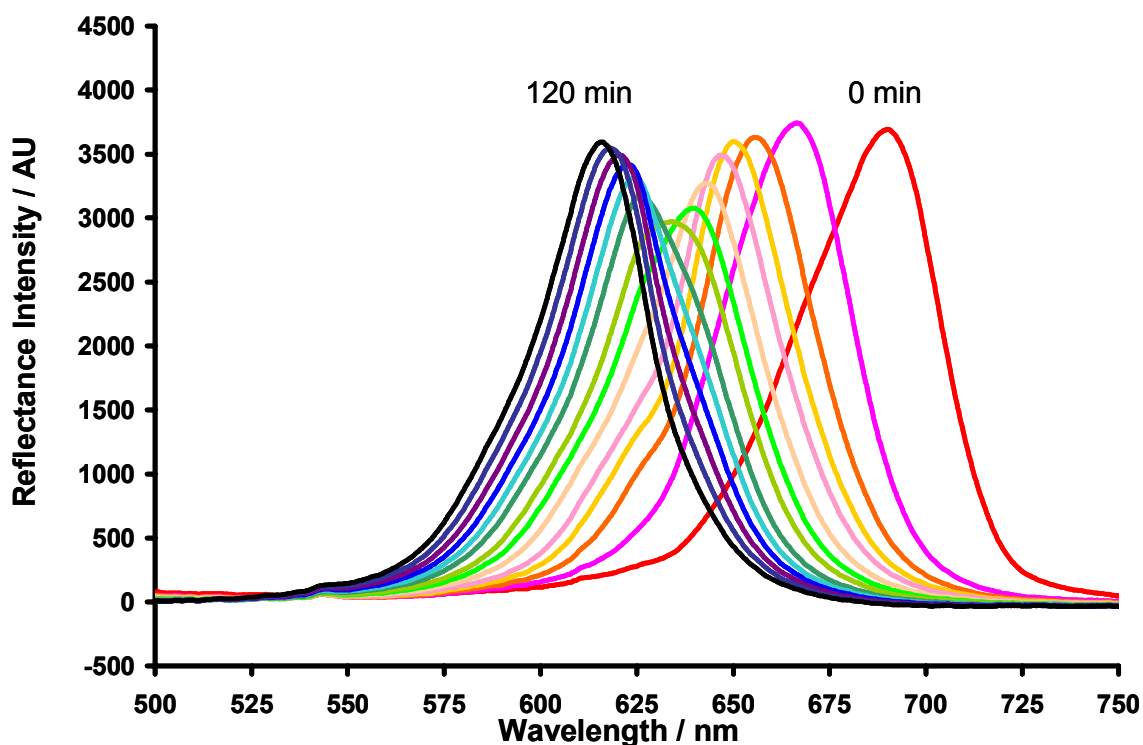
Figure 27: Diffraction spectra of PCCA in presence of 300 μM NH$_3$. The PCCA blue-shifts continuously over the course of 120 min as NH$_3$ reacts with OCl$^-$ and 3-AMP to form an indophenol species which cross-links the hydrogel.

The longest-wavelength diffraction peak ($\lambda_{\text{diffraction}}$ = 691 nm) corresponds to 0 min, directly after the addition of OCl$^-$. The shortest-wavelength diffraction peak ($\lambda_{\text{diffraction}}$ = 617 nm) corresponds to 120 min. The diffraction spectra shown were taken at 5 min intervals for the first 20 min and every 10 min thereafter. The sensor blue-shifts with time as the indophenol cross-links are formed. The change in the primary diffraction wavelength can be detected by a spectrometer, but it can also be observed visually.

Fig. 5 shows the diffraction blue-shift as a function of time for several concentrations of NH$_3$, as well as for a control with no NH$_3$ present. Each sample contained 600 μM OCl$^-$. The rate of blue-shift is faster for higher concentrations of NH$_3$. All samples containing NH$_3$ show diffraction blue-shifts. The control, which contains no NH$_3$, red-shifts.
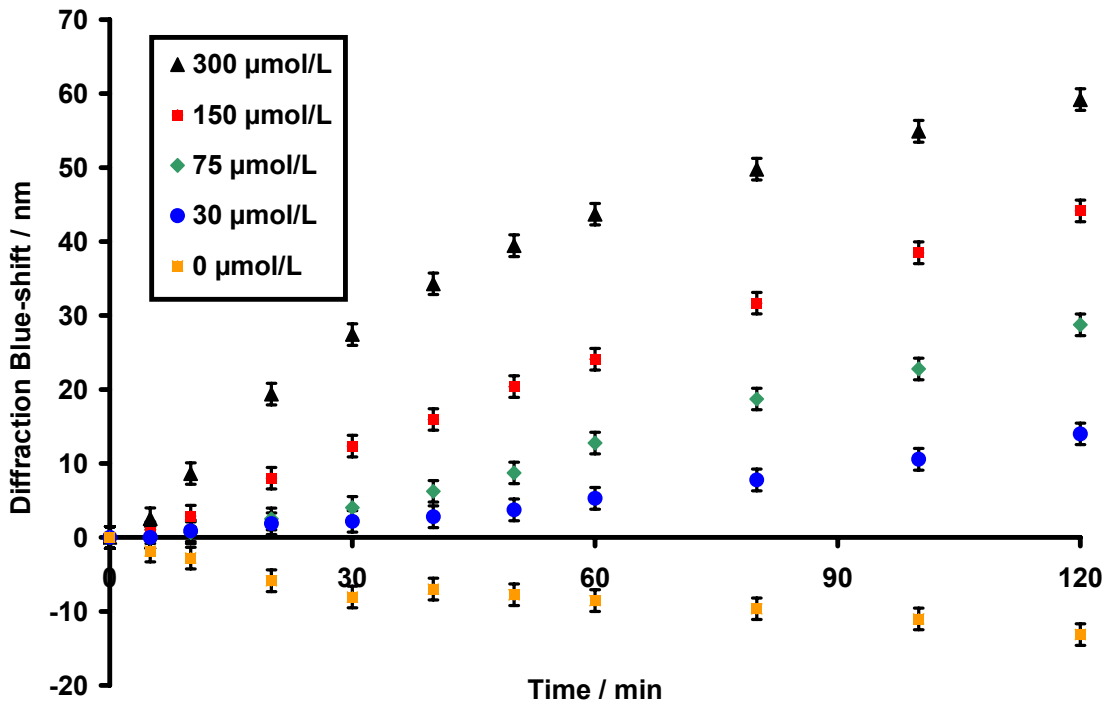
Figure 28: Diffraction blue-shift versus time for ammonia-sensing PCCA in BBS at pH 9.2 containing 600 μM OCl$^-$. The sensor displays distinctly different rates of diffraction shift for differing NH$_3$ concentrations; the control, containing no NH$_3$, actually red-shifts. The error bars are the average over the different time measurements of the standard deviation between replicate trials ($\lambda_{diffraction}$ = ± 1.46 nm, N = 3). The relative standard deviation remained fairly constant over time.

The lack of blue-shift in the control indicates that no cross-links are formed without NH_3 present. The diffraction red-shift is presumably caused by the hydrolysis of the poly(ethylene glycol) cross-links esters at basic pH; this decreases the elastic restoring force of the PCCA and causes the hydrogel to expand. Since the red-shift is accelerated in the presence of OCl^-, we presume the OCl^- accelerates the hydrolysis of the cross-link esters. Our hypothesis that the cross-link ester groups are being hydrolyzed is confirmed by observing an un-functionalized PCCA (no GA or 3-AMP) swell upon addition of $OCl.^-$ The extent and rate of red-shift was independent of the presence of 3-AMP. **Figure 29** shows the NH_3 response calibration curves constructed from the observed shifts at 60 and 120 min in 50 mM BBS. The curve has been corrected by subtracting the red-shift of the control from each spiked sample.
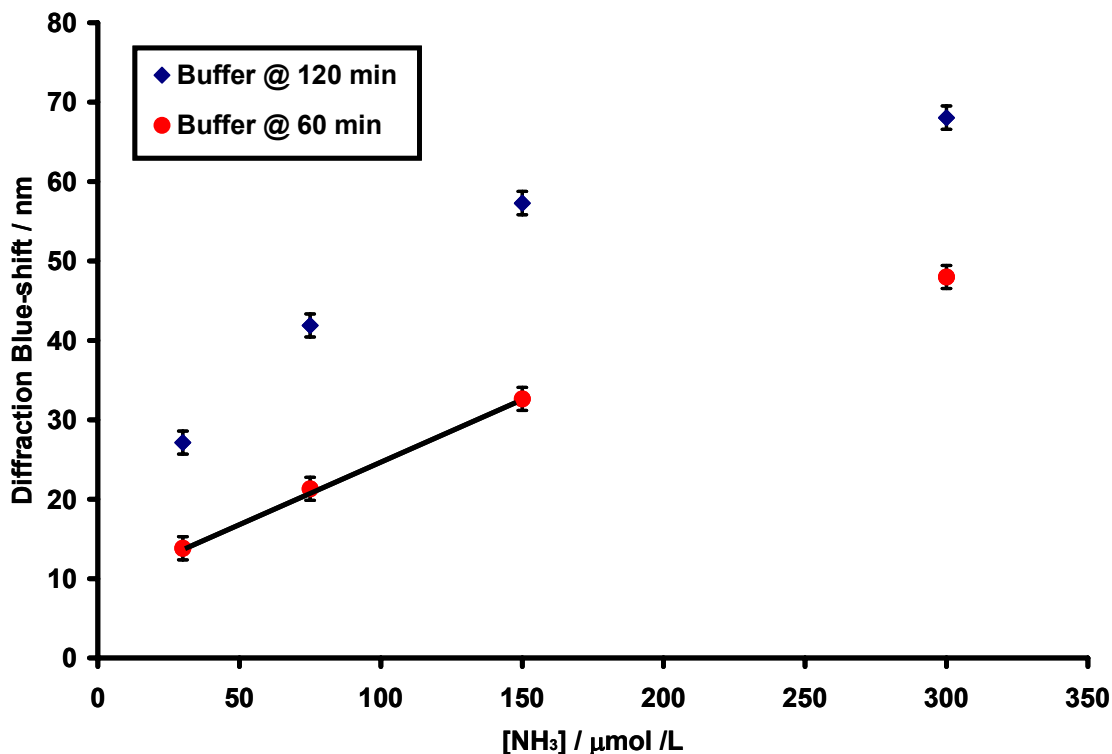
Figure 29: Calibration curve based on the response of our sensor to NH$_3$ in BBS (pH=9.2) containing 600 μM OCl$^-$ at 60 and 120 min. This sensor shows a linear response between 30 and 150 μM NH$_3$ at 60 min.

The response of the sensor is linear at 60 min for NH$_3$ concentrations between 30 and 150 μM, but begins to saturate at NH$_3$ concentrations greater than 150 μM. The response is curvelinear at longer times. The deviation from linearity presumably occurs because the concentrations of available OCl$^-$ and 3-AMP are depleted as the reaction proceeds. This effect is exacerbated at longer time intervals and higher NH$_3$ concentrations. At low concentrations of NH$_3$, the 3-AMP and OCl$^-$ concentrations are present in sufficient excess such that the rate depends mainly on the concentration of NH$_3$. Harfmann and Crouch previously established that the Berthelot reaction is first order with respect to the NH$_3$ when the OCl$^-$ and phenol are in excess.[35] The linear region

of the 60 min calibration was used to calculate a detection limit. This limit was found to be 27 μM NH_3 at a signal to noise ratio of 3/1.

We examined the dependence of response on ionic strength. We utilized samples which were isotonic with serum and which had a salt concentration of 150 mM NaCl. The rate and response was indistinguishable from the behavior of our sensor in 50 mM BBS. These results confirm that the sensing mechanism is not affected by high ionic strength and that the volume change is essentially independent of the ionic free energy of the system.

Sensor Response to NH_3 in Serum

We also examined the response of our sensor to samples in diluted human blood serum. The serum presents a more complex sensing medium than BBS due to the presence of salts, amino acids, and proteins. Although we seek to develop a sensor which works in whole blood, we are first testing our sensor in serum to avoid the errors associated with the generation of NH_3 in stored whole blood.[10] RBCs contain enzymes that can increase the concentration of NH_3 with time after the blood is drawn. This rapidly raises the level of NH_3 in the samples to hyper-physiological levels.

Figure 30 displays the diffraction blue-shift as a function of time for four spiked serum samples (30, 75, 150, 300 μM NH_3 spikes) as well as the normal, unspiked, sample.
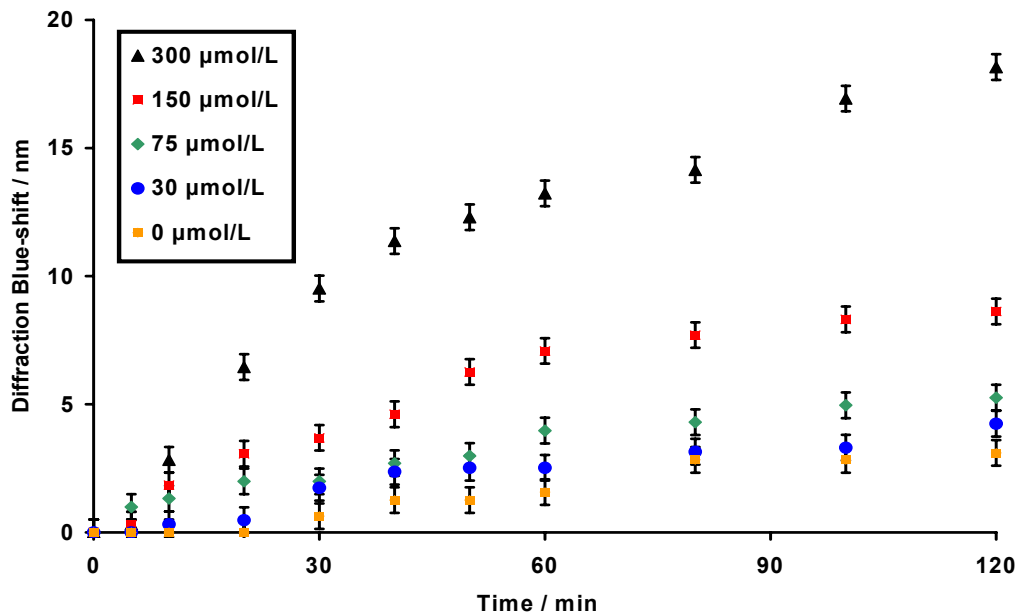
Figure 30: We measured the PCCA response of four spiked serum samples and an un-spiked sample. All samples contained 600 µM OCl⁻ and had a pH of 9. We found the serum contains NH_3 on the order of the physiological concentration for healthy adults. The error bars are the average of the standard deviation between replicate trials ($\lambda_{diffraction}$ = ± 0.57 nm, N = 3).

Unlike the buffer, normal human serum contains a background level of NH_3. To determine the concentration of NH_3 in our unspiked sample, we used a Vitros 950 Chemistry System, the clinical instrument utilized by the University of Pittsburgh Medical Center. According to the Vitros determination, our normal serum solution had a background concentration of 4 µM NH_3.

The most remarkable difference between the sensor in buffer and in serum is the response to low NH_3 concentrations. In buffer without NH_3, the sensor responds to the addition of OCl⁻ by red-shifting $\Delta\lambda$ = 14 nm. In the normal serum solution containing only 4 µM NH_3, the sensor responds to the addition of OCl⁻ by blue-shifting $\Delta\lambda$ = 3 nm. We established that proteins were responsible for the blue-shift by analyzing an

ammonia-free protein-rich solution of BSA (70 mg BSA/ml in BBS). The sensor also responded with a slight blue-shift ($\Delta\lambda$= 3 nm) in the two hours following the OCl$^-$ addition. We conclude the proteins in the serum are primarily responsible for the blue-shift in the unspiked serum.

Our observations correlate well with the Hawkins et al.[36,37] description of the reactivity of OCl$^-$ towards proteins. They showed that OCl$^-$ modifies the amino-acid side-chains without significant degradation to the protein backbone at low OCl$^-$ concentrations. Interactions of this type would result in a reduction of the available OCl$^-$ which would reduce the kinetics and extent of the reaction between OCl$^-$ and NH$_3$. While slow compared to the reaction with NH$_3$, the products of reactions between OCl$^-$ and serum proteins could react further with the 3-AMP species on the hydrogel to cause the slight blue-shift observed.

The diminished response observed in serum can be explained by previous studies, which report that the Berthelot reaction is subject to interference from proteins.[18] Ngo et al.[19] found that a solution containing 0.1% human serum caused an interference of 4%. The manifestations of this interference are obvious in our sensor as the response rate and the spectral window are both decreased by a factor of three in 50% human serum solution. Despite the interference, we were able to establish a calibration curve for the spectral shift in response to the NH$_3$ concentration in serum. **Figure 31** shows the calibration curve of the sensor's response to NH$_3$ at 60 min.
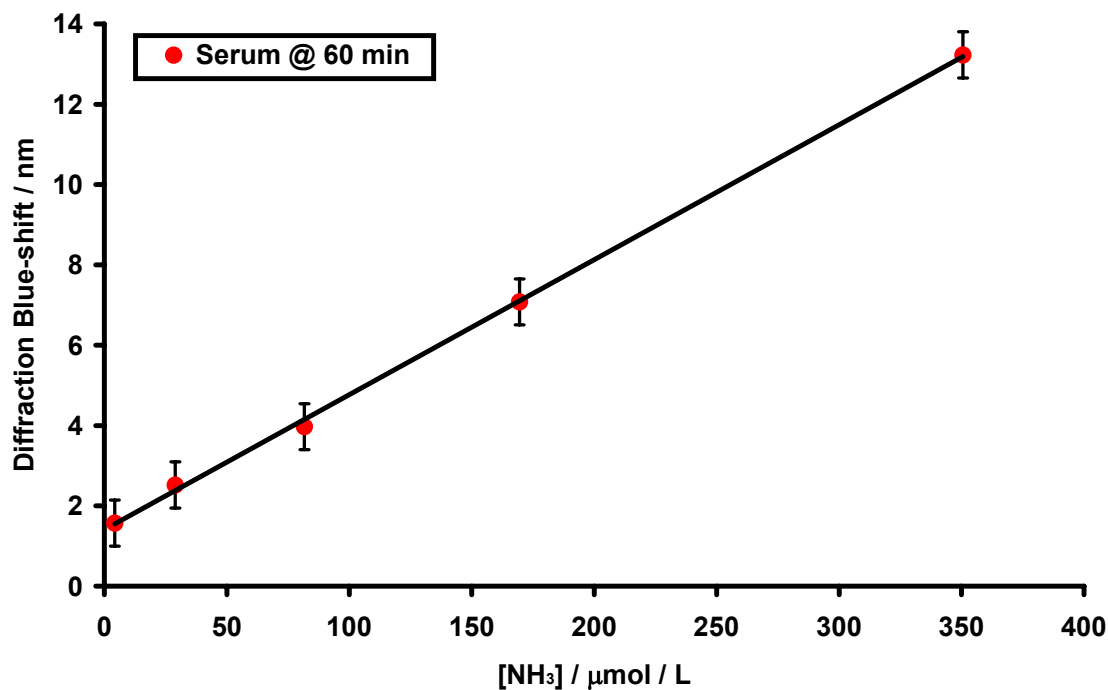
Figure 31: Calibration curve for the response of our sensor to NH$_3$ in a 1:1 solution of serum and BBS at 60 min. Concentrations of NH$_3$ were determined using the Vitros Autoanalyzer. Error bars are equal to the standard deviation ($\lambda_{\text{diffraction}} = \pm 0.57$ nm, N = 3).

The response of the sensor is linear for concentrations of NH$_3$ between 0 − 350 μM. We determined that the detection limit for our sensor was 50 μM NH$_3$ at 60 min, and increases to 60 μM NH$_3$ at 120 min. The detection limit was determined from three times the standard deviation of our control (λ= 0.57 nm). The detection limit for the observed blue-shift (λ= 3.12 nm) was used to calculate the NH$_3$ detection limit utilizing the linear regression. The increase in detection limit with time is due to the increase in the standard deviation of our spectral shifts at longer times and higher concentrations. The detection limit would also be increased at smaller times as the slope of the response versus concentration increases over time. The NH$_3$ present in the unspiked serum is below the detection limit of our sensor and cannot be distinguished from a serum sample

containing no NH$_3$. Furthermore, the 30 μM spiked sample cannot be distinguished from the unspiked sample at the >99% confidence level. **Table 1** compares our sensor with current standards in clinical NH$_3$ sensing.

Clinical Reference Interval	10 - 300 μM NH$_3$
Ammonia Sensitive PCCA	50 – 350 μM NH$_3$
Vitros 950 Chemistry Analyzer	1.0 – 500 μM NH$_3$

Table 1: Comparison of clinical reference interval with PCCA and Vitros NH$_3$ methods.

4.2.4 Conclusions

In the work described here, we devised an NH$_3$ sensitive material in which we utilize the Berthelot reaction in our Polymerized Crystalline Colloidal Array (PCCA) sensing platform. Our material has the capability to quantitatively determine NH$_3$ concentrations between 50 and 350 μM NH$_3$ in human blood serum which brackets the clinically relevant interval. The material responds to 300 μM NH$_3$ additions with a spectral blue-shift of $\Delta\lambda$= 60 nm in BBS and $\Delta\lambda$= 20 nm in serum solution at 120 min. The detection limit is 27 μM NH$_3$ in BBS at 60 min and 50 μM NH$_3$ in 50% serum solution at 60 min with a confidence level of >99%.

Future Work and Outlook

We are currently optimizing our reaction conditions, sample preparation, and hydrogel composition to improve sensitivity, spectral shift, and response time. We anticipate that our technology could be engineered to combine separation and detection into a single system through modification of the diffusion characteristics of our hydrogel

or by utilizing our material's thin film morphology, which could be incorporated into a more complex sensing device. Separation of NH_3 from the sample would prevent interferences (RBCs, proteins, clotting, etc.) from affecting the sensor's performance.

The goal of our optimization is to develop a sensor responsive to NH_3 concentrations over the clinically relevant interval with distinct visual color changes. Our sensor could then be used as a point-of-care device for the detection of blood NH_3 concentrations to monitor conditions deriving from urea cycle disorders, organic acidemias, fatty acid oxidation defects, and hepatic disorders in order to prevent patients from reaching hyperammonemic states. The ability to monitor these conditions at the bedside or at home with an inexpensive, robust system would provide long-term benefits to both patients and health care providers.

4.2.5 Acknowledgments

References

1. Huizenga, J.R.; Gips, C.H.; Tangerman, A. *Ann. Clin. Biochem.* **1996***, 33, 23.

2. Tietz, N.W. *Clinical Laboratory Guide to Laboratory Tests, 3rd Ed.* **1995,** WB Saunders, Philadelphia.

3. Pesce, A.J.; and Kaplan, L.A. *Methods in Clinical Chemistry,* **1987,** CV Mosby Company, St. Louis, MO.

4. Hazell, A.S.; and Butterworth, R.F. Exp. Biol. and Med. 1999, *222*, 99.

5. Campion, M. *Blood Ammonia: a critical measurement,* **2003**, in BIMDG Bulletin Spring 13.

6. Bachmann, C. *Eur. J. Pediatr.* **2003**, *162,* S29.

7. Mondzac, A.; Ehrlich, G.E.; and Seegmiller, J.E. *J. Lab. Clin. Med.* **1965**, *66,* 526.

8. Van Anken, H.C.; Schiphorst, M.E. *A. Clin. Chim. Acta.* **1974**, *56,*151.

9. Bostian, K.A., and Betts, G.F. *Biochem. Journal* **1978**, *173*, 773.

10. Huizenga, J.R.; Tangerman, A.; Gips, C.H. *Ann. Clin. Biochem.***1994**, *31,* 529.

11. Mann, L.T. *Anal. Chem.* **1963**, *35*, 2179.

12. Reay, P.F. *Anal. Chim. Acta.* **1985**, *176*, 275.

13. Lau, K.T.; Edwards, S.; and Diamond, D. *Sens. Actuators B.* **2004**, *98,* 12.

14. Daridon et al. *Sens. Actuators B.* **2001**, *76,* 235.

15. Zellmer, S.; Katenborn, G.; Rothe, U.; Lehnich, H.; Lasch, J.; and Pauer, H.D. *Anal. Biochem.* **1999**, *273*, 163.

16. Berthelot, M. Repert. Chim. Appl. **1859**, *1*, 284.

17. Searle, P.L. *Analyst,* **1984**, *109*, 549.

18. Gips, C.H.; and Reitsma, A. *Clin. Chim. Acta* **1971**, *33*, 257.

19. Ngo, T.T.; Phan, A.P.H.; Yam, C.F. and Lenhoff, H.M. *Anal. Chem.* **1982**, *54*, 46.

20. Krieger, I.M.; and O'Neill, F.M. *J. Am. Chem. Soc.* **1968**, *90*, 3114.

21. Hiltner, P.A.; and Krieger, I.M. *J. Phys. Chem.* **1969**, *73*, 2386.

22. Hiltner, P.A.; Papir, Y.S.; and Krieger, I.M. *J. Phys. Chem.* **1971**, *75*, 1881.

23. Carlson, R.J.; and Asher, S.A. *Appl. Spec.* **1984**, *38*, 297.

24. Runquist, P.A.; Photinos, P.; Jagannathan, S.; and Asher, S.A. *J. Chem. Phys.* **1989**, *91*, 4932.

25. Asher, S.A.; Holtz, J.H.; Liu, L.; and Wu, Z. *J. Am. Chem. Soc.* **1994**, *116*, 4997.

26. Weissman, J.M.; Sunkara, H.B. Tse, A.S.; and Asher, S.A. *Science,* **1996**, *274*, 959.

27. Ito, K.; Nakamura, H.; and Ise, N. *J. Chem. Phys.* **1986**, *85*, 6136.

28. Monovoukas, Y.; and Gast, A.P. *J. Colloid Interface Sci.* **1989**, *128*, 533.

29. Okubo, T. *Acc. Chem. Res.* **1988**, *21*, 281.

30. Asher, S.A. U.S. Patents 4,627,689 (**1986**), 4,632,517 (**1986**), 5,281,370 (**1994**), 5,452,123 (**1995**).

31. Holtz, J.H.; and Asher, S.A. *Nature* **1997**, *389*, 829.

32. Holtz, J.H.; Holtz, J.S.; Munro, C.; and Asher, S.A. *Anal. Chem.* **1998**, *70*, 780.

33. Pan, G.; Kesavamoorthy, R.; and Asher, S.A. *J. Am. Chem. Soc.* **1998**, *120*, 6525.

34. Goponenko, A.V.; and Asher, S.A. *J. Am. Chem. Soc.* **2005**, *127,* 10753.

35. Harfmann, R.G.; and Crouch, S.R. *Talanta.* **1989**, *36*, 221.

36. Davies, M.J. *Biochim. Biophys. Acta.* **2005**, *93,* 1703.

37. Hawkins, C.L.; Pattison, D.I.; and Davies, M.J. *Amino Acids* **2003**, *25*, 259.

CHAPTER 5: PVA Thermo-reversible Gelation Hydrogel Photonic Crystals

5.1 The Synthesis of Thermo-reversible Gelation Hydrogels with an Embedded Crystalline Colloidal Array

By *Kyle W. Kimble, Jeremy P. Walker, and Sanford A. Asher*

Abstract:

We describe here the utilization of thermo-reversible gelation (TG) to embed a crystalline colloidal array (CCA) within a poly(vinyl alcohol) (PVA) hydrogel to form a thermo-reversibly gelled crystalline colloidal array (TGCCA). The TG hydrogel is a physically cross-linked network formed by a process somewhat similar to the well-known freeze-thaw process, which does not involve freezing the solvent. The TGCCA diffraction is similar to that of our previously developed photo-polymerized PCCA. The TGCCA can be irreversibly covalently cross-linked using glutaraldehyde. We demonstrated that the cross-linked TGCCA can be made responsive to chemical stimuli by functionalizing the hydrogel hydroxyl groups. We monitored diffraction of carboxyl or amine functionalized TGCCA as a function of the pH and found diffraction wavelengths titrate with the pK_a of the functional group. We also demonstrated TGCCA can be inexpensively fabricated in arbitrarily large volumes and shapes.

5.1.1 Introduction

We describe here the utilization of thermo-reversible gelation (TG) to embed a crystalline colloidal array (CCA) within a poly(vinyl alcohol) (PVA) hydrogel to form a thermo-reversibly gelled crystalline colloidal array (TGCCA). The TG hydrogel is a physically cross-linked network formed by a process somewhat similar to the well-known freeze-thaw process, which does not involve freezing the solvent.

TGCCA have similar diffraction properties to our previously reported polymerized CCA (PCCA) materials.[1] The simplicity of the synthetic process broadens the range of PCCA-based materials which can now be synthesized. The thermo-reversibility enables the synthesis of interpenetrated polymer network CCA-based

materials where the original hydrogel can be completely removed. It also enables the synthesis of CCA-based materials containing UV and free-radical sensitive chemical groups.

PCCA have been utilized for applications ranging from biosensors[2] to optical filters.[3] They appear brightly colored because the highly charged colloidal particles self-assemble into ordered fcc arrays which Bragg diffract visible light. The wavelength of the diffracted light depends on the spacing of the fcc crystal lattice.

Our original motivation for exploring thermo-reversible hydrogels stems from a need to develop nitrogen-free and low polymer content (<10%) hydrogels that are stable against oxidation and hydrolysis for use as ammonia sensors.[4] PVA hydrogels possess these properties and, additionally, are non-toxic, mechanically robust, and elastic. PVA is inexpensive, safe, biocompatible and already used for *in vivo* applications.[5] PVA hydrogels have recently shown promise for the development of artificial tissues, contact lenses, implantable devices, and as vehicles for drug delivery.[6]

PVA hydrogels have been made through covalently or physically cross-linking PVA polymer solutions. PVA hydrogels have been covalently cross-linked with dialdehydes, gamma-radiation, or the polymerization of PVA macromers.[7] Physically cross-linked PVA hydrogels have typically been made through the well-known freeze-thaw process.[8] In a deviation from the freeze-thaw process, Hyon *et al.* described the preparation of transparent PVA hydrogels from mixed solutions of DMSO and water

without freezing the solvents.[9] In their procedure, PVA was dissolved and poured into a mold at 90°C and the temperature lowered to -20°C. They found optically clear hydrogels formed at the appropriate compositions (PVA concentrations, solvent compositions, and cooling rates) from the cooled liquid.[10] Hydrogels made in non-frozen solvent conditions have been called psychrotrophic gels (from psychria meaning chill); however, this terminology has not been generally adopted. These hydrogels are formed through the homogeneous formation of nano-crystallites throughout the solution.

The psychrotrophic hydrogels developed by Hyon et al. differ substantially from the cryogels made through the better-known freeze-thaw process. A cryogel forms as the solvent freezes and the PVA is concentrated into the non-frozen regions of the solution. The concentration of PVA in the non-frozen regions increases and the PVA crystallizes. The structure of the PVA cryogel is determined by the crystallization of the liquid. They typically appear turbid because the 3-D crystalline polymer network contains large channels formed by the frozen liquid. In contrast, psychrotropic gels are formed through spinodal decomposition. The solution is super-saturated due to the low temperature and unfavorable solvent conditions (cononsolvency) and becomes unstable against infinitesimal fluctuations in composition. The nano-crysallites of PVA form as the solution spontaneously separates into two phases.

The TGCCA synthesized here are optically similar to our previously developed photo-polymerized PCCA. However, the hydrogel can be melted by increasing the temperature. We also demonstrate that the TGCCA can be made thermally stabilized by

utilizing simple dialdehyde cross-linking. The cross-linked TGCCA can be made responsive to chemical stimuli by functionalizing the hydrogel. This expands the chemical and physical properties of PCCA photonic crystal materials.

5.1.2 Experimental

PCCA Preparation.

A typical preparation of a TGCCA involves mixing a solution of poly(vinyl alcohol) (Polysciences, 98 mole % hydrolyzed, MW ~78,000) 5% (w/w) in dimethylsulfoxide (DMSO, Fisher) with the crystalline colloidal array (CCA) solution. The CCA solution contains monodisperse cross-linked polystyrene colloidal particles (110 nm, 10% w/w in water) whose synthesis was previously reported.[11] After adding the PVA solution to the CCA solution, ion-exchange resin (Bio-Rad AG 501-X8 (D) Resin) is added and the mixture agitated until strong diffraction is visually evident (2 min.). The ion-exchange resin is removed from the solution through centrifugation and the TGCCA precursor solution is poured or injected into a cell and the temperature lowered. After 2 hours at −20 ^{o}C, the solvent remains unfrozen, but the TGCCA has gelled and can be removed from the cell.

The rectangular sample shown in **Figure 32** was made by placing a 0.5 ml drop of the TGCCA precursor solution between two square glass plates separated by a 100 μm polyester spacer. When the plates were forced together, the precursor solutions spreads evenly throughout the cell and the excess solution is forced from the cell edges.
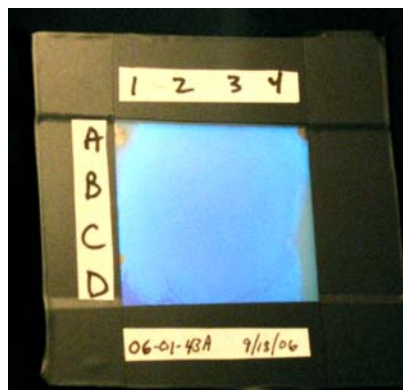
Figure 32: A 3 cm x 3 cm TGCCA was fabricated between glass plates by using a 100 μm thick polyester spacer to separate the TGCCA from the adhesive used to seal the edges of the glass plates. The cell was divided into sixteen 9 mm square regions (A1 – D4) that were analyzed via UV-Vis transmission spectroscopy with a 5 mm diameter aperture.

The glass and quartz plates were cleaned prior to use by soaking in 1 M NaOH (Fisher), with subsequent rinsing with water, acetone (EM Science), and methanol (EM Science). After drying in an oven at 140 $^{\circ}$C, SigmaCote (Sigma) was pipetted onto the warm surface and allowed to evaporate. SigmaCote is a solution of a chlorinated organopolysiloxane in heptane which reacts with surface silanol groups on glass to produce a neutral, hydrophobic, microscopically thin film.[12] The glassware was placed back in the oven at 140 $^{\circ}$C for 20 minutes and, after cooling, rinsed with methanol.

Diffraction and Transmission Measurements.

The backscattered diffraction from a TGCCA was monitored using a fiber-optic diode spectrometer with a tungsten halogen light source (Ocean Optics) and a reflectance probe. The diffraction spectra in **Figure 33** were measured by contacting the fiber optic probe against the glass wall.

The relationship between the diffracted wavelength of light (λ_o) and the lattice spacing closely follows Bragg's law:

$$\lambda_o = 2 \, nd \sin \theta, \quad \textbf{Equation 1}.$$

We utilize back-diffracted light normal to the PCCA surface to characterize the lattice spacing and the volume of the hydrogel. The diffracted wavelength in air, λ_o, depends on the diffracting plane spacing, d, and the refractive index of the system, n. The reflectance from the PCCA is observed normal to the surface ($\theta = 90^o$).

UV-VIS transmission spectra were measured by a Varian Cary 5000 UV-VIS spectrophotometer. Only planar samples with thicknesses of less than 300 μm were examined utilizing transmission measurements. These samples were measured while contained within the glass or quartz plates in which they were prepared. Samples were measured within 1 day of preparation. Locations on the samples were labeled in a grid pattern. Each region of the grid was analyzed independently utilizing a 5 mm round aperture. The spectrometer was run in dual beam mode. The reference beam passed through a cell prepared in an identical manner to those utilized for the TGCCA, but filled with 18 MΩ water.
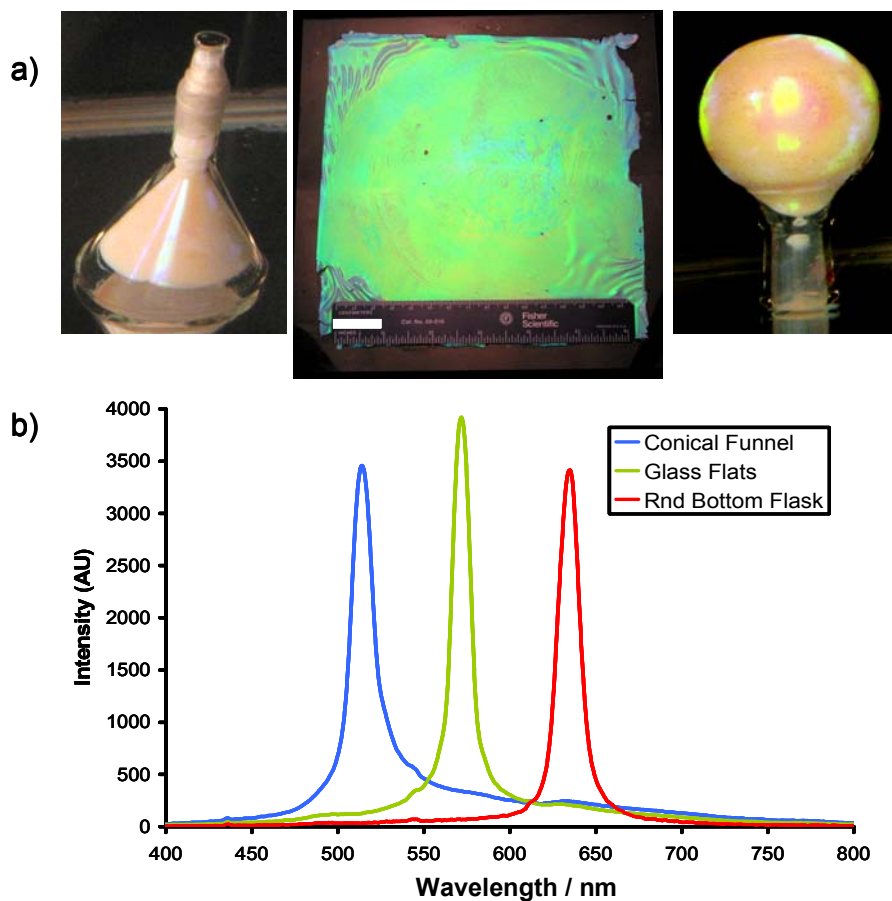
Figure 33: a) A conical funnel, glass plates and a round bottom flask containing the fabricated TGCCA. The planar 16 cm x 16 cm sample shown has a thickness of 500 μm. Included for reference is a 15 cm ruler and a 25 mm scale-bar. The TGCCA in the round bottom flask and funnel have volumes of 50 ml. b) Reflectance spectra from each TGCCA.

Transmission Electron Microscopy of PVA layer.

A 6% solution of 180 nm colloidal particles was mixed with a 5% solution of 78,000 MW PVA in DMSO. The solution was mixed by turning it end-over-end for two hours. A drop of this solution was diluted to 3 mL in a 50% DMSO and water solution and dried on a 75 mesh 3.0 mm O.D. copper TEM grid (Ted Pella). The sample was placed in a vacuum oven at 40 $^{\circ}$C for 2 hours under reduced pressure. The micrograph

was taken with a Jeol JEM-1400 using an accelerating voltage of 80 kV and a magnification of 180,000.

Testing Thermal Reversibility.

A TGCCA was fabricated between a set of cleaned glass plates (6 cm x 6 cm). A 5 mm wide polyester film spacer (~ 100 μm thick, Grafix, Inc.) was cut so as to contain a 36 mm x 36 mm x 100 μm PCCA. This spacer was placed between the plates to provide a uniform TGCCA thickness and to separate the TGCCA precursor solution from the adhesive used to seal the edge of the cell (Instant Krazy Glue, Elmer). The TGCCA precursor was placed in the cell and the cell closed. Excess precursor solution was drawn out of the spacer region by utilizing a Kim-Wipe. After the spacer region had dried, adhesive was added to the edge of the cell and capillary action drew the adhesive into the spacer region. After the adhesive had set, the cell was placed at −20 ^{o}C for 2 hours to gel the sample. The gel was then placed in an oven at 85 ^{o}C for 30 minutes to cause the TGCCA to melt. Melting was confirmed by movement of an air bubble trapped in the cell.

Formation of Covalent Cross-links.

A 40 mL solution of 50% DMSO and water was added to a 125 mL Nalgene straight-side wide-mouth jar. 0.6 ml glutaraldehyde solution (Sigma, Grade II, 25%) and 0.4 ml of concentrated sulfuric acid (J.T. Baker) were then added. A 3 cm x 3 cm (250 μm thick) TGCCA sample was cut into 16 pieces with a razor blade and placed in the

92

Nalgene jar. To quench the reaction, TGCCA pieces were removed and immersed in gently stirred pure water. The bath water was replaced after 5 min.

Conjugation of Carboxylic Acid.

A covalently cross-linked TGCCA was exchanged from pure water to pure DMSO through a gradient with steps at 25%, 50%, 75%, and 100% DMSO. After 2 hours in each solution, the TGCCA was transferred into the more concentrated DMSO solution.   The 100% DMSO solution (200 ml) was replaced 3 times, with 2 hour equilibration times. The TGCCA was placed into a 40 ml solution of DMSO containing 0.22 g of succinic anhydride (Sigma). The reaction was allowed to proceed for 2 hours at room temperature prior to rinsing with DMSO. The TGCCA was then solvent exchanged through the DMSO/water gradient to pure water. Diffraction spectra were taken with a reflectance probe as the carboxylated TGCCA was titrated with 20 mM HCl (Fisher) solution in the presence of 150 mM NaCl. The 20 mM HCl solution was added drop-wise. The pH of the solution was monitored as acid was added. After each addition of acid, the TGCCA was allowed to equilibrate, a spectrum was taken, and the pH recorded.

Conjugation of 3-aminophenol.

0.5 g of 3-aminophenol (3-AMP, 4.6 mmol, Sigma) was dissolved in 10 ml of DMSO (J.T. Baker) and then diluted to 50 ml with 50 mM phosphate buffer solution (PBS, Pierce Biotechnology). The TGCCA was incubated for 4 hours in the 3-AMP solution. 0.5 g of 1-ethyl-3-(3-dimethylaminopropyl) carbodiimide hydrochloride (EDC, 0.52 mmol, Pierce Biotechnology) was dissolved into the solution containing the TGCCA

and the reaction was allowed to proceed for 2 hrs. The 3-AMP functionalized PCCA was rinsed repeatedly with a 150 mM NaCl (J.T. Baker) solution and titrated as above except utilizing 20 mM NaOH (Fisher).

5.1.3 Results and Discussion

TGCCA formed through the thermo-reversible gelation process can be made much thicker than photo-polymerized PCCA because the thickness attainable through UV photo-polymerization is limited by the optical density of the PCCA precursor solution. Particles which strongly scatter or absorb UV light prevent initiation of the free-radical polymerization deep within the hydrogel. Furthermore, the thermo-reversible approach allows the use of photo-chemically unstable molecules to be incorporated within the TGCCA during synthesis.

Another benefit of the TGCCA synthetic process is that it does not require the specialized quartz containers required by the UV photo-polymerization process. The TGCCA shown in **Figure 33** were made in standard laboratory glassware, TGCCA can also be fabricated inside plastic and metal molds.

The feasibility of preparing thick TGCCA is shown in **Figure 33**. Each TGCCA has a volume of 50 ml, about 100-fold larger than typically prepared PCCA (0.5 ml). The samples' iridescence results from the back-diffraction of light by the fcc 111 crystal lattice of the embedded CCA. **Figure 33b** shows the characteristic back diffraction spectra of the TGCCA. The diffracted wavelength of each TGCCA differs because they

were prepared at different colloid concentrations. The lattice spacing and consequently

the diffraction wavelength is controlled by the concentration of the colloidal particles.

Figure 34 shows the reflectance spectra of a series of TGCCA made in plastic cuvettes at

various colloid concentrations. Obviously, the diffracted wavelength can span the entire

visible spectrum.
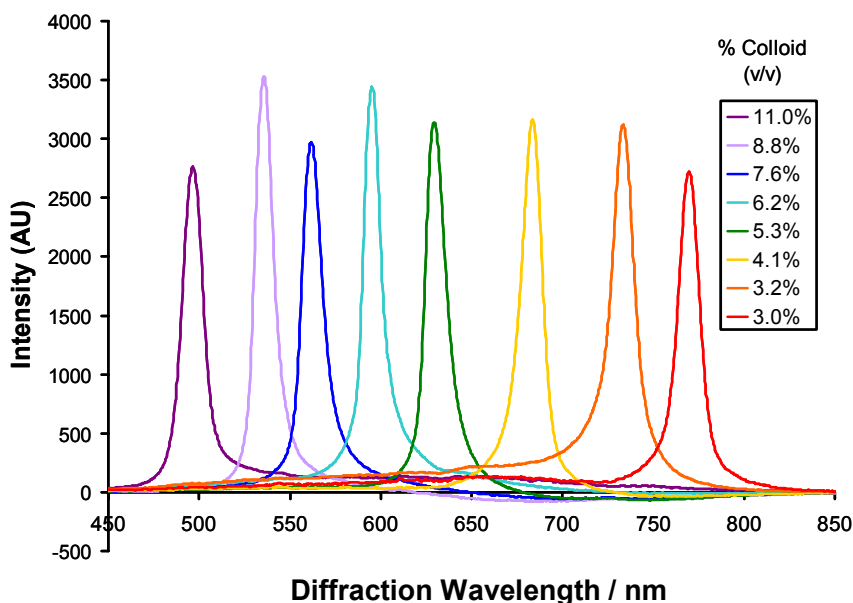
**Figure 34: TGCCA made with 5% 78 KD PVA and 110 nm diameter particles diffract
different wavelengths of light depending on the colloid concentration. TGCCA materials
can be made which diffract anywhere in the visible spectrum by controlling the colloid
concentration.**

DMSO Enables the Embedding of Colloidal Particles

The role of each component within the TGCCA precursor solution was examined

by thermally cycling compositions which lacked one or more of the components

necessary for fabricating a TGCCA. The following table describes the composition of

the samples shown in **Figure 35**:

Table 2: Samples in Figure 35 made with different compositions.

	a	b	c	d	e	f
PVA	5.00%	5.00%	5.00%	5.00%	0.00%	0.00%
Colloid	0.00%	0.00%	7.50%	7.50%	7.50%	7.50%
Water	95.00%	42.50%	87.50%	43.75%	92.50%	46.25%
DMSO	0.00%	42.50%	0.00%	43.75%	0.00%	46.25%

Figure 35 shows the impact of cooling these samples to -20°C for 3 hours and then allowing them to return to room temperature. The photograph was taken with each sample lying on its side slightly tilted. After thermal cycling, sample **a** was a liquid, while sample **b** gelled. Sample **a**, which consists of PVA dissolved in pure water, was subjected to 5 additional thermal cycles. At -20°C, sample **a** appeared frozen; when inverted, the sample did not flow. Furthermore, the surface of the sample was corrugated and air bubbles were dispersed throughout the sample. Upon returning to room temperature, sample **a** returned to the liquid state. Over the course of six additional thermal cycles, sample **a** became more viscous until it gelled and became infinitely viscous after the sixth cycle. Sample **b**, which is PVA dissolved in DMSO and water, gelled after a single cooling cycle.

Samples **c** and **d** are identical to samples **a** and **b** respectively, except that they additionally contain colloidal particles. Before being cooled to -20°C, both samples ordered into a CCA and strongly diffracted light. Sample **c**, made without DMSO, exhibited no diffraction after being cooled to -20°C. Like sample **a**, sample **c** appeared frozen at -20°C with ice protruding from the surface. Unlike sample **a**, sample **c** gelled

after a single thermal cycle.   Sample **d**, made with DMSO, water, colloidal particles and PVA, gelled to form a strongly diffracting TGCCA after a single cooling cycle.

Both samples **e** and **f** are colloidal suspensions containing no PVA. While both CCA initially diffracted light, sample **e** froze at −20°C and the diffraction dissapeared. After returning to room temperature, sample **e** melted and the colloidal particles appeared to be aggregated, with much precipitate. At −20°C, sample **f** remained an unfrozen CCA. Upon returning to room temperature, sample **f** continued to diffract similarly to that prior to the temperature decrease.
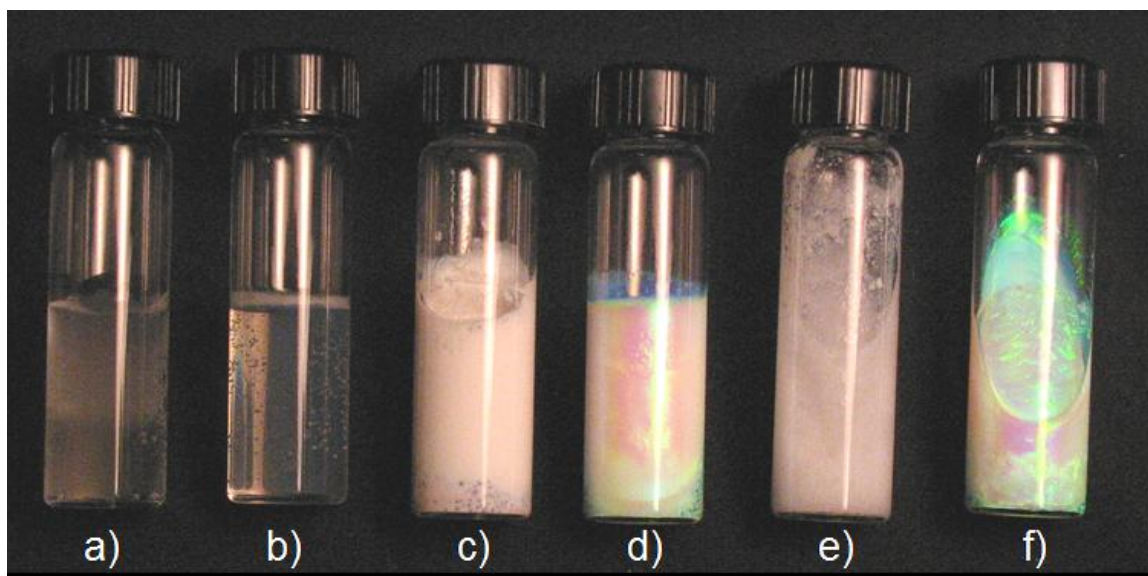
Figure 35: All samples were maintained at −20°C for 3 hours and photographed after warming to room temperature. Sample (a) was cycled six times between −20°C and room temperature. a) 5% PVA in pure water. b) 5% PVA in a 50% DMSO/water. c) 5% PVA and 7.5% colloidal particles in pure water. d) 5% PVA and 7.5% colloidal particles in a 50% DMSO/water. e) 7.5% colloidal particles in pure water. f) 7.5% colloidal particles in 50% DMSO/water.

Samples **a** and **b** demonstrate two different mechanisms of PVA gelation. Without DMSO, the solution freezes and the hydrogel that forms is called a cryogel or a freeze-thaw gel. The mechanism of formation for this type of hydrogel has been studied

extensively. Sample **e** and **f** were included to demonstrate the affect of solvent freezing

on CCA ordering. Freezing causes the particles to aggregate extensively and become

disordered presumably due to exclusion of the particles to the interfaces between frozen

crystallites. DMSO depresses the freezing point of the solution below -20°C and CCA

remains ordered (sample **f**). Sample **c**, made without DMSO, froze during the thermal

cycling. The presence of the PVA did not prevent the CCA from disordering upon

solvent freezing. Sample **d** forms an ordered TGCCA because the DMSO depresses the

freezing point of the solution and causes the PVA to gel.

The PVA phase diagram depends on the concentration of both the water and

DMSO. The mechanism of gelation for PVA in DMSO and water solutions was

thoroughly described by Hoshino *et al*. in 1996.[13] A critical aspect of the gelation is the

cononsolvency of PVA in a solution of DMSO and water.[14] Cononsolvency describes

the phase behavior where PVA is soluble in both water and DMSO individually but

crystallizes out of water–DMSO mixtures.   Cononsolvency is observed because water

and DMSO interact strongly to form stable DMSO-hydrates. PVA interacts less

favorably with DMSO-hydrates than with either water or DMSO. Therefore, PVA

extensively forms inter-chain hydrogen bonds in a solution of DMSO-hydrates. This

inter-chain hydrogen bonding leads to the formation of nano-crystallites. The formation

of nano-crystallites occurs quickly at -20°C, but more slowly at room temperature.   The

turbidity of the hydrogel depends on the size of the crystallites formed. Hoshino *et al.* [13]

showed that the hydrogels made with 60% DMSO were clear when crystallized at

temperatures below -20°C. However, hydrogels synthesized at higher temperatures

became progressively more turbid due to the increased crystallite size. Similarly, Takeshita *et al.* showed that DMSO-water solutions consisting of greater than 76% (*w/w*) DMSO, form clear hydrogels even at room temperature.[15]

The cononsolvency effect is strongest when the solution is ~ 60% (*w/w*) DMSO (mole ratio of water to DMSO is 2.5 – 2.9).[16] Thus, the solvent composition we use to form TGCCA is slightly water-rich (50% DMSO). At this composition, all DMSO is fully hydrated and additional free water is present in solution. With additional free water present, the PVA crystallization depends on the solution temperature. The gel phase occurs when the nano-crystallites become effective cross-links between polymer chains. Initially, inter-chain hydrogen bonding dominates the crystallite formation.[13] Hoshino *et al.* showed through wide angle x-ray scattering (WAXS) of a Mo K_α incident beam (λ=0.71 Å) that the Bragg distance corresponding to the inter-chain hydrogen-bonded PVA (4.00 Å) changes to that corresponding to PVA crystals (4.39 Å) with time. Water-rich or DMSO-rich solutions crystallize more slowly; free water or free DMSO inhibit crystallization by interacting with the PVA hydroxyls and preventing inter-chain hydrogen bonding.

The properties of the TGCCA depend on the concentration of colloidal particles. We found that hydrogels made without embedded colloidal particles gel more slowly than the TGCCA hydrogels. A TG hydrogel made without an embedded array of colloidal particles took 12 times longer to solidify compared to a similarly prepared TGCCA **(Table 3)**.   This is the opposite behavior compared to UV photo-polymerized

hydrogels. Without colloidal particles, photo-polymerized hydrogels polymerize more quickly because the light is not absorbed by the particles.

Table 3: **The presence of the embedded array of colloidal particles increases the rate of gelation.**

	2 hours	4 hours	8 hours	24 hours	48 hours
TGCCA	gel	gel	Gel	gel	Gel
TG	viscous solution	viscous solution	viscous solution	viscous solution	Gel

Furthermore, we were able to synthesize TGCCA at lower PVA concentrations in the presence of colloidal particles. A TGCCA was synthesized with 2% PVA while a TG hydrogel without embedded particles could not be made at this PVA concentration using a single thermal cycle. Not only did the presence of colloidal particles increase the rate of gelation, but they also made the hydrogel more robust. Hydrogels formed without embedded colloidal particles swelled more upon exposure to water, and dissolved more quickly in a hot water bath than TGCCA.

It appears that the presence of colloidal particles significantly alter the distribution of PVA in solution. This hypothesis is supported by previous literature reports which indicate that PVA adsorbs onto polystyrene colloidal particles to form PVA rich shells.[17] We used TEM to examine whether PVA adsorbed onto our colloidal particles. We removed a small quantity of TGCCA precursor solution, prior to gelation, and diluted it into a 50% solution of DMSO and water (same DMSO:H_2O ratio as the precursor solution). After depositing a drop of this solution onto a TEM grid and drying in a vacuum oven, we utilized TEM to image the particles. **Figure 36** shows a TEM image

indicating the presence of a ~10 nm layer of PVA layer on the particle surface. A sphere without PVA on the surface would have a smooth surface and would not exhibit the electron density increase at the particle edge.
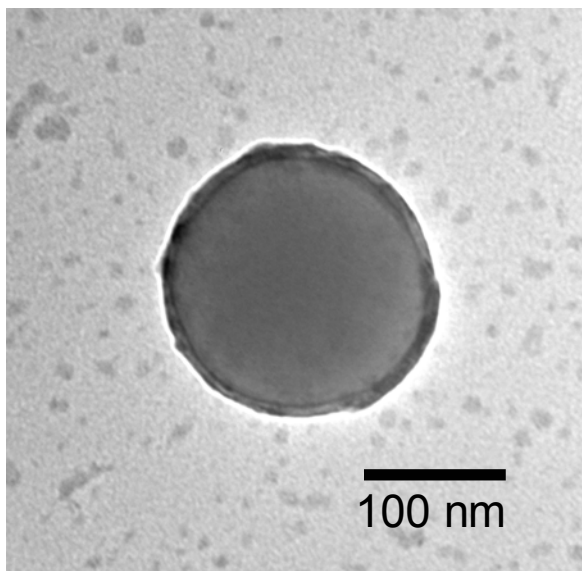
Figure 36: TEM image of a 180 nm PS colloidal particle incubated in a PVA solution. An ~10 nm layer of PVA appears to be adsorbed to the particle surface.

The thickness of a PVA layer adsorbed onto a polystyrene colloidal particle depends on the properties of the solution, the concentration of the PVA, the temperature and the nature of the particles (size, composition, cross-linking, surface charge, and even the prevalent counter-ion). The layer thickness we observed correlates well with Van de Ven's measurement of the increase in particle radius due to the adsorption of PVA onto polystyrene colloidal particles (5-20 nm) determined utilizing dynamic light scattering.[17] The adsorption causes the concentration of PVA in the vicinity of the particle surface to be higher than it is in the solution. We believe this increased concentration in the vicinity of the colloidal particle facilitates the formation of nano-crystallites of PVA.

Thermal Reversibility

We studied the impact of thermal cycling on the diffraction of light by the TGCCA **(Figure 37)**. The sample consisted of 3% PVA in a solution of 50% DMSO and water with approximately 5% colloidal particles by volume. 0.5 mL of the solution was placed onto a glass plate inside a polyester spacer. Another glass plate sandwiched the sample and squeezed excess solution out of the spacer edges **(Figure 37)**.

We measured the transmission of light through the sample to probe ordering of the CCA in both the liquid and the gel phase (**Figure 37** CCA on left and TGCCA on right). We first placed the sample in a −20 ^{o}C bath for 2 hr, which caused the CCA to gel and form a TGCCA. After the sample returned to room temperature, we took a photograph and acquired spectra. We then subjected the sample to 85 ^{o}C for 30 minutes, causing the TGCCA to melt into a CCA. After returning to room temperature, another photograph was taken and additional spectra acquired. The photographs and spectra from five thermal cycles are shown in **Figure 37.**

Initially, the diffraction spectra did not change as the CCA gelled into TGCCA. In **Figure 37** (row 1), the black and red traces are nearly identical. This is consistent with the similarity seen between the CCA and TGCCA photographs. After heating to 85 ^{o}C, the CCA and the TGCCA spectra and photograph are still very similar.
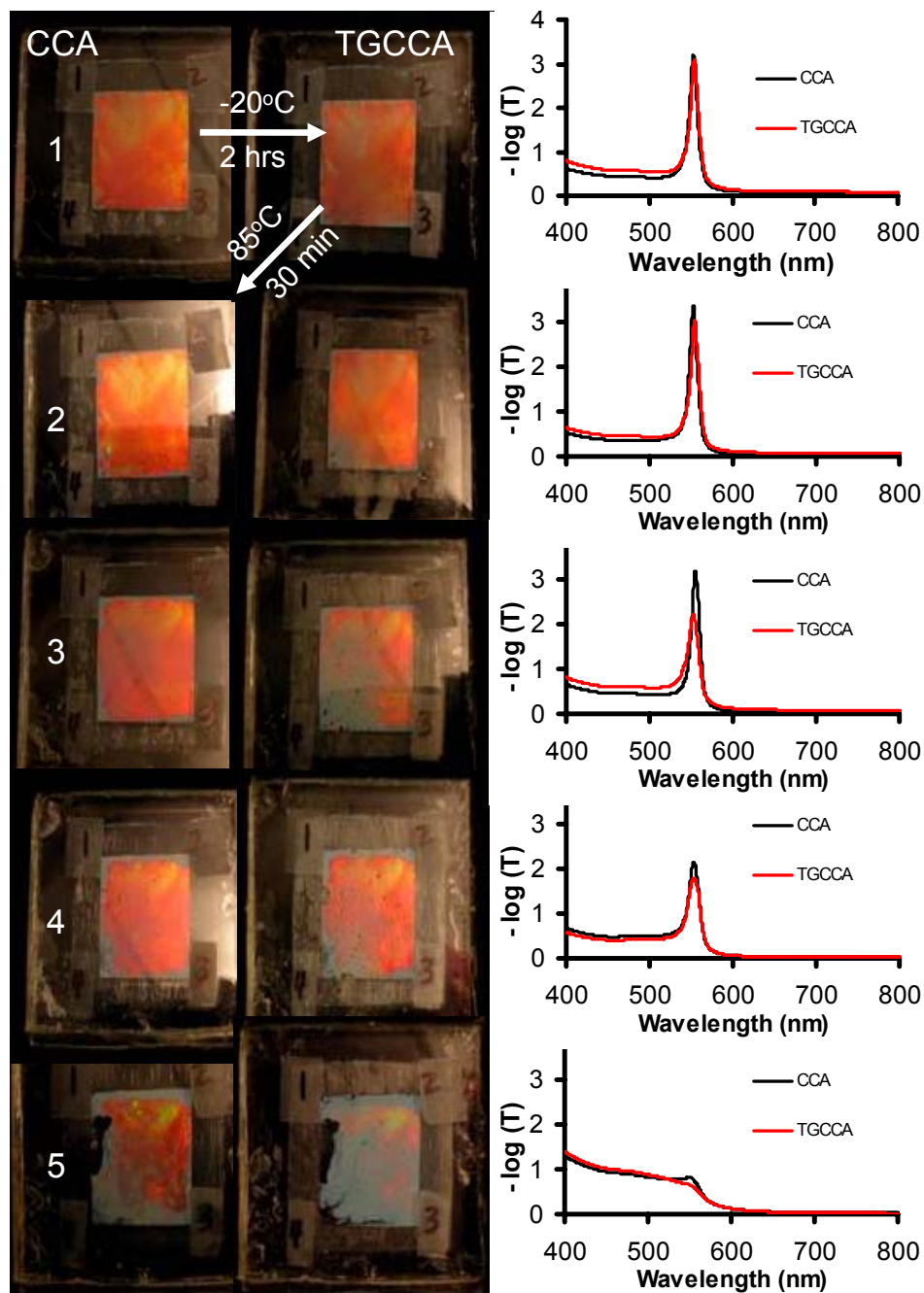
Figure 37: Photographs of CCA (left) thermally cycled to form TGCCA (right). The conditions for the thermal cycling are shown on photographs 1 and 2. On the right, average transmission spectra through four locations in both the CCA (black trace) and the TGCCA (red trace) are shown. The colloidal particles disorder, starting at the edges, with increasing thermal cycling.

Upon cooling the sample and forming a TGCCA for the second time, disorder becomes evident in the lower left-hand corner of the sample. Heating the sample causes

the gel to melt and the size of the disordered regions increase within the sample and around the edges. Upon cooling the sample to reform the TGCCA, the lower left portion of the sample becomes increasingly disordered and the diffraction peak height decreased. The sample becomes increasingly disordered with additional thermal cycling until only small regions within the sample diffract.

Figure 37 shows that the sample can be thermally cycled between the liquid and solid state, but multiple cycles negatively impact the diffraction.   The diffraction decrease at the edge of the cell suggests that the leaching of ionic impurities from the vicinity of the spacer and adhesive is responsible for the disorder.

Comparison of TGCCA to Photo-polymerized pAMD PCCA Ordering.

Figure 38 compares the transmission spectra of a TGCCA to that of a typically prepared pAMD photo-polymerized PCCA; each gel was ~100 μm thick and made with the same 110 nm diameter colloidal particle. Both the TGCCA and the photo-polymerized PCCA were made by injecting the respective precursor CCA solutions between quartz plates separated by a 100 μm parafilm spacer. The TGCCA's diffraction peak (FWHM) was narrower at 17 nm compared to the 25 nm for the photo-polymerized pAMD PCCA. The standard deviation of the TGCCA diffraction peak maxima was found to be $\sigma = 1.8$ nm and the standard deviation of the photo-polymerized sample was found to be $\sigma = 3.0$ nm. The FWHM (bandwidth) expected for a CCA made from 110 nm is expected to be approximately 14 nm according to dynamical Bragg diffraction theory,[18] thus both the TGCCA and the PCCA are larger than expected.
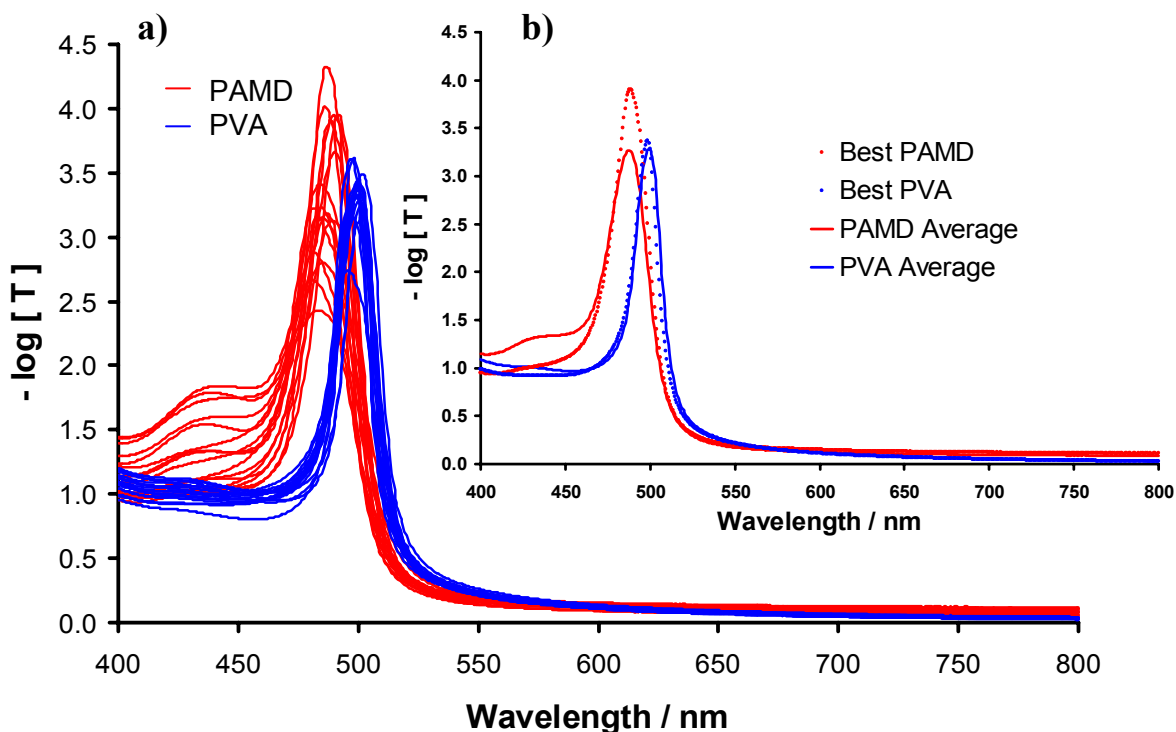
Figure 38: a) Sixteen transmission spectra were taken of a single photo-polymerized PCCA and of a single TGCCA. Each spectrum comes from a different 9 x 9 mm area of the PCCA and TGCCA. b) The average and best spectra from the sixteen spectra.

Figure 38b shows the average diffraction spectrum and the narrowest single diffraction spectrum for both the PVA TGCCA and the photo-polymerized PAMD PCCA. The PCCA shows much more variability in diffraction between different regions. The best PCCA region shows a much higher diffraction than the TGCCA. However, the poorer PCCA regions displaying a diffraction shoulder. A perfect fcc lattice, where the 111 planes were oriented perpendicular to the incident light, would show no diffraction until approximately half the wavelength of light diffracted by the 111 planes (~250 nm). Thus, both the PCCA and the TGCCA are imperfect CCA. The overall narrower diffraction bandwidth of the TGCCA indicates superior ordering.

Cross-linking the Hydrogel

Thermo-reversible gelation results in PVA nano-crystallite physical cross-links that melt at higher temperatures. To create a covalently cross-linked hydrogel, we used glutaraldehyde to cross-link the PVA hydroxyls. We explored two different concentrations of cross-linking reagents and monitored the impact of different cross-link concentrations by removing pieces of the sample at different reaction times and transferring them into pure water. The samples were then heated to 85 $^{\circ}$C for 30 minutes.

PVA TGCCA without covalent cross-links dissolve very rapidly at 85 $^{\circ}$C because the nano-crystallites which physically cross-link the hydrogel melt and dissolve. The cross-link density determines the equilibrium hydrogel volume, which we monitor by measuring the wavelength of the diffracted light **(Figure 39).**

Figure 39a shows the diffraction spectra from samples removed at different times from a 1.5% glutaraldehyde cross-linking solution. **Figure 39b and c** show the diffraction as a function of reaction time for cross-link formation in 1.5% and 0.15% glutaraldehyde solutions.
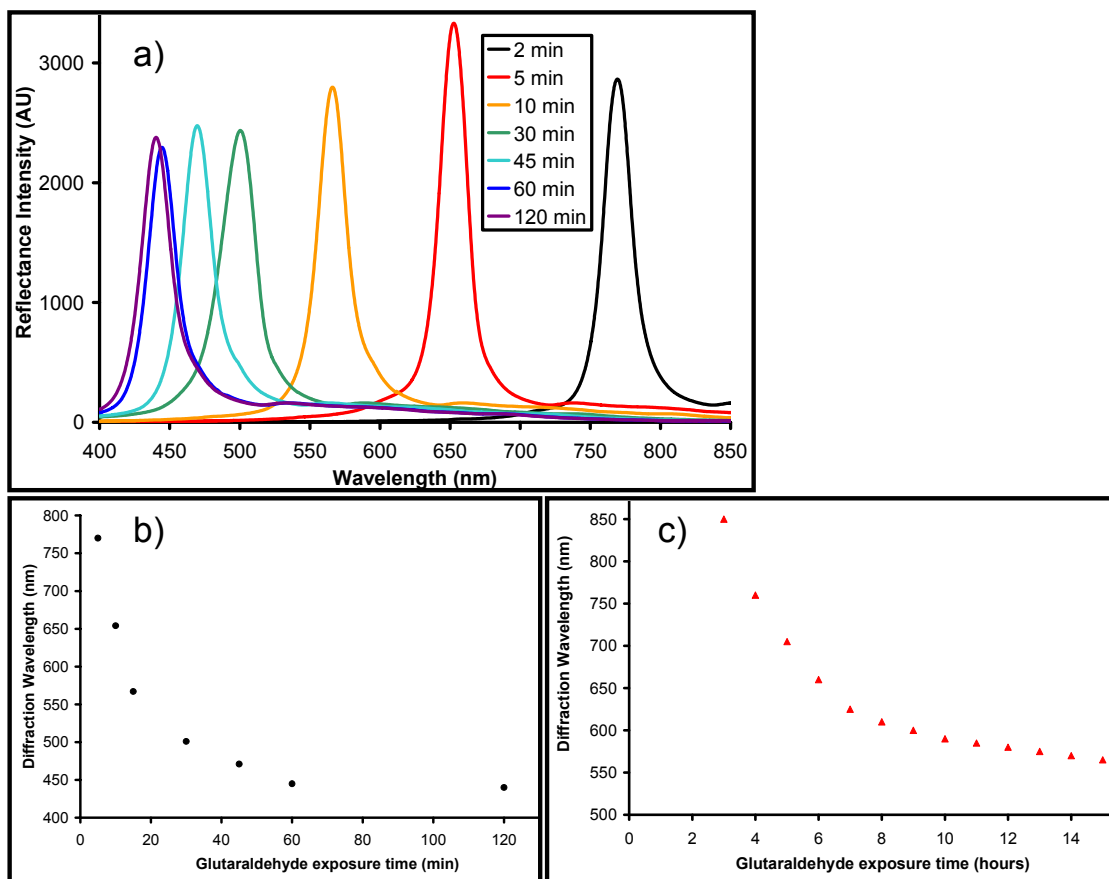
Figure 39: a) Room temperature diffraction spectra of TGCCA cross-linked by 1.5% glutaraldehyde solution after melting PVA physical cross-links. The diffraction peak wavelength is a function of the cross-linking time in b) 1.5% and c) 0.15% glutaraldehyde.

With 1.5% glutaraldehyde, the cross-linking reaction occurs quickly and 2 min. was sufficient to form a stable hydrogel, which did not dissolve upon heating. After 60 min., the 1.5% glutaraldehyde cross-linked hydrogel no longer blue-shifts. This probably indicates that the 50-fold excess of glutaraldehyde has cross-linked every PVA hydroxyl group after ~ 60 min. for the 1.5% glutaraldehyde solution.

A thermally stable hydrogel formed in 3 hours with 0.15% glutaraldehyde. As with the higher concentration of glutaraldehyde, the diffraction wavelength blue-shifts

with increasing reaction times; however, the cross-linking reaction is slower (note that the abscissa is in units of hours).

Functionalization of the Hydrogel.

We can prepare a TGCCA chemical sensor by attaching chemical recognition groups to the hydrogel. We covalently cross-linked a 3 cm x 3 cm x 100 μm TGCCA by using a 0.15% glutaraldehyde solution as described above. We then reacted succinic anhydride with the PVA hydroxyls to functionalize the TGCCA with carboxylates. These pendant carboxylic acids make the TGCCA sensitive to pH.[19] We also further modified the carboxylated TGCCA with amines using carbodiimide chemistry to link 3-AMP to the carboxylates.

Figure 40 shows both the diffraction spectra and the titration behavior for carboxylated and aminated TGCCA. The low pH TGCCA shows a peak maximum at ~445 nm which redshifts to ~490 nm as the pH increases to pH = 6. The midpoint of the titration curve indicates an effective TGCCA carboxylate pK_a ~3.5. For the amine coupled TGCCA we see a similar titration curve but with a pK_a ~9.6. In the absence of TGCCA functionalization we observe little pH dependence of the diffraction.
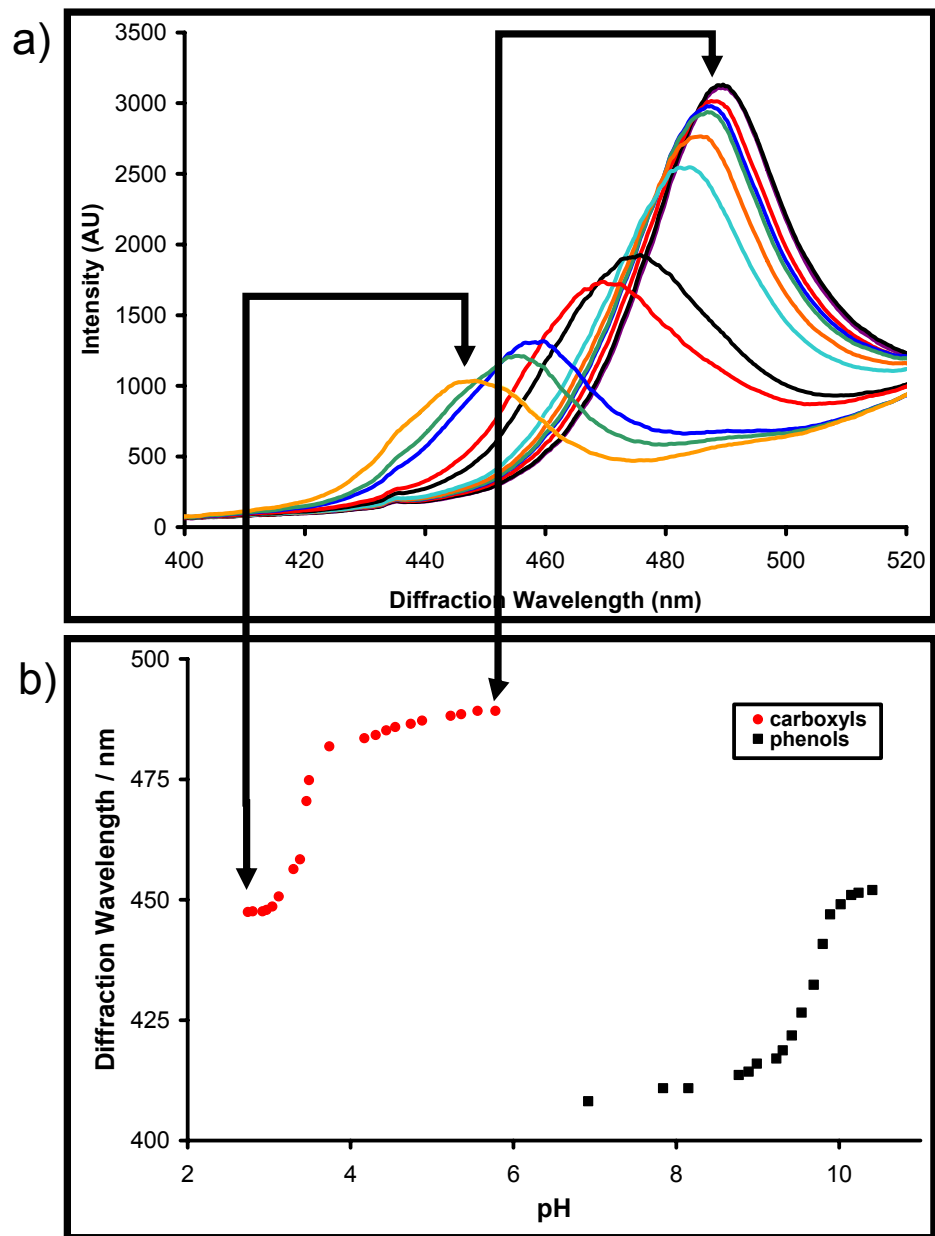
Figure 40: a) **The diffraction spectra for a TGCCA functionalized with carboxylic acid groups exhibits a blue-shift in its diffraction wavelength as the carboxylate is protonated. b) The titration curves for a carboxyl and 3-amniophenol functionalized TGCCA.**

5.1.4 Conclusions

We describe the reversible synthesis of a new type of CCA-based material made by embedding a CCA within a physically cross-linked PVA hydrogel. PVA hydrogels are non-toxic, biocompatible, mechanically robust, and elastic. The TGCCA diffraction is similar to that of our previously developed photo-polymerized PCCA. The TGCCA can be irreversibly covalently cross-linked using glutaraldehyde. We demonstrated that the cross-linked TGCCA can be made responsive to chemical stimuli by functionalizing the hydrogel hydroxyl groups. We monitored diffraction of carboxyl or amine functionalized TGCCA as a function of the pH and found diffraction wavelengths titrate with the pK_a of the functional group. We also demonstrated TGCCA could be fabricated in arbitrarily large volumes and shapes. Our new method fabricates inexpensive homogeneously diffracting chemically modifiable TGCCA.

References

1. Weissman, J. M., Sunkara, H. B., Tse, A. S., Asher, S.A., *Science* **1996,** *274*, 959.

2. Ben-Moshe M.; Alexeev V.L.; Asher S.A. *Anal. Chem.* **2006**, 78 (14), 5149-5157.

3. Pan G.S.; Kesavamoorthy R.; Asher S.A. *Phys. Rev. Lett.* **1997**, 78 (20), 3860-3863.

4. Kimble K.W.; Walker J.P.; Finegold D.N.; Asher S.A. *Anal. And Bioanal Chem.* **2006**, 385 (4): 678-685.

5. Kaneo, Y.; Hashihama, S.; Kakinoki, A.; Tanaka, T.; Nakano, T.; Ikeda, Y. *Drug Metab. Pharmacokinet.* **2005**, 20 (6), 435-442.

6. Peppas, N.A.; Hilt, J.Z.; Khademhosseini, A.; Langer, R. *Adv. Mater.* **2006**, 18, 1345-1360.

7. Nuttelman C.R.; Henry S.M.; Anseth K.S. *Biomaterials*, **2002**, 23, 3617-3626.

8. Lozinsky V.I.; Galaev I.Y.; Plieva F.M. *Trends in Biotechnology*, **2003**, 21 (10), 445-451.

9. Hyon, S.-H.; Cha, W.-I.; Ikada, Y. *Polym. Bull.* **1989**, 22, 119-122.

10. Hassan, C.M.; Peppas, N.A. *Macromolecules* **2000**, 33, 2472-2479.

11. Reese C.E.; Guerrero C.D; Weissman J.M.; Lee, K.; Asher S.A. *J. Colloid Interface Sci.* **2000**, 232 76-80.

12. SIGMACOTE product information sheet:
    http://www.sigmaaldrich.com/sigma/product%20information%20sheet/sl2pis.pdf

13. Hoshino, H.; Okada, S.; Urakawa, H.; Kajiwara, K. *Polymer Bulletin* **1996**, 37, 237-244.

14. Young, T.; Chuang, W. *Journal of Membrane Science* **2002**, 210 (2) 349-359.

15. Takeshita, H.; Kanaya, T.; Nishida, K.; Kaji, K. *Macromolecules* **2001**, 34, 7894-7898.

16. Takahashi, H.; Kanaya, T.; Nishida, K.; Kaji, K. *Polymer* **2003**, 44, 4075-4078.

17. Van den Ven, T.G.M.; *Adv. Colloid Interface Sci.* **1994**, 48, 121-140.

18. Rundquist, P. A., Photinos, P., Jagannathan, S., Asher, S. A., *J. Chem. Phys.*, **1989,** *91*, 4932.

19. Goponenko, A.V.; and Asher, S.A. *J. Am. Chem. Soc.* **2005**, *127,* 10753.

CHAPTER 6: Summary and Future Work

6.1 Summary

Our work towards the development of a clinically useful ammonia sensor led to the development of several new polymeric backbones for embedding crystalline colloidal arrays. Utilization of these new hydrogels facilitated the development of a sensor responsive to physiological concentrations of ammonia within bodily fluids. We were also able to modify this hydrogel system to develop an organophosphate sensor. Development of these sensors demonstrates that the poly-hydroxyethyl acrylate hydrogels can be used as the basis of new PCCA sensor materials.

The poly(vinyl alcohol) (PVA) thermo-reversible gelled crystalline colloidal array (TGPCCA) is another new material we developed which further expands the number of hydrogel materials available for the development of new CCA applications. This material takes advantage of a new synthetic strategy for the formation of photonic materials. It enables the simple and inexpensive synthesis of photonic materials with 3-dimensional sizes previously unattainable. We made this physically cross-linked hydrogel thermally stable by introducing covalent cross-links. We then showed that simple functionalization of the hydrogel results in a stimuli responsive sensing platform.

Chapter 3 describes a poly(acrylamide) (pAMD) ammonia sensitive material. We discuss the different analytical approaches to determining ammonia concentrations in bodily fluids and discuss the Berthelot or indophenol reaction. This commonly used solution-based reaction was incorporated onto our hydrogel as a means of inducing a hydrogel volume transition in response to ammonia. In this reaction, ammonia reacts

with hypochlorite to form a monochloramine. The monochloramine reacts with two 3-aminophenol molecules attached to the hydrogel backbone, forming a covalent cross-link. The formation of additional covalent cross-links increases the elastic restoring force for the hydrogel and causes the hydrogel to shrink. We were forced to abandon this pAMD as the hydrogel backbone because it reacts with hypochlorite which was a key component of our sensor's response mechanism.

In Chapter 4, we discuss the development of new hydrogel systems and how those new hydrogels enable the development of sensor materials. We first attempted to develop a poly(hydroxyethyl methacrylate) (pHEMA) based hydrogel PCCA. We quickly shifted towards using a more water soluble analogue, poly(hydroxyethyl acrylate) (pHEA), in order to minimize the polymer content of the PCCA sensor. The pHEA polymer backbone proved effective for the development of an ammonia sensor. Not only was our new hydrogel system useful for the development of an ammonia sensor, its general applicability was shown by its use for the development of a second-generation organophosphate sensor (Appendix). With the new pHEA PCCA, we developed a bimodular sensing approach utilizing two complimentary chemical recognition groups. Organophosphate hydrolase creates a local pH gradient by hydrolyzing the analyte paraoxon. The 3-aminophenol is titrated by this change in pH and actuates a volume phase transition due to a change in the free-energy of mixing.

We also examined alternative hydrogel materials to develop novel PCCA. In Chapter 5, we show that thermo-reversible gelation hydrogels can be used to embed

CCA. Because these hydrogels are thermally reversible and prepared without utilizing covalent chemical reactions, it presents potential advantages for sensor development. We studied the mechanism and the resulting material characteristics, and found that we could synthesize a wide range of TGCCA compositions. We created TGCCA with diffraction wavelengths spanning the entire visible spectra. We observed that the colloidal particle concentration strongly impacts the TGCCA properties. Utilizing simple chemical modifications, we were able to transform the TGCCA into a thermally stable, stimuli responsive PCCA. The simplicity of this approach, coupled with the unique attributes of PVA makes this new synthetic technique an attractive alternative for the development of PCCA materials.

6.2 Future Work

6.2.1 Optimization of the Ammonia Sensor

While the ammonia sensor is already capable of displaying sufficient sensitivity within the clinically relevant ammonia concentration range in both buffer and serum solutions, it still needs to be optimized. The original goal of our research was two-fold. First, we sought to develop a sensor which could be used to establish the concentration of ammonia in a point-of-care type device. Secondly, we sought to develop a general sensing approach which could be extended to quantify other analytes such as an amino acids.

Efforts to improve the ammonia sensor should focus on switching to our newly developed poly(vinyl alcohol) PVA polymer backbone. PVA should be an ideal backbone for the ammonia sensor because it is generally recognized as biocompatible and proteins do not adhere to it.[1] It also shows a low degree of reactivity with biological fluids.[2] Our current pHEA sensor is limited because it is made with 18% (w/w) polymer. We believe that this high polymer content hydrogel has substantial physical entanglements which prevent large volume phase transitions which decrease the sensor's sensitivity. We were unable to lower the percent polymer of this sensor because microsyneresis occurs at lower polymer concentrations. The newly developed PVA TGCCA hydrogels can be made with only 2.5% polymer. Furthermore, since we have already shown that 3-AMP can be coupled to PVA, development of a PVA sensor requires only optimizing the synthetic and sensing conditions. Therefore, we expect that

the PVA sensor will be a substantial improvement over the previous pHEA hydrogel because it will have lower polymer content.

The presently designed ammonia sensor also responds too slowly to be used to determine the concentration of NH_3 in capillary blood. We anticipate the use of the PVA TGCCA will allow us to improve our reaction kinetics. Literature has shown the Berthelot reaction can be very fast (2-3 minutes) when the reaction conditions are optimized.[3] In order to increase our reaction rate we must be able to increase the concentration of phenol within the hydrogel. The PVA hydrogel is post-synthetically modified with phenol, therefore, optimization of this reaction parameter can be separated from the polymerization optimization. The pHEA ammonia sensor utilized epoxy groups incorporated during the polymerization to attach the 3-AMP. Increases in the epoxy-containing monomer caused microsynerisis and therefore the concentration of 3-AMP was limited by the epoxy content of the hydrogel. Coupling 3-AMP through a step which is completely independent of the synthesis should allow for the incorporation of much higher concentrations of phenol which should increase the reaction rate.

In order to develop a robust clinical sensor from our ammonia sensing PCCA, we would also need to develop a mechanism for eliminating some of the common interferences present in a typical sample. This obstacle has been addressed primarily by separating the ammonia from the sample prior to its determination.[4,5] A commonly used approach which we could apply to our research involves raising the pH of the analytical sample such that the ammonium ions are quickly and completely converted to ammonia

gas. A gas permeable membrane could then be used to separate the ammonia from the complex biological matrix and sequester it into a solution ideal for the determination of the ammonia. The permeability of ammonia through various polymer membranes has been described and the concept has been incorporated into commercially available electrodes.[6,7] Another potential approach involves on-line gas dialysis which effectively removes >90% of the ammonia by dialyzing against an acid.[8] In preliminary experiments we have been able to sense the ammonia which has crossed a low molecular weight dialysis membrane. We placed a serum sample spiked with ammonia inside a 1000 MWCO dialysis tube and placed that tube in the solution surrounding our ammonia sensing PCCA. The sensor did respond to the ammonia in the sample, however the response times were slower. While slower, this type of separation may be a viable option for future versions of our ammonia sensing PCCA. It has not been a viable option for the development of electrodes, due to the transport of interfering ions across the membrane, however, our high selectivity makes dialysis a viable option.

6.2.2 Development of a Phenylalanine Sensor

The impetus for developing an ammonia sensor was not solely for use in determination of blood ammonia levels. Ammonia is a product of the catabolism of many clinically important amino acids. The first amino acid sensor we would attempt to develop is for phenylalanine (phe) because of its immediate impact on people with phenylketonuria (PKU).

117

PKU is caused by an inborn deficiency in phenylalanine hydroxylase, preventing the conversion of phenylalanine to tyrosine and leading to high blood levels of phenylalanine. Untreated, PKU leads to severe neurological deficits and is associated with many other health problems from decreased vision to asthma.[9,10] The incidence of PKU in the United States is approximately one in 15,000 live births.[11] Early detection and dietary control are essential to prevent severe mental retardation in patients with PKU. Dietary modifications should begin within 7 days of birth, and all states currently screen for PKU in newborns. Blood samples must often be sent to an outside laboratory, and results may not be received for days.

During the first year of life of a PKU patient, phenylalanine levels should be measured every week in order to maintain serum phenylalanine below 6 mg/dL thus preventing mental retardation. The NIH consensus statement on PKU recommends that after the first year, Phenylalanine testing occur twice a month until the age of 12 and once a month after the age of 12. Testing should also occur twice a week during the pregnancy of a woman who has PKU.[11] Tight control of serum phenylalanine levels is critical during neurological development and remains important later in life.[9]

Due to the necessity and frequency of monitoring phenylalanine in PKU patients, the NIH consensus statement recommends the development of a home testing method for serum phenylalanine. A simple test that does not have to be sent to an outside laboratory for analysis would also be useful in neonatal screening. As an estimated 4.2 million

children will be born in the US in 2005[12], the potential market for a simple, rapid phenylalanine test is very large.

Current clinical testing for phenylalanine in infants is conducted using the Guthrie bacterial inhibition test[13], fluorometry, and ion-exchange chromatography of blood.[2] Tandem mass-spectrometry is also gaining popularity, though it is not available in all laboratories. The Guthrie test requires that the blood sample be applied overnight to a bacterial culture in order to determine the concentration of phenylalanine in the blood. The overnight wait is not desirable in dealing with infants, whose diet must be regulated quickly in order to minimize adverse effects of the disease. The fluorometric techniques are very sensitive, however false negatives can occur due to interference from antibiotics as well as inadequate samples or poor sample handling.[14]

The reference interval is 70-206 µM phenylalanine for normal birthweight and 121-254 µM phenylalanine for low birthweight infants.[6] The test is more accurate when administered 2-3 days after birth because initiation of protein metabolism causes the level of phenylalanine to rise in affected cases. The general cutoff for phenylalanine levels used by most labs is 4 mg/dL (240 µM). Levels can climb as high as 1800 µM if untreated for 10 days.[15]

Our sensor will utilize an enzyme which is specific for L-phenylalanine. Many enzymes that have previously been utilized to sense phenylalanine can also react with tyrosine. Hsiung et. al.[16] reported an enzyme electrode based on the use of L-

phenylalanine ammonia lyase (PAL), which reacts only with phenylalanine without interference from L–tyrosine. We will utilize this reaction to produce ammonia in our sample. The initial sample could be split and PAL can be added to half of the blood or plasma sample in order to catalyze the conversion of L-phenylalanine. The ammonia sensor developed here-in could be used on both samples to determine the concentration of ammonia. The increase in the ammonia concentration will be stoichiometric with the phe concentration. We have already demonstrated that our ammonia sensing PCCA displays sensitivity to concentrations of ammonia within the reference interval for phenylalanine.

References

1. Kaneo, Y.; Hashihama, S.; Kakinoki, A.; Tanaka, T.; Nakano, T.; and Ikeda, Y. *Drug Metab. Pharmacokinet.* **2005**, *20*, 435-442.

2. Chatterjee, J.; Haik, Y.; and Chen, C.J. *BioMag. Res. Tehcnol.* **2004**, *2*, 2-4.

3. Lau, K.T.; Edwards, S.; Diamond, D. *Sensors and Actuators,* **2004**, 98, 12-17.

4. Huizenga, J.R.; Tangerman, A.; Gips, C.H. *Ann. Clin. Biochem.* **1994**, 31, 529-543.

5. Searle, P.L. *Analyst*. **1984,** 109: 549-568.

6. Tarsiche, I; Hopirtean, E.; Ciurchea, D. *Meas. Sci. Technol.* **1997**, 8, 1367-1371.

7. Meyerhoff, M.E.; Fraticelli, Y.M.; Greenberg, J.A.; Rosen, J.; Parks, S.J.; Opdycke, W.N.; *Clin. Chem.* **1982**, 28(9), 1973-1978.

8. Fraticelli, Y.M.; Meyerhoff, M.E. *Anal. Chem.* **1983**, 55, 359-364.

9. Koch, R.; Burton, B.; Hoganson G. *J. Inherit. Metab. Dis.* **2002** 25(5), 333-346.

10. Jones, S.J.; Turano, G.; Kriss, A.; Shawkat, F.; Kendall, B.; Thompson, A.J., *J. Neurol. Neurosurg. Psychiatry* **1995,** 59(3), 260-265.

11. National Institutes of Health Consensus Development Conference Statement: phenylketonuria: screening and management, October 16-18, 2000; *Pediatrics* **2001**, 108(4), 972-982.

12. CIA, The World Factbook, http://www.cia.gov/cia/publications/factbook/geos/us.html#People

13. Guthrie, R.; Susi, A. *Pediatrics*. **1963**, 32, 338-343.

14. Holtzman, C., Slazyk, W.E., Cordero, J.F. *Pediatrics* **1986**, 78, 553-558.

15 Tietz, N.W.; *Clinical Laboratory Guide to Laboratory Tests*. 3rd ed. Philadelphia, W.B. Saunders, **1995**.

16. Hsiung, C.P.; Kuan, S.S.; Guilbault, G.G. *Anal. Chim. Acta*. **1976,** *90*, 45-49.

Appendix 1: pHEA as a Broadly applicable Sensing Platform

Photonic Crystal Sensor for Organophosphate Nerve Agents Utilizing the Organophosphorus Hydrolase Enzyme

J.P. Walker, K.W. Kimble, and S.A. Asher, November, 2006

A.1 Introduction

Synthetic organophosphorus compounds (OPs), such as parathion and paraoxon, are widely used agriculturally in both the United States and worldwide as pesticides and insecticides.[1] These compounds are also structurally similar to chemical warfare agents (CWAs) such as sarin, soman and VX. OP compounds are commonly found in agricultural wastes at levels between 1 – 10,000 ppm.[1] These compounds are potent inhibitors of the enzyme acetylcholinesterase (AChE), because they prevent breakdown of the neurotransmitter acetylcholine at the neural synapse.[2] The inhibition of acetylcholine breakdown and subsequent accumulation results in loss of muscular function and can result in paralysis or death if untreated.[3,4] Due to the widespread use of these agents in agriculture, a high risk of food and ground water contamination exists. The neurotoxicity of OP compounds is of immense concern, given their potential for use in chemical terrorism. Due to this threat, there is intense interest in developing sensors which can rapidly and selectively detect OP compounds for environmental analysis as well as for military/ law enforcement applications such as counter terrorism and

battlefield detection of OP agents. Rapid detection is a crucial element for preventive response, exposure treatment, and decontamination.

Several types of techniques exist for detection and identification of OPs. Thin layer chromatography, HPLC and GC/MS techniques are commonly used and provide nanomolar detection limits.[5,6] These techniques are, however, expensive and time consuming, requiring significant sample preparation and skilled technicians for operation, which limits their practical use in field detection. Molecularly imprinted polymers (MIPs) which have very high selectivity towards OP substrates have also been developed. These sol-gel films utilize silanes which are functionalized to create OP-binding templates. Detection of the sequestered OP molecules is done using fluorescence or electrochemistry.[7]

Recent research has focused on developing sensors which utilize biological recognition elements such as enzymes to detect and quantify OPs. These sensors provide a significant advantage over current chemical sensing techniques because they utilize specific enzymes which have very high affinities for OP analytes. For example, AChE and Organophosphorus Hydrolase (OPH, also called phosphotriesterase) have been extensively utilized in biosensor development.

AChE is inhibited by OPs at the catalytic serine site, which prevents turnover of acetylcholine at the neural synapse.[2] Several sensors utilize AChE either by directly using it to bind an OP and measuring the sensor's response, or by measuring changes in the

amount of substrate turnover caused by exposure to OPs. [8-12] A flow injection technique utilizing immobilized AChE has been developed where AChE is immobilized on a polymer substrate. [8] A sample solution containing OP is then exposed to the immobilized enzyme. A solution containing an enzyme substrate and reagent which reacts to form a chromophore upon substrate catalysis is added. The absorbance of the chromophore is monitored to detect changes in enzyme activity caused by OP inihibition. Leon-Gonzalez and Townshend achieved 8 nM OP detection limits with this technique.[8]

Langmuir-Blodgett multilayer sensors have also been developed utilizing AChE along with several other recognition elements. These sensors, which monitor changes in fluorescence caused by OP binding, also achieved nM detection limits.[9,10] Amperometric sensors have also been fabricated which utilize AChE to detect very low OP concentrations.[11] These techniques can be easily miniaturized and are less expensive. Thus, they are more suitable for field detection than most other types of sensors. However, they are subject to interference from the other oxidizable substances present in real samples. [11] A piezoelectric sensor which monitors the binding of cholinesterase to inhibitors using a mass-sensitive quartz crystal was also recently developed. The sensor is capable of detecting 10^{-10} M paraoxon.[12]

We previously demonstrated a photonic crystal sensor which acts as a dosimeter and which operates in low ionic strength solution that detects OPs based on a change in the ionic free energy of the system due to creation of a charged species that forms when parathion inhibits AChE.[13] Binding of OP shifts the wavelength of visible light Bragg

diffracted by the PCCA. This sensor achieves unprecedented (fM) detection limits; however it only works in low-ionic strength solution, and, thus, is not ideally suited for use in real samples.

Sensors which utilize AChE are fundamentally limited in their development for two primary reasons. First, AChE can be irreversibly inhibited by several other species, such as carbamates and some neurotoxins[7]. These interferences could cause false positive results for OP detection. Alternatively, they could cause false negatives by preventing OP binding to AChE altogether. Secondly, AChE is irreversibly inhibited by OPs[7], so sensors are not continuous or reusable, which increases the cost of performing the analysis. In light of these limitations, researchers have begun to explore the utility of other enzymes for OP detection.

Several researchers have utilized the recombinant enzyme organophosphorus hydrolase (OPH) instead. The development of the recombinant enzyme has facilitated the development of sensors which take advantage of this enzyme's unique properties. OPH is a ~ 35 kDa protein normally present as a homodimer. OPH contains a divalent metal ion cofactor (usually Zn^{2+} or Co^{2+}) which catalyzes the hydrolysis of OP esters at pH 8-10, releasing two protons in the process.[14-16] The enzyme is not subject to as significant a degree of interference from other species as is AChE, which can be inhibited by carbamates in addition to OPs. Another advantage of OPH is that it is a recombinant enzyme; researchers have altered the sequence of the enzyme through site-directed

mutagenesis in order to produce OPH species which catalyze specific OP species more efficiently.[17] The catalytic reaction of OPH is illustrated in **Figure 41**.
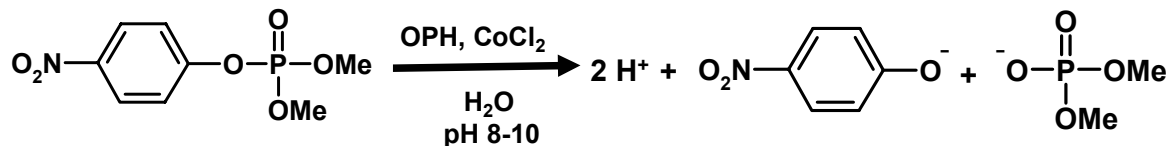
Figure 41: OPH hydrolyzes methyl-paraoxon, an organophosphorus pesticide, into p-nitrophenolate and dimethylphosphate at basic pH, producing two protons in the process.

Several types of sensors which utilize OPH have been developed. Potentiometric sensors based on measuring the pH changes caused by the OPH catalyzed degradation of OP species have been developed.[16,18,19] For example, Mulchandani et.al. reported a 2 μM detection limit with one such system.[16] Amperometric sensors utilizing OPH have also been developed.[,20,21,22,23] These sensors oxidize p-nitrophenol, a paraoxon hydrolysis product, which is then detected at a carbon paste electrode. Detection limits as low as 20 nM have been demonstrated.[21] Another sensor employed a bacterium which oxidizes 2-nitrophenol to CO_2, consuming O_2 in the process. The O_2 consumed, measured by an oxygen electrode, correlates with the concentration of OP present. The detection limit for this technique was reported to be 0.2 μM OP.[23]

OPH has also been recently utilized not only for sensing applications, but also for decontamination of OP-containing samples.[24,25] Current chemistry-based decontamination techniques frequently require use of caustic materials, however these strong alkalis can damage the contaminated objects as well as the environment.[25] OPH can eliminate use of caustics because it selectively hydrolyzes OP species. The possibility

of producing multi-use reversible enzymatic systems capable of OP detection and decontamination would provide a significant advantage for anti-terrorism preparedness and for contaminant clean-up. Such systems would provide a rapid, cost-effective single approach for initial detection, decontamination, and the monitoring of the decontamination process.

We demonstrate in this paper the development of a novel, inexpensive sensor for detection of OP species based on our previously developed intelligent polymerized crystalline colloidal array (IPCCA) photonic crystal sensing materials. These IPCCAs utilize an array of colloidal particles[26-31] polymerized into a hydrogel[32-35] network which Bragg diffracts light in the visible spectral region. We utilize our recently-developed general bimodular sensing motif originally demonstrated for sensing creatinine.[36] The first sensing element is an enzyme, which reacts with the analyte to produce a steady-state pH gradient inside the hydrogel. The pH change is then detected by the second sensing element, which titrates to cause a sensing response.

Our OP-sensing IPCCA contains OPH, which degrades the OP methyl-paraoxon to p-nitrophenolate and dimethylphosphate at pH 9.7, producing two protons. These protons protonate the secondary sensing element, 3-aminophenolate (3-AMP), causing a steady-state volume change in the PCCA. The wavelength of diffracted light shifts in response to the steady-state volume change of the hydrogel. **Figure 42** illustrates this sensing motif.

Figure 42: a) CCAs form due to electrostatic repulsion between particles. The particle spacing is such that the array Bragg diffracts visible light. The lattice is locked into place by a poly(2-hydroxyethyl acrylate) hydrogel network. The backbone is functionalized with both organophosphorus hydrolase (OPH) and 3-aminophenolate. As OPH reacts with methyl-paraoxon, p-nitrophenolate and dimethylphosphate, as well as two protons are produced. This produces a steady-state pH gradient between the interior and exterior regions of the hydrogel. The lower pH inside the hydrogel protonates the phenolates. As a result, the solubility of the hydrogel network decreases, which shrinks the hydrogel and blue-shifts the IPCCA diffraction. **b)** The diffraction peak of the IPCCA blue-shifts in response to the analyte concentration.

Our PCCA sensor platform relies upon a volume phase transition phenomenon which occurs in the hydrogel matrix due to changes in the free energy of the system. For this sensor, the volume change is caused by a change in the free energy of mixing (ΔG_{mix}) of the hydrogel.[37] The back-diffracted light follows Bragg's Law: $\lambda_o = 2\,n\,d\,\sin\theta$.

The wavelength (λ_o) of light diffracted by the IPCCA's 111 plane of the fcc lattice depends upon the plane spacing (*d*), the refractive index (*n*) of the system, and the Bragg glancing angle, θ. Because we are sampling normally incident light, $\sin \theta$ is unity. We demonstrate that our sensor reversibly detects the OP pesticide methyl-paraoxon at submicromolar concentration levels in lab buffer solution as well as in stream water samples.

A.2 Experimental

PCCA Preparation

Figure 43 depicts the synthesis and functionalization of the OP IPCCA sensor. 2-hydroxyethylacrylate (2-HEA, 0.94 g, 8.1 mmol, Sigma), acrylamide (AMD, 0.02 g, 0.28 mmol, Fluka), poly(ethylene glycol-200) dimethacrylate (PEGDMA-200, 0.09 g, 0.25 mmol, Polysciences), glycidyl acrylate (GA, 0.04 g, 0.37 mmol, Sigma) and ethylene glycol (1.95 g, 31 mmol, J.T. Baker) were mixed and treated with Al_2O_3 to remove inhibitors from the monomers. The mixture was centrifuged to separate the monomer from the Al_2O_3. 1.015 g of this solution was mixed with the colloid suspension (1.0 g, 5-10% w/w dispersion, polystyrene latex spheres, 120 nm).[26-31] AG501-X8 (D) ion exchange resin (~ 0.1 g, 20-50 mesh, mixed bed, Bio-Rad) and 10 % diethoxyacetophenone (DEAP, 10 μL, 4 μmol, Aldrich) in dimethylsulfoxide (DMSO, J.T. Baker) were mixed into the suspension in a 2-dr vial. After 15 min, the mixture was centrifuged to remove the ion-exchange resin and was injected between two quartz discs separated by a 125 μm-thick Parafilm spacer. The colloidal particles self-assemble into a crystalline colloidal array (CCA), resulting in a liquid film which diffracts light. The film

was exposed to 365 nm UV light from mercury lamps (Blak Ray) for 3 hrs. A pHEA/AMD hydrogel network with PEGDMA cross-links forms around the CCA, resulting in a polymerized CCA (PCCA).[32-35] The quartz cell enclosing the hydrogel was opened in Nanopure water and the PCCA was allowed to equilibrate with water.
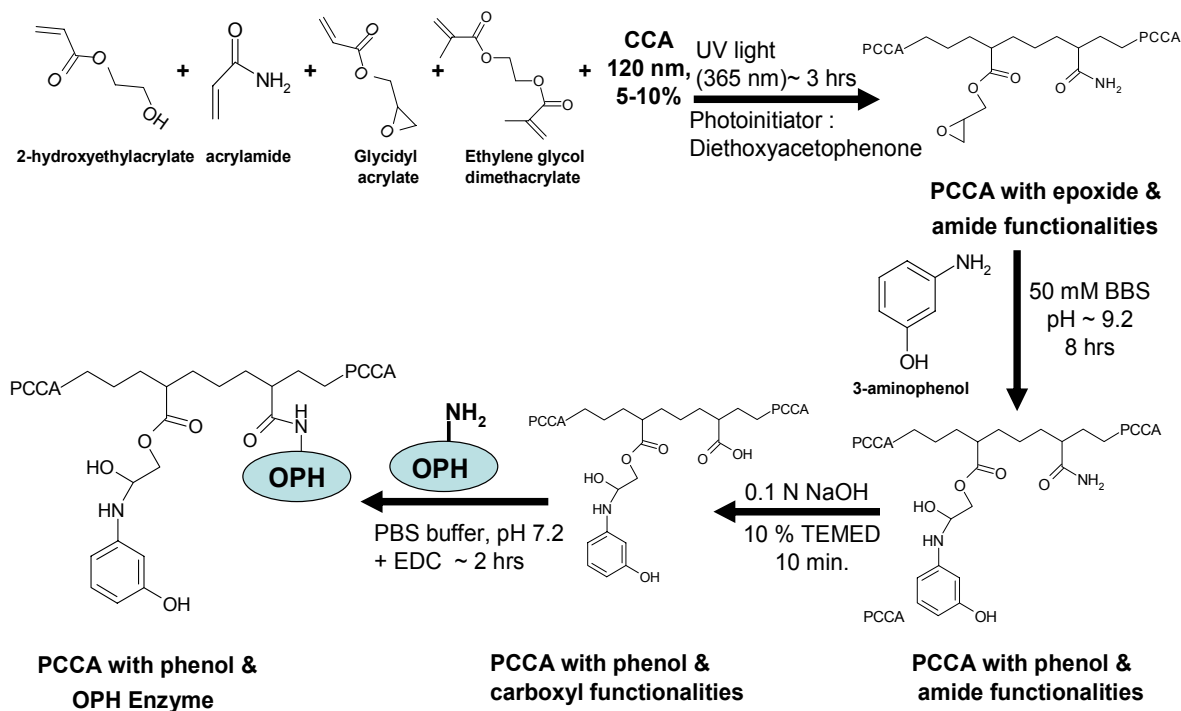
Figure 43: Preparation of the IPCCA and functionalization with 3-aminophenol and OPH. The 3-AMP is first coupled via epoxide ring opening. The pendant amides are subsequently hydrolyzed to form carboxylates, which are carbodiimide-coupled to amines on the OPH enzyme.

Attachment of 3-Aminophenol

The PCCA was placed into a 50 mM borate buffer solution (BBS, pH 9.2, J.T. Baker) to equilibrate before coupling. 0.5 g of 3-aminophenol (3-AMP, 4.6 mmol, Sigma) were dissolved in 10 ml DMSO (J.T. Baker) and then diluted to 50 ml with 50 mM BBS. The solution and PCCA were placed in a 125 ml plastic container (Nalgene) and allowed to react for 8 hours. After reacting, the PCCA was rinsed hourly for 6 hours with BBS. A blank gel (hydrogel in which CCA is replaced with H_2O) was prepared and functionalized according to the above protocol. UV-VIS spectra of the blank gel were measured by a Varian Cary 5000 UV-VIS spectrophotometer to confirm attachment of 3-AMP by monitoring the absorbance at 290 nm. The sensor typically contains a 13 mM concentration of 3-AMP.

Attachment of Organophosphorus Hydrolase

The PCCA was then hydrolyzed in a 50 mL solution of NaOH (0.1 M, J.T. Baker) containing 10 % v/v N,N,N',N'-tetramethylethylenediamine (TEMED, Aldrich) for 10 min. The hydrolyzed PCCA was washed for 2 hrs with 150 mM NaCl (J.T. Baker). UV-VIS Spectra were recorded to confirm that phenols remained attached to the hydrogel after hydrolysis.

A piece of the PCCA (1 cm x 1 cm x 125 μm) was allowed to adhere to a plastic petri dish (Falcon). A coupling solution of enzyme was made by dissolving 6 mg Organophosphorus Hydrolase (OPH, EC 3.1.8.1., 6 mg solid, MW 35,000, Lybradyn, Inc.) in 200 μL of 0.1 M phosphate buffer (PBS, Pierce Biotechnology). The PCCA was

incubated overnight in the enzyme solution to allow the OPH to diffuse into the hydrogel. Next, 0.1 g of 1-ethyl-3-(3-dimethylaminopropyl) carbodiimide hydrochloride (EDC, 0.52 mmol, Pierce Bitoechnology) was dissolved into 100 μL of 0.1 M 2-(N-morpholino)ethanesulfonic acid (MES, pH 4.7, Pierce Biotechnology). The EDC solution was added, and the reaction was allowed to proceed for 2 hrs. The sensor was rinsed in 150 mM NaCl (J.T. Baker) and stored overnight until testing in 0.1 M PBS solution at 4 ^{o}C. UV-VIS spectra were also recorded for a blank hydrogel treated exactly the same way. OPH attachment was confirmed by monitoring the absorption difference spectrum of the blank hydrogel functionalized with 4-amino-2-nitrophenol instead of 3-AMP. The absorption difference spectrum was generated by subtracting spectra of the sample before and after coupling.

Solutions & Diffraction Measurements

The PCCA was stored in 0.1 M PBS (pH 7.4) at 4 ^{o}C at all times when not being tested. We made the following buffer test solution (BTS) which contained: 2 mM $Na_2B_4O_7 \cdot 10\ H_2O$ (J.T. Baker), 5% v/v methanol (Fisher), 0.05 mM $CoCl_2 \cdot 6H_2O$ (Fisher), and 150 mM NaCl (J.T. Baker). The test solution pH was adjusted to ~9.7 with 0.1 M NaOH (Fisher).

The PCCA diffraction was monitored using a fiber-optic diode spectrometer with a tungsten halogen light source (Ocean Optics) using a reflectance probe. All measurements were conducted with the PCCA adhering to the bottom of the petri dish with stirring using a magnetic stir bar.

The sensor was first titrated to confirm that the 3-AMP was attached and that the sensor responded to titration of the attached phenols with 20 mM NaOH (Fisher). We used these data to confirm the pK_a of the attached phenols.

We then tested the sensor with a control as well as in a series of BTS dilutions of the OP pesticide methyl-paraoxon (ChemService, Inc.) ranging in concentration from 2.4 μM to 1 mM. The IPCCA was pre-equilibrated in BTS for 30 min. prior to exposure to the methyl-paraoxon solutions. Diffraction spectra were recorded until the diffraction stopped shifting, indicating that the sensor had reached steady-state. Responses typically were saturated in about 50 min. The sensor was subsequently rinsed and re-equilibrated in BTS. The sensor was subsequently exposed to a new methyl-paraoxon solution. Two sensing runs were performed with the sensor on consecutive days. We utilized the range of concentrations from 0 – 24 μM methyl-paraoxon to calculate the detection limit.

We also performed several control experiments in order to confirm that the response was due to a change in the free energy of mixing of the PCCA. We tested the sensor with various components absent in order to prove that the sensing response was produced by titration of the pendant phenolates by the protons produced during the OPH hydrolysis of methyl-paraoxon. Several control studies were also performed to confirm the hypothesis that the sensor displays a steady-state response and not an equilibrium response.

Finally, the response of the sensor was tested in stream water to determine the sensor performance in a real sample matrix. Water samples were obtained in July, 2006 from a small stream behind the Plantations housing development in Saxonburg, PA. The the sample was first filtered through a 2 μm filter to remove particulate matter. Then, the stream water samples were prepared by adding 5% (v/v) methanol to help solubilize the OP,150 mM NaCl, 0.05 mM $CoCl_2 \cdot 6H_2O$, 2 mM $Na_2B_4O_7 \cdot 10\ H_2O$, and adjusting the pH to 9.7 with 0.1 M NaOH. This solution was used in place of the BTS to make serial dilutions of methyl-paraoxon via the protocol used previously.

A.3 Results & Discussion

UV-VIS Confirmation of Sensing Element Attachment

The conjugation of 3-AMP and OPH to the hydrogel matrix was monitored on a colloid-free hydrogel (blank gel) through absorption spectroscopy (**Figure 44**). Each sensor was rinsed for several hours with 150 mM NaCl solutions to remove unreacted species. The 3-AMP is initially present at a concentration ~ 25 mM, but the hydrolysis step necessary for coupling OPH also hydrolyzes some of the ester bonds between the phenolate and the hydrogel, leaving ~ 13 mM phenol attached to the hydrogel (**Figure 44a**). OPH attachment to a blank hydrogel was confirmed by monitoring the tyrosine/tryptophan absorbance at 280 nm. Prior to OPH coupling, 4-amino-2-nitrophenol, which does not have an absorbance maximum at 280 nm, was attached to the blank hydrogel instead of 3-AMP. Thus spectral overlap between OPH and 3-AMP was avoided. **Figure 44b**. displays the difference spectrum of the blank hydrogel before and

after OPH coupling. Using the extinction coefficient of the OPH monomer, 26,740 M^{-1}cm^{-1} at 280 nm,[38] we calculated an 8 μM OPH concentration in the hydrogel using the difference spectrum.

We also proved that OPH was attached to the sensor by monitoring the 412 nm absorbance of p-nitrophenol, an OP hydrolysis product, in BTS containing methyl-paraoxon, and found that the rate of hydrolysis was ~ 400 times greater in the presence of an OPH-functionalized PCCA than in the presence of a PCCA lacking OPH. The OPH hydrolysis rates are typically 40-2450 times faster than in a 0.1 N NaOH solution.[39] This result also demonstrates that functional OPH is attached to the PCCA.

Figure 44: UV-VIS absorbance spectra of CCA-free hydrogels. a) displays the spectra at various stages of 3-AMP coupling. The blue line is the spectrum of a blank pHEA hydrogel prior to conjugation, the green spectrum is the blank after coupling with 3-AMP, and the red spectrum is after hydrolysis and rinsing. b) shows the spectra of a pHEA hydrogel with 4-amino-2-nitrophenol attached before (green) and after (red) OPH coupling. The blue difference spectrum represents the absorbance difference after coupling OPH. The peak at ~ 280 nm in the difference spectrum indicates OPH attachment. 4-amino-2-nitrophenol, which absorbs at ~ 430 nm instead of ~280 nm, was coupled instead of 3-AMP in order to avoid dominating overlap between the absorbance peaks of 3-AMP and OPH.

PCCA Titration in Test Buffer

We monitored the diffraction of the PCCA with 3-AMP attached in BTS in order to determine the pK_a of the phenol groups, which should be close to the pK_a of 3-acetamidophenol (**Figure 45**). Both the borate buffer (pK_a = 9.2) and the 3-acetamidophenol (pKa = 9.65) groups titrate at their expected pK_a values.[40] We observed that when the pH rises above the inflection point of the buffer, the sensor diffraction wavelength shifts. We conclude that the response is due to the deprotonation of the phenols, which makes the free energy of mixing of the hydrogel more favorable.[37] The titration and diffraction measurements show inflection points at pH ~ 9.6, the pK_a of the conjugated phenol. These measurements were repeated on the same PCCA after rinsing to demonstrate reproducibility and reversibility of the response.
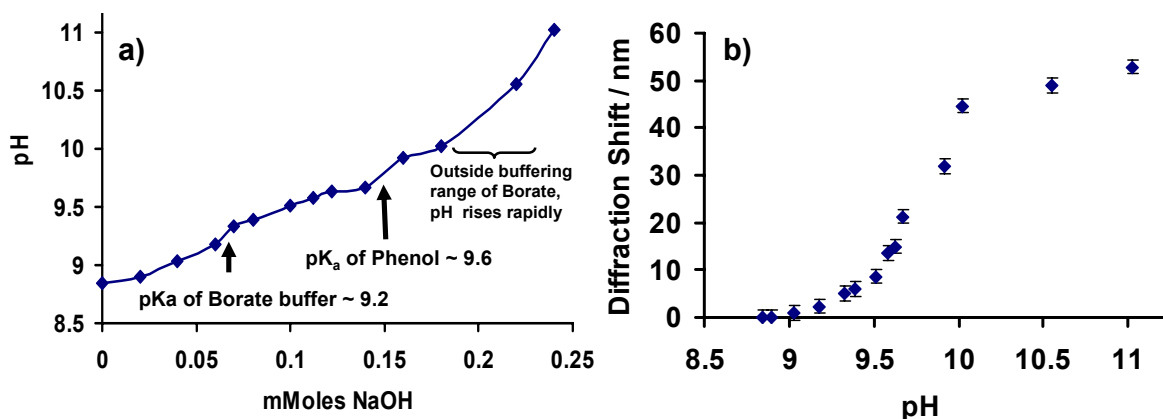
Figure 45: **a) The solution pH versus the number of millimoles NaOH added. The pK_a of the borate buffer (pH ~ 9.2) and the 3-AMP (pH ~ 9.6) are apparent. b) Diffraction red-shift of the PCCA as a function of the pH. We see that while the titration of the buffer occurs, there is very little response from the PCCA. But, as the phenol groups are titrated, we see the PCCA diffraction red-shifts. The inflection point in (b) occurs at the phenolate pK_a, indicating that the diffraction response is due to the phenol titration.**

Dependence of PCCA Diffraction on Methyl-Paraoxon Concentration

Our IPCCA organophosphate sensor contains both 3-aminophenol and OPH, which catalyzes the hydrolysis of methyl-paraoxon and releases protons.[16] The products, p-nitrophenol and dimethyl hydrogen phosphate, have pK_a which are lower than the buffered solution pH of 9.2 (7.22 and 1.24, respectively)[40] and thus decrease the internal pH of the IPCCA and protonates the pendant phenolates. This causes a steady-state reduction in the free energy of mixing, causing the gel to shrink. This volume change blue-shifts the diffraction in proportion to the concentration of methyl-paraoxon.

Figure 46 shows the methyl-paraoxon concentration dependence of our IPCCA sensor diffraction in BTS. The diffraction wavelength blue-shifts with increasing concentration of methyl-paraoxon. The shift essentially saturates by 240 μM methyl-paraoxon. At lower concentrations (≤24 μM) the response is quite linear, so a detection limit can be calculated. This concentration range is shown in the inset of **Figure 46a**. The detection limit is determined by the concentration of analyte that gives a response equal to 3 standard deviations of the blank. We calculate a 0.2 μM detection limit. Some AChE-based sensors achieved lower detection limits (typically 1-10 nM) because AChE irreversibly binds OPs and/or because AChE shows an extremely fast hydrolysis rate. Our current reversible sensor achieves the same level of detection as OPH-based biosensors based on potentiometry.[16,18,19] However, these new IPCCA OP sensors based on OPH are reversible, as evident by our use of the same sensor for replicate measurements.
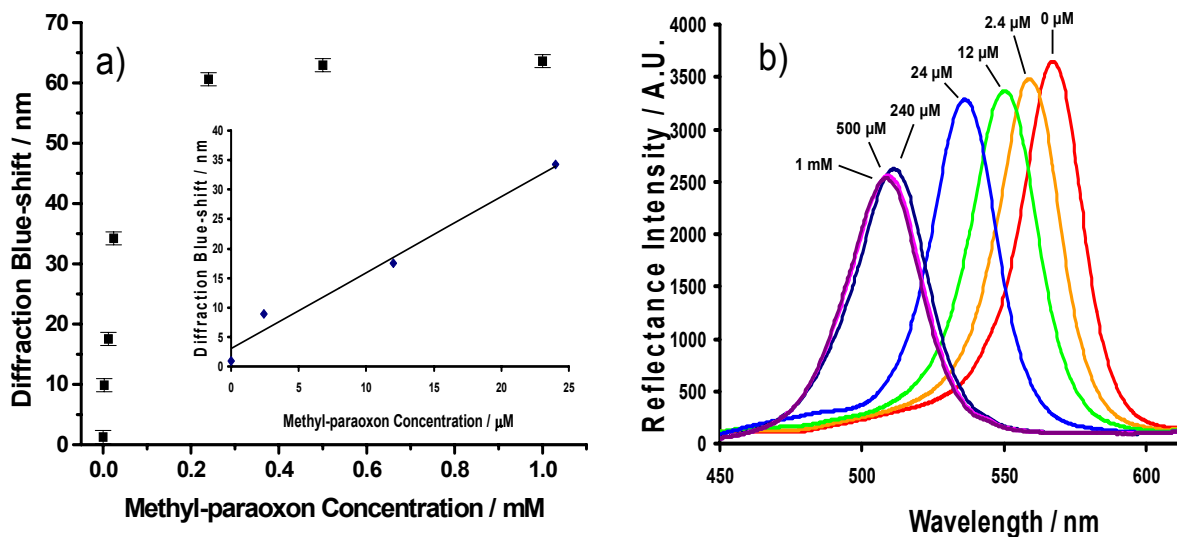
Figure 46: a)The PCCA diffraction wavelength as a function of methyl-paraoxon concentration in BTS. Inset is the range (0-24 µM methyl-paraoxon) used to calculate the limit of detection. b) shows the representative diffraction spectra of the PCCA at several methyl-paraoxon concentrations. The standard error in the measurement was σ = 1.1 nm for 2 replicates.

Confirmation of Sensing Mechanism

Sharma et.al. previously demonstrated a similar bimodular sensing approach utilizing the PCCA sensing platform in which a hydroxide enzyme hydrolysis product titrated a phenol, producing a steady-state pH gradient between the interior and exterior of the hydrogel, which changed the free energy of mixing, producing a diffraction wavelength shift proportional to the analyte concentration.[36] We performed several control experiments which confirmed that our sensor was also bimodular and responded to analyte through a decrease in the free energy of mixing of the hydrogel produced by the steady-state pH gradient within the sensor, which titrates pendant phenolates.

We also tested the sensor with OP in the absence of either 3-AMP or OPH to prove that the sensing response was due to a bimodular motif. The PCCA functionalized

with OPH, but lacking 3-AMP showed only a small ~1 nm diffraction wavelength blue-shift for 240 μM methyl-paraoxon.

A PCCA with 3-AMP and no OPH attached was also exposed to a 240 μM methyl-paraoxon solution. Under these conditions, the sensor actually blue-shifted ~ 3 nm after 60 minutes. This is very small compared to the normal sensing response of the IPCCA with OPH attached (~ 62 nm). This small blue-shift may result from the slow hydrolysis of methyl-paraoxon in the basic solution, catalyzed by the hydrogel. The hydrolysis produces a few protons that cause the gel to shrink slightly.

We performed studies to confirm that the sensing response resulted from a steady-state response and not an equilibrium response. We monitored the absorbance of a 12 μM methyl-paraoxon in BTS solution exposed to an OPH-functionalized IPCCA via UV-VIS of the solution in order to calculate the rate of production of p-nitrophenol, which absorbs at 412 nm. Using the rate of the p-nitrophenol absorbance increase, we calculated that it would take over 3 hrs for the sensor to hydrolyze all of the methyl-paraoxon. However, our sensor achieves full response in 50 minutes and thereafter remains stable for over an hour (**Figure 47**). After 2 hrs, the sensor begins to red-shift back towards the starting diffraction. We observed a similar response for 2.4 μM methyl-paraoxon concentration.

This response plateau occurs because the sensor reaches a steady-state after about 1 hr where the rate of H^+ diffusion out of the gel is equal to the rate of H^+ production from the OPH-mediated hydrolysis of methyl-paraoxon. After 2 hrs, the 12 μM methyl-

paraoxon is depleted by the enzyme, and the sensor subsequently red-shifts. Our observations are consistent with the steady-state bimodular results reported by Sharma et. al.[36]
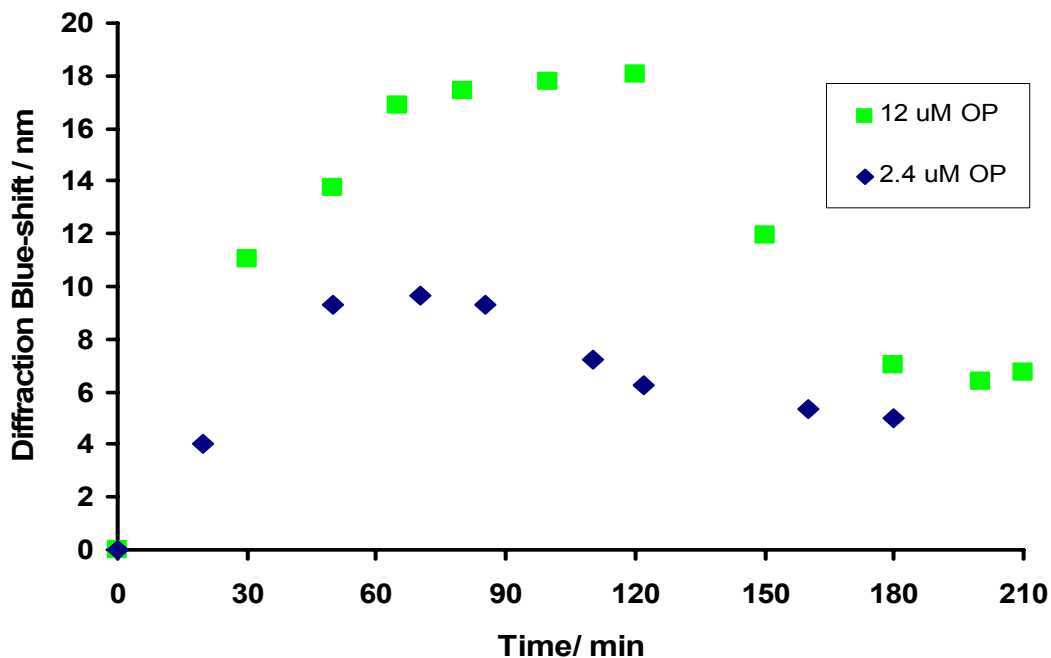
Figure 47: Time dependence of the diffraction blue shift at two different methyl-paraoxon concentrations. Steady-state is established within ~ 60 min. The diffraction red-shifts at longer times due to depletion of the analyte.

Stream Water Testing

We exposed the same sensor to both methyl-paraoxon in BTS as well as in a prepared stream water sample to compare the response of the sensor to laboratory samples and to environmental samples (**Figure 48**). The sensor displays a blue-shift of ~ 52 nm in response to 1 mM OP in BTS solution, compared to a blue-shift of ~ 46 nm to 1 mM OP in the stream water sample. The responses in stream water are consistently about 16 % smaller than in BTS at concentrations above saturation (>250 μM OP).

In order to determine why the spectral window is reduced in stream water, we titrated the stream water sample to determine whether there was another natural buffer present, such as calcium carbonate, which would increase the effective buffer concentration and reduce the spectral window of the sensor. The stream water did not require much base to increase the pH significantly, and no inflection point was found. The spectral window was not reduced by the presence of a natural buffer.
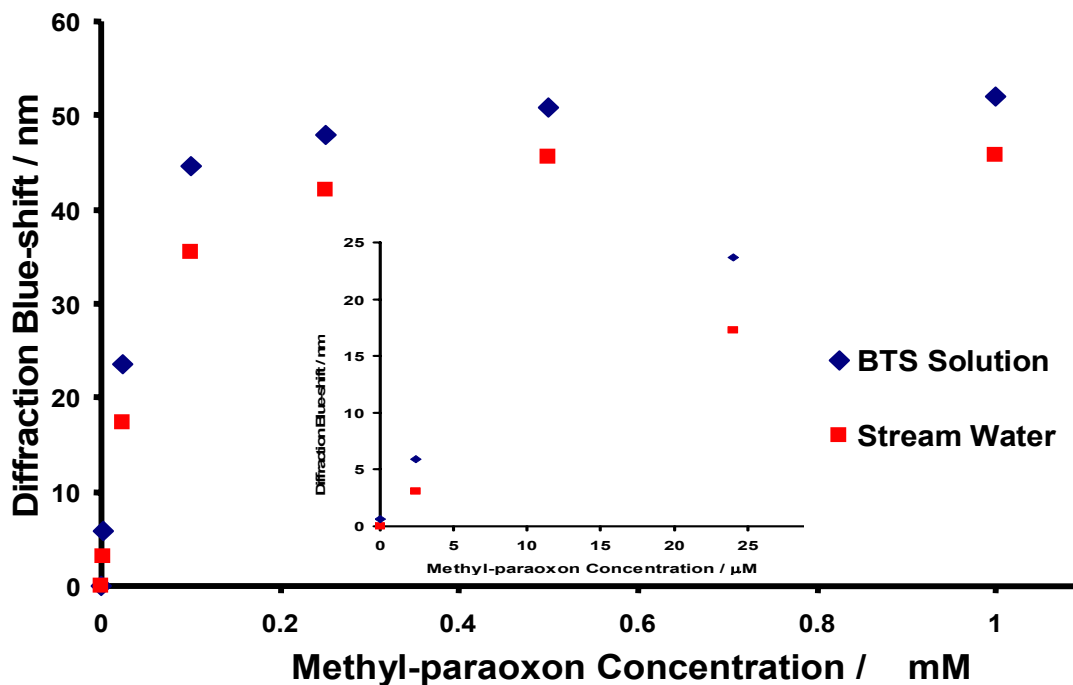
Figure 48: PCCA OP sensor diffraction wavelength as a function of methyl-paraoxon pesticide concentration in both BTS and filtered stream water. The sensor displays a 16% smaller response in stream water compared to its response in BTS. The inset shows the concentrations ≤ 24 μM methyl-paraoxon.

A possible cause for the reduction in the spectral window in real samples is the presence of other species which function as OPH inhibitors, which could cause the OPH to turn over the methyl-paraoxon at a slower rate. A slower turnover rate would decrease

the steady-state pH gradient, which would cause less protonation of the phenolates, which would result in a smaller diffraction blue-shift.

A.4 Conclusions

We developed a sensor which is capable of determining submicromolar concentrations of the organophosphate pesticide methyl-paraoxon. Organophosphorus hydrolase enzyme immobilized inside the hydrogel catalyzes the hydrolysis of methyl-paraoxon, producing protons which create a steady-state pH gradient in the hydrogel. Pendant phenolates are protonated as a result of this pH gradient, causing a decrease in the free energy of mixing of the hydrogel, which shrinks the gel and blue-shifts the wavelength of light diffracted by the CCA proportional to the concentration of OP in solution. The OPH-based photonic crystal sensor operates at high ionic strength and is reversible, so that it can be used as a continuous sensor for environmental sample solutions. We observe submicromolar detection limits in buffer solution and in a stream water sample. We demonstrated that our sensor works in environmental samples by sensing methyl-paraoxon in stream water solutions. We are currently working to increase the spectral window to span the entire visible region and to increase the sensitivity and speed of the sensor response.

A.5 Acknowledgments

142

References

1. Hopkins, E.H.; Hippe, D.J., Frick, E.A.; Buell, G.R. *Organophosphorus pesticide occurrence and distribution in surface and ground water of the United States, 1992-97.* **2000,** U.S. Geological Survey Open File Report 00-187, Denver, CO.

2. Burtis, C.A.; Ashwood, E.R. (Eds). Cholinesterases from *Tietz Textbook of Clinical Chemistry,3rd Edition,* **1999**, W.B. Saunders, Philadelphia, 708-711, 939-940

3. Radic, Z.; Pickering, N.A.; Vellom, D.C.; Camp, S.; Taylor, P. *Biochem.* **1993**, *32*, 12074-12084.

4. Dziri, L.; Boussaad, S.; Tao, N.; Leblanc, R.M. *Langmuir* **1998**, *14*, 4853-4859.

5. Zaugg, S.D.; Sandstrom, M.W.; Smith, S.G.; Fehlberg, K.M. *Determination of pesticides in water by C-18 solid phase extraction and capillary column gas chromatography/mass spectrometry with selected-ion monitoring.* **1995,** U.S. Geological Survey Open-File Report 95-181, Denver, CO.

6. Agency for Toxic Substances and Disease Registry (ATSDR). Toxicological profile for methyl parathion. **2001**, Update. Atlanta, GA: U.S. Department of Health and Human Services, Public Health Service.

7. Marx, S.; Zaltsman, A.; Turyan, I.; Mandler, D. *Anal. Chem.* **2004,** *76*, 120-126.

8. Leon-Gonzalez, M.E.; Townshend, A. *Anal. Chim. Acta*, **1990,** 236, 267-272.

9. Constantine, C.; Mello, S.V.; Dupont, A.; Cao, X.; Santos, D.; Oliveira, O.N.; Strixino, F.T.; Pereira, E.C.; Cheng, T.; Defrank, J.J.; Leblanc, R.M. *J. Am. Chem. Soc.*, **2003**, *125*, 1805-1809.

10. Mello, S.V.; Mabrouki, M.; Cao, X.; Leblanc, R.M.; Cheng, T.; Defrank, J.J. *Biomacromolecules* **2003**, *4*, 968-973.

11. Sacks, V.; Eshkenazi, I.; Neufeld, T.; Dosoretz, C.; Rishpon, J. *Anal. Chem.* **2000**, *72*, 2055-2058.

12. Halamek, J.; Pribyl, J.; Makower, A.; Skladal, P.; Scheller, F.W. *Anal. Bioanal. Chem.* **2005,** *382*, 1904-1911.

13. Walker, J.P., Asher, S.A. *Anal. Chem.* **2005**, *77*, 1596-1600.

14. Lai, K., Dave, K.L., and Wild, J.R. *J. Biol. Chem.* **1994**, *24*, 16579-16584.

15. Donarski, W. J.; Dumas, D.P.; Heitmeyer, D.P.; Lewis, V.E.; Raushel, F.M. *Biochem.* **1989**, *28*, 4650-4655.

16. Mulchandani, P.; Mulchandani, A.; Kaneva, I.; Chen, W. *Biosens. Bioelectron.* **1999**, *14*, 77-85.

17. Cho, C.M.; Mulchandani, A.; Chen, W. *Appl. Environ. Microbiol.* **2004**, *70*, 4681-4685.

18. Rogers, K.R.; Wang, Y.; Mulchandani, A.; Mulchandani, P.; Chen, W. *Biotechnol. Prog.* **1999**, *15*, 517-521.

19. Rainina, E.; Efremenco, E.; Varfolomeyev, S.; Simonian, A.L.; Wild, J.R. *Biosens. Bioelectron.* **1996**, *11*, 991-1000.

20. Mulchandani, A.; Mulchandani, P.; Chen, W.; Wang, J.; Chen, L. *Anal. Chem.* **1999**, *71*, 2246-2249.

21. Mulchandani, P.; Chen, W.; Mulchandani, A. *Environ. Sci. Technol.* **2001**, *35*, 2562-2565.

22. Lei, Y.; Mulchandani, P.; Wang, J.; Chen, W.; Mulchandani, A. *Environ. Sci. Technol.* **2005**, *39*, 8853-8857.

23. Lei, Y.; Mulchandani, P.; Chen, W.; Mulchandani, A. *J. Agric. Food Chem.* **2005**, *53*, 524-527.

24. LeJeune, K.; Wild, J.R.; Russell, A.J. *Nature.* **1998**, *395*, 27-28.

25. DeFrank, J.J.; Beaudry, W.T.; Cheng, T.; Harvey, S.P.; Stroup, A.N.; Szafraniec, L.L. *Chem. Bio. Interact.* **1993**, *87*, 141-148.

26. Asher, S.A.; Flaugh, P.L.; Washinger, G. *Spectroscopy* **1986**, *1*, 26-31.

27. Carlson, R.J.; Asher, S.A. *Appl. Spectrosc.* **1984**, *38*, 297-304.

28. Weissman, J.M.; Sunkara, H.B.; Tse, A.S.; Asher, S.A. *Science* **1996**, *274*, 959-960.

29. Reese, C.E.; Guerrero, C.D.; Weissmann, J.M.; Lee, K.; Asher, S.A. *J. Coll. Interface. Sci.* **2000**, *232*, 76-80.

30. Flaugh, P.L.; O'Donnell, S.E.; Asher, S.A. *Appl. Spectrosc.* **1984**, *38*, 847-850.

31. Rundquist, P.A.; Photinos, P.; Jagannathan, S.; Asher, S.A. *J. Chem. Phys.* **1989**, *91*, 4932-4941.

32. Asher, S.A.; Holtz, J.; Liu, L.; Wu, Z.; *J. Am. Chem. Soc.* **1994**, *116*, 4997-4998.

33. Holtz, J.H.; Asher, S.A. *Nature* **1997**, *389*, 829-832.

34. Holtz, J.H.; Holtz, J.S.; Munro, C.H; Asher, S.A. *Anal. Chem.* **1998**, *70*, 780-791.

35. Asher, S.A.; Holtz, J.H.; Weissman, J.M.; Pan, G. *MRS Bull.* **1998**, (October), 44-50.

36. Sharma, A.C., Jana, T., Kesavamoorthy, R., Shi, L., Virji, M.A., Finegold, D.N., Asher, S.A. *J. Am. Chem. Soc.* **2004**, *126*, 2971-2977.

37. Flory, P.J. *Principles of polymer Chemistry;* Cornell University Press: Ithaca, NY, **1953**.

38. Lybradyn GS-10 OPH product specifications, Lybradyn, Inc. **2006**. Oak Brook, IL.

39. White, B.J.; and Harmon, H.J. *Biosens. Bioelectr.* **2005**, *20*, 1977-1983.

40. *Lange's Handbook of Chemistry,* 15th e d. Dean, J.A., Ed.; McGraw-Hill Publishers,: New York, **1999**, Chapter 8.